Development and Characterization of Controlled Delivery Systems for rhBMP-2

D i s s e r t a t i o n

zur Erlangung des akademischen Grades

doctor rerum naturalium (Dr. rer. nat.)

vorgelegt der

Naturwissenschaftlichen Fakultät I

Biowissenschaften

der Martin-Luther-Universität Halle-Wittenberg

von

Herrn Alexander Lochmann

geb. am 22.06.1981 in Karl-Marx-Stadt, jetzt Chemnitz

Gutachter

1. Prof. Dr. rer. nat. habil. Karsten Mäder
2. Prof. Dr. rer. nat. habil. Elisabeth Schwarz
3. Prof. Dr. rer. nat. habil. Michaela Schulz-Siegmund

Halle, den 11. März 2011

Nothing in life is to be feared, it is only to be understood.

Maria Skłodowska-Curie

Meiner Familie

Table of Contents

1 **Introduction** 1

1.1 Preface 1

1.2 The Backbone of It All – Development of Bone Defect Regeneration 2

1.2.1 The Family of Bone Morphogenetic Proteins 4

1.3 Drug Delivery Options for rhBMP-2 6

1.3.1 Microparticles in Drug Delivery 9

1.4 Research Objective 12

2 **Experimental** 14

2.1 Expression, Extraction and Purification of rhBMP-2 14

2.1.1 Isolation of Inclusion Bodies 14

2.1.2 Solubilization of Unfolded rhBMP-2 16

2.1.3 Renaturation 16

2.1.4 Control of Refolding 16

2.1.5 Purification 18

2.2 Modification of rhBMP-2 19

2.2.1 Carboxyfluorescein Labelling 19

2.2.2 Rhodamine Labelling 19

2.3 Stability of rhBMP-2 20

2.3.1 Aggregates 20

2.3.2 Stability of rhBMP-2 in Release Media 23

2.3.3 Freeze-thaw Recovery of rhBMP-2 and the Influence of Microsphere Degradation Products on rhBMP-2 Stability 25

2.4 Production of Microspheres 26

2.4.1 Residual Solvents 28

2.4.2 Thermal Analyses of Polymers and Microspheres 28

2.5 Characterization of Drug-loaded Microspheres 29

2.5.1 Size Distribution 29

2.5.2 Surface Morphology 30

2.5.3 Drug Distribution 30
2.5.4 Encapsulation Efficiency 31
2.6 In Vitro Release Studies 31
2.6.1 *In Vitro* Degradation of the Microspheres 31
2.6.2 Release Determination 32
2.6.3 *In Vitro* Activity of Released rhBMP-2 33
2.7 Microspheres in Scaffolds 34
2.8 Microspheres in Gel 34
2.8.1 Chitosan-based *In Situ*-Forming Implants 35
2.8.2 Hydrophobically Modified Hyaluronic Acid Gels 35
2.9 In Vivo Investigation of rhBMP-2-loaded Microspheres 36
2.9.1 Frequently Applied Techniques 36
2.9.2 System Optimization 39
2.9.3 Bone Formation Assessment in a Mouse Ectopic Model 40
3 **Results and Discussion** 44
3.1 Extraction and Purification of rhBMP-2 44
3.2 Modification of rhBMP-2 47
3.2.1 Carboxyfluorescein Labelling 47
3.2.2 Rhodamine Labelling 48
3.3 Analysis of rhBMP-2 50
3.3.1 Aggregates 50
3.3.2 Stability of rhBMP-2 in Release Media 58
3.3.3 Freeze-thaw Recovery of rhBMP-2 and the Influence of Microsphere Degradation Products on rhBMP-2 Stability 59
3.3.4 Solubility, Aggregation and Stability: Conclusion 60
3.3.5 Considerations towards rhBMP-2 Encapsulation 62
3.4 Production of Microspheres 63
3.4.1 Residual Solvents 68
3.4.2 Thermal Analyses of Polymers and Microspheres 69
3.5 Characterization of Drug-Loaded Microspheres 71
3.5.1 Size Distribution 71

3.5.2 Surface Morphology 74
3.5.3 Drug Distribution 75
3.5.4 Encapsulation Efficiency 77
3.6 In Vitro Release Studies 79
3.6.1 *In Vitro* Degradation of Microspheres 80
3.6.2 Release Determination 84
3.6.3 *In Vitro* Activity of Released rhBMP-2 88
3.7 Microspheres in Scaffolds 89
3.8 Microspheres in Gel 90
3.8.1 Chitosan-based *In Situ*-forming Implants 90
3.8.2 Hydrophobically Modified Hyaluronic Acid Gels 92
3.9 In Vivo Investigation of Loaded Microspheres 93
3.9.1 Injection of Microspheres dispersed in Liquid 93
3.9.2 Injection of Microspheres dispersed in Gel 93
4 **Synopsis and Conclusions** 111
5 **Abstrakt in deutscher Sprache** 119
6 **Appendices** 120
6.1 List of Abbreviations 120
6.2 List of Media and Buffer Solutions 123
6.2.1 Isolation and Purification of rhBMP-2 123
6.2.2 SDS-PAGE 124
6.2.3 Microsphere Fabrication Standard Buffers 124
6.2.4 *In vitro* Release and Stability 125
6.2.5 *In vitro* Activity Assay 125
7 **References** 126

1 Introduction

1.1 Preface

This study has been carried out in the course of three consecutive projects of the Translational Centre for Regenerative Medicine in Leipzig. Consequently, the research work was focussed on the translation from conceptual towards preclinical research. Several outcomes, e.g. the protein aggregation and stability pattern, offer the potential for further investigations to gain deeper insights into the involved mechanisms. In spite of this fact, the project design enabled the direct usage of the obtained results for further steps of development. Parts of this thesis have been published in research papers.

Brand names and trademarks that were used in this thesis have not been labelled specifically. The absence of labelling does not identify an item as non-proprietary.

Mean values and standard deviations are indicated in order to ensure the comparability of the obtained results with other data. However, as a result of the small numbers of samples in some experiments, tests on Gaussian distribution were omitted in several cases. Hence, it should be kept in mind that in small groups normality was not tested but assumed.

1.2 The Backbone of It All – Development of Bone Defect Regeneration

"To be the backbone of something:" As expressed in many sayings, the 'backbone' is regarded as an inherent part of an entity, as a necessity for existence. The United Nations and the World Health Organization declared the first decade of this century to be the *Bone and Joint Decade*[1]. In fact, only few other tissues can be found which possess such an essential importance to human life. Logically, bone has the highest ability for regeneration amongst all tissues[2]. Being subject to constant building, rebuilding and decomposition processes, bone tissue can bridge defective areas well, especially when the periosteum is still intact. Unlike other tissues, which heal by the formation of scars after an encroachment of fibroblasts, the initial blood clot is slowly replaced by newly forming bone. However, if the bone defect exceeds a certain limit, the regenerative ability of the organism will be exhausted. The space is then filled with connective tissue, resulting in a so-called non-union or pseudo-arthrosis. In conjunction with these effects, the term critical size defect is often used. The critical size, as defined by Schmitz, Hollinger and Kleinschmidt, is the "smallest intraosseous wound that would not heal by bone formation. ... Less than 10 % of bone regeneration [can be observed] during the lifetime ..."[3] The critical size of a defect depends on the regenerative potential of the patient, which has been described to decrease with age[3]. Up to 10 % of all fractures are estimated to show impaired healing, with patients suffering not only from morbidity, but also from psychosocial stress[4]. The need for sufficient care is further enhanced by socioeconomic reasons, such as high costs for the health care systems due to long hospitalisation times.

While the excision of misfunctioning, ill or malign tissues has been performed for ages[5], the substitution of missing or removed tissues has proven much more complicated. Implantation of substitutes such as a gold plate in the frontal bone defect of a Peruvian chief[6], or the use of fir-wood inserted into long bone defects by the Aztecs in the 16th century[7] may be regarded as pioneering work in the field. With advances in aseptic surgery and anaesthesia in the middle of the 19th century, the issue of bone grafting was successfully addressed in modern surgery.

Three types of grafts can be distinguished[8]:

(I) autograft, derived from tissues of the patient,

(II) allograft, obtained from one or more individuals other than the receiving patient,

and (III) xenograft, gained from another species.

The first recorded bone allografting process was accomplished in 1880 by Sir William Macewen[7]. He succeeded in grafting an 11 cm defect in the humerus of a three-year-old boy. As early as 1889, Senn proposed the use of decalcified bone matrix as an alternative to Macewen's method, being the first to use a processed bone material with inherent growth factors[9]. Senn had initially been searching for a suitable carrier to bring iodoform as an antiseptic into defect areas and was surprised to see them closing as a result of the treatment. Fifty years later, Rainsford Mowlem popularized the use of tissue derived from the iliac crest of the patient to repair maxillofacial and long bone defects[10,11]. Circumventing the immunogenicity, disease transmission and excessive resorption seen in allografts and xenografts, autologous cancellous bone has been the gold standard for decades[12]. However, several drawbacks are inherent in this method. Donor site pain and morbidity, infection and extra blood loss are considerable adverse effects[13]. Unacceptable failure rates of 13 - 30 % have been reported[14]. Moreover, the autologous bone harvestable at potential donor sites, such as the iliac crest, is limited, especially in osteoporotic or pediatric patients[13].

A milestone in bone defect regeneration was set by Marshall Urist. In a series of animal experiments, he investigated fractions of decalcified bone matrix in ectopic sites[15-17]. Urist was the first to postulate the autoinductive potency of bone and linked it to a fraction he had isolated therefrom[15]. In the 1980s, experiments with fractions containing Bone Morphogenetic Proteins (BMPs) were performed. The understanding of endochondral bone formation of the molecular and cellular level has since progressed[18]. Sampath and Reddi proposed a simple and reliable bioassay for the assessment of ectopic bone formation[19]. Later, the advances in recombinant expression and the demonstration of the biological activity of recombinant BMPs[20] enabled the study of single molecules.

Meanwhile, a novel discipline of science was being created. In 1993, Tissue Engineering was defined as "a new field,... [applying] the principles of biology and engineering to the development of functional substitutes for damaged tissue" by Langer und Vacanti[21].

They identified three main strategies of Tissue Engineering:

(I) the use of isolated cells or of cell substitutes

(II) tissue-inducing substances

and (III) cells placed on or within matrices.

All of these strategies as well as several peripheral approaches are applied today in bone defect regeneration research. While one part of research is focussed on scaffold materials and their optimization, other studies address the combinations of scaffolds with cells or injectable systems with cells. Growth factor and gene delivery are further advancements in the field, so that a broad variety of combinations is currently being investigated. Recent progress includes the combined delivery of an osteogenic growth factor, mesenchymal stem cells and an antibiotic oligomer by means of a hydrogel[22]. A bone bioreactor, as proposed by Stevens et al., showed the generation of new vital bone by creation of an artificial subperiosteal space at the tibia of rabbits[23]. The direct percutaneous gene delivery of an adenovirus-modified cytokine was demonstrated to be successful in a critical size femur defect in rats[24]. The most promising and best investigated growth factors for bone tissue engineering are found in the group of Bone Morphogenetic Proteins.

1.2.1 The Family of Bone Morphogenetic Proteins

Bone Morphogenetic Proteins are a subgroup of the TGF-β superfamily. The group of cytokines was originally defined by their ability to induce formation of bone and cartilage in ectopic sites *in vivo*[15,19]. This property is unique, as no other growth factor is capable of turning connective tissue cells into osteoprogenitors[25]. The identification of a common structural characteristic led to a re-evaluation of the term BMP and made the structure a part of their definition. The BMP structure is highly conserved. Seven cysteines can be found in one molecule. Six of these thiol groups form three intramolecular disulphide bonds. The rigid structure obtained therefrom is termed ‘cystine knot’. The seventh thiol group links two BMP molecules to each other, resulting in the native dimer. Homodimers are more frequently found than heterodimeric BMPs, both types were reported to be bioactive[26]. About 20 homodimeric BMPs are known, and there are still controversial opinions on the nomenclature and number of members[2,26-28]. The multitude of synonyms illustrates a heterogeneous denomination practice. Many BMPs are also referred to as ‘growth and differentiation factors’ (GDF)

or as 'osteogenic proteins' (OP). A rough classification divides BMPs *sensu stricto* into four subfamilies:

(I) BMP-2 (BMP-2a) and BMP-4 (BMP-2b),

(II) BMP-5, BMP-6 (Dvr6), BMP-7 (OP-1), BMP-8 (OP-2),

(III) BMP-3 (osteogenin) and BMP-3b (GDF-10),

and (IV) BMP-9 (GDF-2), BMP-11 (GDF-11).

The role of BMPs in endochondral bone formation was reviewed by Ten Dijke et al. and Tsumaki and Yoshikawa[29,30]. A recent update of BMP signalling in bone development and repair was published by Rosen[31]. Bone morphogenetic proteins 2-7 and 9 mediate osteoinduction[12]. While BMP-3 and BMP-3b have been described as negative regulators, complete bone morphogenesis has been shown for BMPs 2, 4, 6, 7, and 9[26]. The most potent inducers of bone formation have been identified in BMP-2 and BMP-4[32]. BMP-2 induces endochondral ossification via cartilaginous intermediates, the same process as is found in the epiphyseal growth plates. After an induction stage, which includes the release of growth factors and cytokines from a hematoma at the fracture site, inflammation and subsequent cartilage formation can be observed. With further healing, the cartilage becomes hypertrophic and calcification starts, new blood vessels spread into the area. Osteoblasts can be detected in the region and slowly, the extracellular matrix becomes mineralized. The final step of endochondral ossification is characterized by remodelling processes. wherein lamellar bone and hematopoietic bone marrow appear.

In high doses, BMPs can also predetermine the second way of bone formation[25]. The so-called 'intramembraneous ossification' is characterized by direct transformation of primitive mesenchymal cells into osteoprogenitor cells and subsequent osteoblast formation. Increased osteoclast activity and initial localized bone resorption after administration of high doses of BMPs have also been reported[28].

Apart from functions in bone and cartilage morphogenesis, limb formation and skeleton patterning, various other roles in different tissues have been reported for most BMPs[2], so that recently Reddi proposed an additional denomination of BMPs as 'body metabolo-genes'[33] or 'body morphogenetic proteins'[2]. BMPs 8b, 10, and 12-18 mainly exhibit other physiological roles. They may be seen as BMPs *sensu lato*. BMP-1, a protease known to support a microenvironment beneficial for bone formation, has been excluded from the BMP family, lacking the structural characteristics of other BMPs.

In their recombinant form, BMPs have already made their way from bench to bedside. RhBMP-2 and rhBMP-7 (OP-1) are marketed for spinal fusion and long bone non-unions in tibiae, respectively[26]. The use of rhBMP-2 in other clinical settings, including craniofacial surgery[34], pyogenic vertebral osteomyelitis[35] and reconstructive surgery of the skull[36], has been reported. In spite of higher costs and a lower production efficiency[37], commercially available rhBMP-2 products are still based on the expression in Chinese hamster ovary (CHO) cells. In eukaryotic cells, the protein will be produced in glycosylated state allowing the omission of a refolding process[38]. Uludag et al. reported Asp-338 to be the glycosylation site of the protein, bearing between five and nine mannose residues[39]. Recently, it was shown that unglycosylated rhBMP-2, derived from *E. coli* and refolded correctly, yields the same osteoinductive activity as CHO-derived rhBMP-2[37] and is retained better at its site of application due to lower solubility[40,41]. Furthermore, *E. coli*-derived rhBMP-2 has been shown to be active *in vivo* even after direct dissolution in mixtures of organic solvent and synthetic polymer[42]. From this point of view, prokaryote-derived rhBMP-2 appears to be beneficial for sustained release applications.

1.3 Drug Delivery Options for rhBMP-2

BMP-2 is in clinical use since 2002. More than 500'000 patients worldwide have been treated so far[43]. In a meta-analysis, Mussano et al. concluded that a slight improvement in efficacy with the use of BMPs compared to conventional treatment is achieved, although a minimum concentration of 1.5 mg/ml was needed for sufficient results with the used collagen delivery systems[44]. The extra cost of a treatment with rhBMP-2, in addition to the standard care, amounts to at least € 3'000 and may reach up to € 10'000 per single treatment in Germany[45,46]. These high costs are one factor to limit the clinical use of the protein[12].

How can these drawbacks be tackled? Several different strategies were reported recently[47-54]. In addition to the search for alternative osteo-inductive proteins[50] or more stable BMP-2 derivates[47], most approaches are focussed on dose minimization and on tailored release of the expensive growth factors. Although the initial concentration of the growth factor may be physiological, Seeherman et al. speculated that osteogenic factors are often not present long enough to recruit sufficient responding cells in a bone defect[55]. Hence, the augmentation by growth factor delivery will be needed for an extended period of time to

guarantee a continuation of the regeneration process. BMP-2 is a chemotactic agent[56], lower doses than the clinically applied have been shown to be sufficient in many bone defect models. At present, the main focus has to be laid on dose reduction by controlled delivery of the growth factor. It was shown by several groups, that a better retention of rhBMP-2 at the implantation site resulted in superior osteoinductivity and significantly higher bone scores in rodents[14,57,58]. Li and Wozney speculated that a faster release is tolerated better by species with a high regeneration potential, whereas humans may need a more sustained release for optimal performance[59]. Takahashi and coworkers demonstrated that a healing in skull bone defects of monkeys can be achieved with doses as low as 5 μg when released in a controlled fashion. Although not strictly meeting the criteria of a critical size defect model, these results support the opinion of low dose efficiency of rhBMP-2 in higher animals[60]. The supply of an optimized delivery system is expected to ameliorate the osteoinductive outcome at lower doses, reducing costs and the frequency of adverse effects. Tabata pointed out "the importance of drug delivery in tissue engineering", suggesting protection of the growth factor against proteolysis by the drug delivery system and prolonged retention at the intended site of action[61]. According to Brekke, an ideal osteoinductive bone graft substitute would include the following characteristics[62]:

(I) biocompatibility,

(II) absence of allergic reaction and transmission of disease,

(III) gross architectural qualities such as porosity and flexibility,

(IV) osteoconduction, i.e. support of attachment of bone-forming cells by the matrix[63],

(V) chemotaxis,

(VI) delivery/control of osteoinductive protein,

(VII) promotion of angiogenesis and vascularization,

and (VIII) compliance with administrative regulations.

Babensee and coworkers defined as follows[64]: "A tissue-engineered implant is a biologic-biomaterial combination in which some component of tissue has been combined with a biomaterial to create a device for the restoration or modification of tissue or organ function."

Several rhBMP-2 delivery systems have been conceptualised, five of which meet most of Brekke's criteria:

(I) mineral paste,

(II) scaffolds, mainly of composite origin,

(III) hydrogels, often chemically modified,

(IV) microparticulate systems,

and (V) combinations of (I) to (IV).

The growth factor may either be incorporated into or soak-loaded onto the delivery systems[58,65-68]. Soak-loading has a main drawback: If the interactions between matrix and growth factor are weak, tremendous burst releases can be found, which is wasting most of the cytokine within the first hours. If, on the other hand, the matrix and the growth factor do interact strongly with one another, the rhBMP-2 effect will be limited due to incomplete release. El-Ghannam et al. compared different mineral scaffolds as potential carriers for rhBMP-2[69]. They found extremely low release rates of rhBMP-2 adsorbed to the minerals. Less than 1 % of the initially immobilized amount was released within the investigated period of seven days. Another disadvantage of pasty materials is an impaired biodegradability. Low porosity and high particle size impair bone growth into these areas. Paste remnants are often detected even after long investigation periods[70].

The biodegradability of scaffolds is easier to control. Composite materials, including natural components of bone[71] in order to mimic a bone matrix which has to be populated with osteoblasts and remodelled, are frequently used. Unfortunately, an almost irresolvable problem inheres in scaffold matrices: high porosity and high stability controvert one another. If the pore size is too low, the exchange of nutrients and waste products from the inner part is impeded, resulting in impaired cell growth. Furthermore, the cytokine loading process can often be accomplished only by soak-loading. Whang and coworkers reported a decrease in pore size of their composite scaffolds after loading with rhBMP-2 and found no cell growth within the scaffold, probably due to insufficient nutrient supply[72].

Alternatively, hydrogels may hinder mass transport to a lesser extent. Functionalized gels allow for a bioresponsive nature of the implant. Lutolf et al. demonstrated that healing of critical size calvarial defects in rats can be achieved after administration of 5 μg of rhBMP-2 in matrix metalloproteinase-sensitive hydrogels with careful choice of the gel formation parameters[73]. Most advantageous in gel systems are their

ease of application and the perfect fit into the defect area. Because of the already impaired blood supply in the fractured bone, the elevation of muscle attachments is often omitted, so that an optimal placement of scaffolds loaded with growth factors is rarely possible[38]. Injectable systems can be delivered to these areas more easily. However, the lack of stability may impede their use in some clinical applications. A controlled release can only be achieved to some extent by modifications such as crosslinking or the introduction of moieties with a high affinity for rhBMP-2.

Microparticulate systems are a very promising strategy in drug delivery. In addition to the chance for a tailorable release, microparticles open up a large opportunity for combination e.g. with scaffolds[74], hydrogels[75] and even mineral pastes[76], allowing for a fusion of these systems' advantages.

1.3.1 Microparticles in Drug Delivery

The term *microparticle* originates from the Greek *μικρόσ*, expressing *small*, and the Latin *particula*, the diminutive of *part*. Microparticles are defined by their size, being in the range of millionths of meters. The most frequently reported range is 1 – 100 μm[77], although one order of magnitude above and below may be included in broader definitions[78]. Microparticles have gained importance in several branches like food, chemical and pharmaceutical industries. Reports estimate the number of different methods filed in patent offices to be at least 2'000[79]. Hence, microparticles are a heterogeneous group with regard to their micromorphology. Three main types can be distinguished[79] (Fig. 1.3-1):

(I) microcapsules (originating from *capsa*, the Latin word for *container* or *box for books*),

(II) microspheres (derived from *σφαίρα*, the Greek word for *ball*)

and (III) more complex structures such as hollow spheres or spherical aggregates.

Microcapsules are composed of a drug-loaded, solid, liquid or gaseous core and a polymeric wall which constitutes the release barrier. In contrast, microspheres contain the active ingredient homogeneously distributed, either dispersed or dissolved in the matrix throughout the entire particle without the presence of an outer shell.

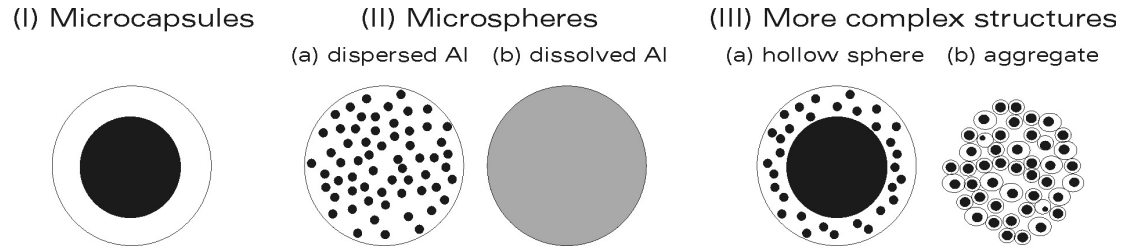

Fig. 1.3-1: Typical microparticle morphologies (Drawing mod. from Ref. 79). The polymer matrix is depicted in white, the active ingredient (AI) in black.

Various excipients have been used for the production of microparticles. Parenteral delivery and the intended step-by-step substitution by bone tissue require biodegradable systems. Schwartz circumvented the use of polymeric components by precipitating rhBMP-2 in order to produce microparticles[80]. However, his work was not focussed on controlled delivery, but on the stabilization of rhBMP-2 in solution.

Natural derived polymers like dextran, chitosan, alginate and starch have been used for microparticulate rhBMP-2 delivery[40,52,81]. Patel et al. demonstrated the adaptability of gelatine microparticles for the controlled delivery of rhBMP-2[48]. Apart from batch-to-batch variations, however, natural polymers used in microspheric delivery were shown to reach desirable release kinetics only after chemical modification[48,51-53], which raises production costs, safety concerns and may cause difficulties on the way towards the clinic. As a consequence, the use of synthetic polymers is very reasonable. Amongst them, polyesters are the most frequently utilized group due to their documented biocompatibility and biodegradability[82,83]. Polylactic acid, polyglycolic acid and their copolymers exhibit low immunogenicity and have been approved for parenteral application[84]. In addition to the mentioned advantages, modifications in the polymer molecular weight, in the end-capping of the polymer chains and in the variation of the lactic/glycolic acid ratio and sequence enable distinct release and degradation profiles. In Germany, five active pharmaceutical ingredients are currently marketed as poly(lactic-co-glycolic acid) (PLGA) microparticles, four of them being peptides[85].

Interestingly, all three main techniques[77,83,86,87] for microsphere preparation are utilized in the production of at least one market product[79], illustrating that neither

(I) spray drying

nor (II) phase separation

nor (III) emulsion - solvent evaporation techniques represent the one ideal way to produce microparticles.

The advantages of spray drying include simplicity and good scale-up possibilities, but its use is limited in small batch sizes[83], which were necessary in this study due to a variation of different parameters. The control of particle size remains difficult, and as particle size is one of the main factors influencing release kinetics, this may be regarded as another main drawback of spray drying.

Phase separation approaches are based on the incompatibility of two polymeric components. The technique is limited in the fabrication of particles in the lower micrometer size range[83], thus disqualifying delivery through standard syringes. Furthermore, coacervation techniques are often regarded as problematic due to the amount of residual solvents and coacervants remaining in the microspheres. In contrast to other techniques, mainly microcapsules are obtained with this method. However, the use of microspheres rather than microcapsules is more advantageous for controlled delivery purposes, because dose dumping through damaged membranes can be precluded.

Originally patented in 1970, the double emulsion method has by now been studied for nearly twenty years for the encapsulation of proteins[88,89]. The simplicity regarding apparative demands makes this method an ideal laboratory technique. On the other hand, a multitude of parameters influences the particle characteristics, so that double emulsion techniques are described to be less reproducible. However, the possible use of small batch sizes enables a convenient formulation development if all parameters are carefully monitored.

In contrast to numerous soak-loading approaches[58,65-68], only few authors report on microspheric PLGA-based delivery systems with incorporated rhBMP-2[74,90-93]. Some of them work with extremely high doses[74] or denaturing agents[92] although the need for a well-balanced delivery of active protein is widely accepted[40,52,91].

1.4 Research Objective

In clinically used rhBMP-2 kits, the growth factor is simply adsorbed to collagen sponges in high amounts before application. Apart from the danger of disintegration and antibody formation, collagen matrices are known to have a very limited loading and retention capacity for growth factors[28,94,95], being below 80 μg of rhBMP-2 per gram of collagen[96,97]. Numerous studies are also found depicting adverse effects of the potent treatment[98-101], and high doses have been directly attributed to a higher probability of severe adverse effects[102]. Recently, Axelrad and Einhorn reviewed the use of BMPs in orthopaedic surgery. They reported an adverse effect incidence of 23 to 27 %[103]. Consequently, there is a clear medical need for substantial improvement.

In spite of its clinical use, the most desirable release profile as well as the needed dose of rhBMP-2 are still controversial[7,49,52,55,104]. About 2 ng of BMP-2 can be found in one gram of powdered bone[54,55]. In demineralized bone matrix, about 20 to 120 ng of BMP-2 per gram of bone matrix were found[105,106]. The latter system has been described to induce bone formation *in vivo*, so that these low doses were postulated to be sufficient for a successful induction of healing of bone defects.

Although PLGA is regarded as the gold standard in biodegradable polymers[78], it exhibits a main drawback. The autocatalytic degradation of the polymer and a low permeability for degradation products have been demonstrated to acidify the inherent part of polyester-based implants. This causes a drop in the local pH during release, reinitiating inflammation processes. Compared to non-pegylated poly-α-hydroxy acids, pegylated polyesters have been described to decrease acidification within microspheres[107], keeping a better microenvironment for both growth factor and surrounding tissue. PEG itself was reported to stabilize growth factors during microencapsulation[108,109]. Neither encapsulation of rhBMP-2 into PEG-PLGA diblock polymers nor effects of PEG coencapsulation have been investigated for rhBMP-2 so far. Until now, pegylated poly-lactic-co-glycolic acid diblock copolymers have not been used for microsphere production with any formulation. The development of a suitable delivery system has to be accompanied by appropriate and extensive characterization. The colocalization of rhBMP-2 delivery and subsequent bone formation has not been demonstrated yet by means of fluorescence imaging, nor has a monitoring of bone formation by means of optical imaging been accomplished. The novel technique of benchtop magnetic resonance

imaging, operating at low static magnetic field strength of 0.5 T, has not been evaluated to picture the process of calcification and bone formation.

Based on these prerequisites, the aim of this study was to develop a suitable low-dose delivery system for non-glycosylated rhBMP-2. Four consecutive parts were accomplished in this study:

(I) the extraction and purification of the growth factor,

(II) the selection and development of a method to produce a variation of different suitable delivery systems,

(III) a thorough *in vitro* investigation of the developed formulations and a selection of promising candidates,

(IV) *in vivo* evaluation of the selected candidates by means of non-invasive imaging techniques such as optical imaging (OI), benchtop-magnetic resonance imaging (BT-MRI), computer tomography (CT) and as well as the histological proof of the outcome.

2 Experimental

All chemicals were obtained from Sigma, Taufkirchen, Germany, and at least of reagent grade unless otherwise stated. The polymers RGPd 5055, RGPd 50105 and RG 503 were purchased from Boehringer, Ingelheim, Germany.

2.1 Expression, Extraction and Purification of rhBMP-2

Escherichia coli BL 21(DE3) cells were transformed for overexpression of rhBMP-2 genes by the recombinant therapeutic protein group, Institute of Biochemistry and Biotechnology, Martin-Luther-University Halle[110]. This host strain has been used for the production of inclusion bodies of rhBMP-2 earlier[111].

2.1.1 Isolation of Inclusion Bodies

Deep frozen BL 21 cells with inclusion bodies (IB) were kindly provided by Prof. Dr. Elisabeth Schwarz. The isolation and solubilization of inclusion bodies was accomplished according to a protocol of Rudolph et al.[112]

A schematic overview of the process is given in Fig. 2.1-1. The composition of the used buffers is provided in appendix 6.2. In the first step, the thawing cell agglomerate was resuspended in *IB Isolation Buffer I* (step a). Then, 1.5 mg of lysozyme per gram of cells were added for the decomposition of the cell wall, followed by an incubation period of 30 minutes at 4 °C. In step (b), the cells were disrupted by high pressure dispersion generated in a MicronLab 40-Gaulin homogenizer. Three to four passages with 80 to 120 MPa pressure were conducted. Nucleic acids were degraded by Benzonase/ $MgCl_2$ for 30 minutes. Cell wall associated proteins were dissolved by addition of half the volume of *IB Isolation Buffer II*, which contains 6 % (w/v) of Triton X-100. Soluble proteins and impurities were excluded by centrifugation ((c); 20'000 rpm; 10 minutes). The precipitate ('pellet') was resuspended in *IB Isolation Buffer III* and step (c) was repeated five more times.

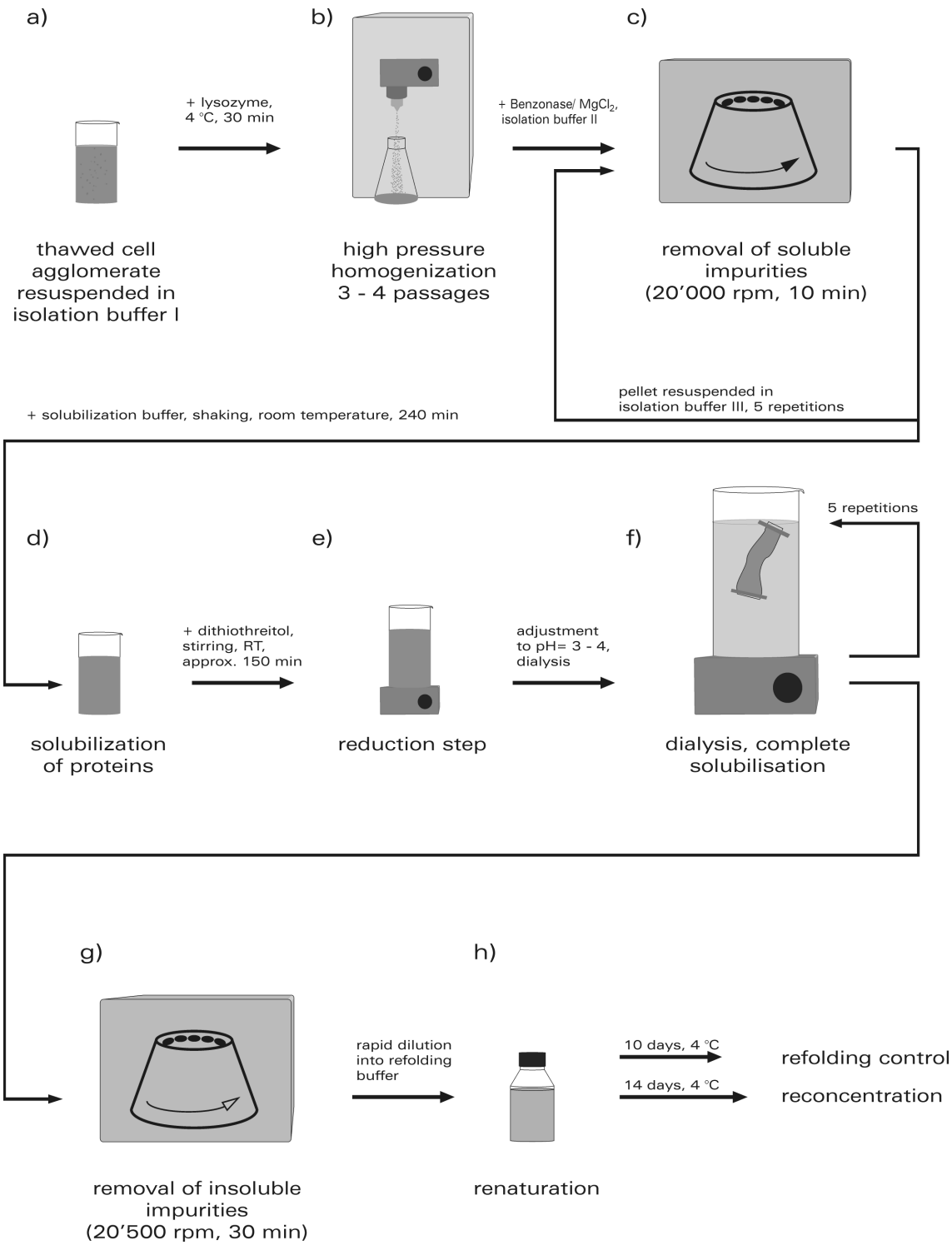

Fig. 2.1-1: Schematic depiction of the isolation, solubilization and renaturation of rhBMP-2.

2.1.2 Solubilization of Unfolded rhBMP-2

The pellet was dissolved in 5 ml of *Solubilization Buffer* per gram of inclusion bodies (step d). After four hours of shaking, 200 mM of dithiothreitol (DTT) were added (e). The solution was stirred for two to three hours at room temperature. The pH of the solution was decreased to pH 3-4 by dropwise addition of acetic acid and dialysed at least five times against its tenfold volume of DTT removal buffer (f). Insoluble remnants were removed by centrifugation ((g); 20'500 rpm; 30 minutes).

2.1.3 Renaturation

The supernatant obtained in the previous step contained unfolded monomeric rhBMP-2 and impurities such as DNA parts. The concentration of protein was estimated by UV spectroscopy and corrected for those impurities. For the refolding process, a volume equivalent to 100 mg of rhBMP-2 was diluted rapidly into 1 l of *Renaturation Buffer* (Figure 2.1-2, (h)). The *Renaturation Buffer* was completed with the redox system after filtering and degassing. In one batch, the redox system published by Vallejo and Rinas[113] was used instead of the standard *Renaturation Buffer*. Any other step was conducted according to the standard protocol. The renaturation step was always carried out at 4 °C.

2.1.4 Control of Refolding

Dimerization as a marker of formation of the native state was controlled by means of SDS-PAGE. After ten days, a sample was taken and dialysed against *Arginine Removal Buffer* (i). Two samples of 1000 µl were withdrawn from the dialysis and investigated. For reconcentration, 100 µl of 0,1 % sodium deoxycholate was added to each reaction tube. RhBMP-2 was subsequently precipitated by the addition of 200 µl trichloroacetic acid. After centrifugation, the precipitates ('pellets') were washed with acetone, dried and resuspended in either reducing or non-reducing *buffer for SDS-PAGE* (j). The samples were loaded onto precast polyacrylamide gels (composition see appendix 6.2) and subjected to a separation distance of 6 cm at a voltage of 175 V. After the separation, the gels were stained with Coomassie brilliant blue. Unspecifically attached dye was washed away with destaining solution.

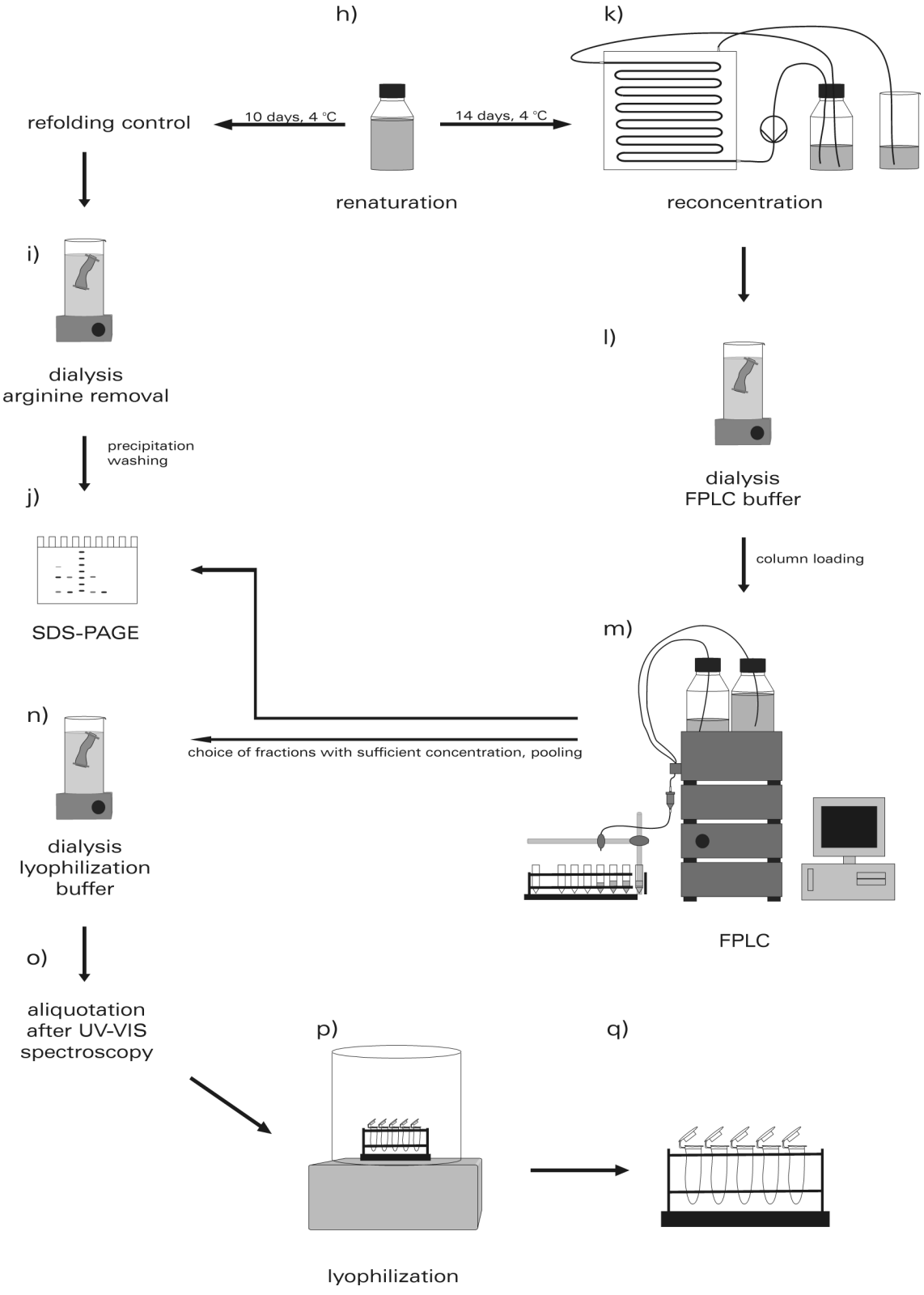

Fig. 2.1-2: Schematic depiction of the renaturation and purification steps of rhBMP-2.

2.1.5 Purification

14 days later, the batch was reconcentrated to 20 – 25 % of its original volume and subsequently dialysed against the tenfold volume of *Purification Buffer I* (steps k; l). The heparin binding segment of rhBMP-2[114] served as affinity link during FPLC purification (step m; Äkta FPLC, Amersham Pharmacia Biotech). RhBMP-2 and monomers as well as oligomers and other polycationic residues interact with the heparin sepharose column[113]. The gradient, with increasing salt concentration due to higher amounts of *Purification Buffer II* led to subsequent elution of these components.

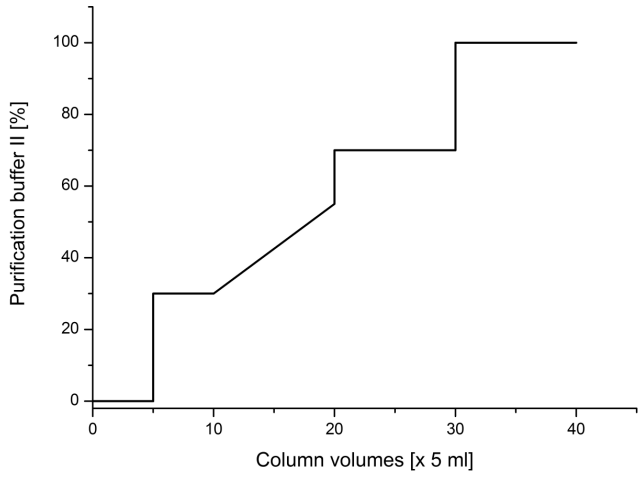

Fig. 2.1-3: Schematic representation of the buffer gradient applied in FPLC purification.

Fractions of the eluate were collected and subjected to SDS-PAGE (j). Fractions with pure rhBMP-2 dimers were pooled, dialyzed against *Lyophilization Buffer* (n), assessed for concentration by means of UV spectroscopy and aliquoted into Eppendorf tubes (o). These were covered with cannula-perforated caps and freeze-dried (p). In the reconstitution phase, the rhBMP-2 condition was checked on a routine basis for the typical features of a UV spectrum and concentrations of the reconstitutes were determined for each batch by means of ELISA. Unless stated otherwise, solutions with 12 µg/ml of rhBMP-2 were used for all *in vitro* investigations.

2.2 Modification of rhBMP-2

2.2.1 Carboxyfluorescein Labelling

Carboxyfluorescein-N-hydroxysuccinimide was purchased in activated form. It was dissolved in dimethyl sulphoxide (125 mg/ml) and diluted with phosphate buffer, pH 6.0, to a final concentration of 1,25 mg/ml. 30 µl of the diluted, activated dye solution were added to 1 ml of rhBMP-2 solution. The mixture was shaken at a temperature of 37 °C for 2.5 hours and then dialysed six times against sodium acetate (20 mM, pH 4.5). All fluorescing solutions were protected from light.

2.2.2 Rhodamine Labelling

For the rhodamine labelling, the fluorescence label had to be activated prior to coupling. 80 mg of rhodamine B were dissolved in 2 ml of dimethyl sulphoxide. 25 mg of N,N'-dicyclohexylcarbodiimide and 25 mg of N-hydroxysuccinimide (NHS) were added to the reaction vessel. The mixture was protected from light and moisture and stirred for two days with a magnetic bar at room temperature. After filtration, the solution was diluted 24fold with sodium acetate buffer (20 mM, pH 5.5). 20 µl of the diluted activated dye solution were added to 500 µl of a chilled rhBMP-2 solution. A rhBMP-2/activated rhodamine B ratio of 1:1.85 was chosen. The mixture was shaken for 3 hours at 37 °C and subsequently dialysed four times against 500 ml of *Ac Buffer* (sodium acetate, 20 mM, pH 4.5).

SDS-PAGE was used for labelling control. 10 µl of the sample were mixed with 10 µl of *SDS buffer*, prepared without bromophenol blue. After finishing the run, the gel was subjected to fluorescence imaging (CRI Maestro, CRI Inc. Woburn, US). Pictures of the gel were generated using the green filterset. Acquisition time was set automatically. The image was compared with the result of subsequent conventional staining.

The labelling efficiency was determined with fluorescence spectroscopy (Perkin Elmer MPF 44). The slit widths were set to 6 nm. Excitation and emission were recorded at λ_{ex}=555 nm and λ_{em}=578 nm, respectively. One data point per second was recorded. A calibration curve was generated with concentrations from 500 pmol/l to 500 nmol/l. The data points were corrected with the arithmetic mean of the respective background scans. All measurements were carried out threefold and the mean of all 216 data points was used as the sample value. All fluorescence experiments were carried out under light protection.

2.3 Stability of rhBMP-2

2.3.1 Aggregates

Due to the high tendency of rhBMP-2 to form aggregates[80,114-116], an estimation of aggregation probability and aggregate sizes was undertaken. Various techniques were employed for the exclusion of artifacts and an appropriate overview of the samples. Resulting from different preparation procedures, possible sample alterations and so emerging bias were expected to be easier detectable.

2.3.1.1 MALDI-TOF-MS

The experiments were carried out with a delayed extraction time-of-flight (TOF) mass spectrometer (Voyager DE PRO, Applied Biosystems, Weiterstadt, Germany). Different batches of rhBMP-2 dissolved in *Ac* or *AcPEG Buffer* were used in the process. At the time of investigation, they had either been stored at 4 °C for six months or were freshly reconstituted. The samples were embedded either 5:1 or 10:1 (v/v) into sinapinic acid in acetonitrile/ 0.1 % trichloroacetic acid (1:1, w/v). The samples were vortexed for 30 seconds, centrifuged down to the bottom of the tube again (60 s, 13'000 rpm) and spotted in quantities of 1 µl onto a steel matrix. The presence of PEG in the matrix of *AcPEG* samples prevented crystallization of the sinapinic acid. As a result, these samples had to be excluded from evaluation.

An accelerating voltage of 25 kV was applied, the grid voltage was set to 90 % and a delay time of 200 ns was chosen.

2.3.1.2 Asymmetric Flow Field Flow Fractionation

In contrast to the MALDI experiments, Asymmetric Flow Field Flow Fractionation (AF4) is more capable of detecting high molecular weight fractions of molecules[117].

The basic principle of the method is a separation according to diffusion ability. Two main flows are applied to the sample in the flow chamber:

(I) a linear flow from the injection point towards the two detectors

and (II) a transversal flow, termed crossflow, towards a membrane (molecular weight cut off 5 kDa).

This membrane, situated at the bottom of the crossflow channel, prevents the molecules from vanishing. In principle, fractions appear in the order of increasing molecular weight, because the diffusion velocity of smaller molecules from the membrane is higher, shortening the time for their reappearance in the main flow area and hence a faster transport of the analyte fraction through the channel.

An Eclipse F instrument (Wyatt, Santa Barbara, USA), connected to a multi angle light scattering detector (Dawn EOS) and a refractive index detector (Shodex RI-101) in combination was used. In the channel, a spacer height of 350 µm and a regenerated cellulose membrane (cut off 5 kDa; Microdyn Nadir GmbH, Wiesbaden, Germany) were applied.

The detector flow was set to 1.0 ml/min and the *Ac Buffer* was used for elution. The method utilized in running the system was optimized during the first runs. The final parameters are indicated in figure 2.3-1. Astra software (Version 4.90.08; Wyatt) was applied for result evaluation. The processing towards molecular weight data was accomplished according to the Debye equation (dn/dc = 0.185).

Different batches of rhBMP-2, dissolved in *Ac* or *AcPEG Buffer*, were used for the experiment. A sample of rhBMP-2 in phosphate buffer, pH 6.0, was also included, because it was suspected to have a higher aggregation tendency based on recovery data from previous ELISA experiments and information from the literature on its solubility profile[80,114].

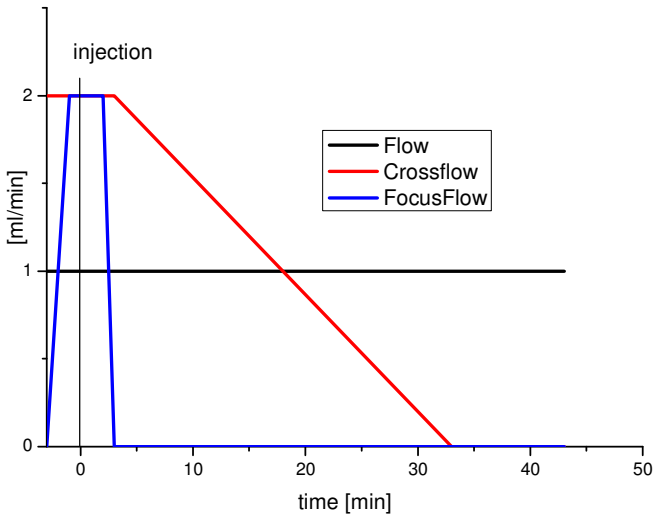

Fig. 2.3-1: Asymmetric flow field flow fractionation: schematic depiction of the applied flow scheme during sample analysis.

2.3.1.3 Photon Correlation Spectroscopy (PCS)

Dynamic light scattering methods are frequently used in the determination of hydrodynamic diameters. Translational, rotational and vibrational motions of particles lead to light intensity fluctuation over time. The time dependency of light scattering intensity is measured and correlated with the Brownian motion of the molecules. Based on the precondition of small, independently moving particles, the obtained diffusion coefficient D may be used to calculate the hydrodynamic diameter from the Stokes-Einstein relation, where r_h denotes the hydrodynamic radius of the particle, and k_b is the Boltzmann constant. The influence of sample temperature (T) and dispersant viscosity (η) on the outcome is also reflected in equation 2.3-1.

$$r_h = \frac{k_b T}{6\pi\eta D} \qquad (2.3\text{-}1)$$

For PCS measurements, one sample of each batch was freshly reconstituted in sterile-filtered *Ac Buffer*. Ten runs with a measurement time of 20 seconds each were executed with a HPPS instrument (Malvern). The measurement was done at least in triplicate for each sample.

Measurements were repeated one week after reconstitution. A refractive index of 1.45 for the protein and a buffer viscosity and refractive index equivalent to water were assumed for result calculation (Dispersion Technology Software, v. 4.20, Malvern).

2.3.1.4 Nanoparticle Tracking Analysis

Nanoparticle tracking analysis (NTA) is a novel technique whose measuring principles are quite similar to PCS. In ideal samples, corresponding results to PCS can be obtained[118]. A laser beam (40 mW at 640 nm, width of approximately 50 µm) is sent through a glass slide into the sample chamber. Here, the laser beam can be scattered by particles in the analyte solution. The diffused light caused by these particles is visualized in a microscope and imaged by means of a CCD camera. 30 images per second were acquired on a field of view of 100 µm x 80 µm. Imaging software is used to track those bright areas, but not the particles themselves. The Brownian motion of those bright areas corresponds to the hydrodynamic size of the particles, which can be calculated once again according to the Stokes-Einstein equation (eq. 2.3-1). For this reason, the software calculates the three-dimensional

Brownian motion from the time-dependent, two-dimensional bright spots. According to the manufacturer, the system is able to detect light scattered by protein aggregates as small as 30 nm[119]. The advantage of the system over PCS is the tracking of single particles, so that multimodal distributions, as expectable in protein aggregation, can be detected more easily. One of the drawbacks, however, is a bias towards larger sizes[120]. The scattering intensity, which is proportional to the sixth power of the particle diameter in rayleigh scatterers, causes masking of weak scatterers by strongly scattering large particles. For the measurements, a LM20 device was used (Nanosight Ltd, Amesbury, United Kingdom). Two samples of 07-II BMP-2 (for details, see table 3.1-1), a freshly reconstituted one and another one in solution for six weeks, were diluted with *Ac Buffer* to a concentration of around $5 \cdot 10^8$ detectable scattering centres per ml. 500 µl were introduced into the sample chamber. The scattered light in the sample chamber was imaged continuously over a period of 40 seconds. Data were evaluated by means of NTA software (Nanosight Ltd.). For comparison, blank *Ac Buffer* was also analyzed.

2.3.1.5 UV Spectroscopy

Samples were taken for concentration determination and rough estimation of purity during rhBMP-2 purification. 12 µl were diluted with the respective buffer (*Ac*, *AcPEG*, or *Phos*, for details see 6.2.3) to a total volume of 120 µl. Spectra were recorded from 240 nm to 340 nm in triplicate, the respective buffer was used as blank. The concentration was calculated according to Lambert-Beer's Law, with an absorption coefficient of 18'200 $mol^{-1}cm^{-1}l$ for rhBMP-2 at 25 °C and 280 nm.

2.3.2 Stability of rhBMP-2 in Release Media

In a preliminary screening, ten different buffer systems based on phosphate buffer were tested for rhBMP-2 recovery. The detectable concentration was assessed either immediately after dilution of rhBMP-2 into these systems or after 9 days. The influence of salt concentration was also examined. Either phosphate buffered saline, pH 7.4, according to the European Pharmacopeia[121] (PBS R), or phosphate buffer of the same composition, prepared without sodium chloride (PB), was used. An overview of the tested buffers is provided in table 2.3-1.

Table 2.3-1: Buffer systems investigated for rhBMP-2 stability. Percentages represent mass per volume.

Phosphate Buffer (PB)	Phosphate Buffered Saline (PBS R)
PB	PBS R
PB + polysorbate 20, 0.05 %	PBS R + polysorbate 20, 0.05 %
PB + polysorbate 80, 0.1 %	PBS R + polysorbate 80, 0.1 %
PB + Solutol HS 15, 0.1 %	PBS R + Solutol HS 15, 0.1 %
PB + arginine, 0.8 M	PBS R + arginine, 0.8 M

Each sample was prepared from the same batch of rhBMP-2. 10 µl of freshly reconstituted rhBMP-2 in *Ac Buffer* were diluted 1:100 with the respective buffer-to-investigate. All samples were prepared in duplicate and investigated by means of ELISA (Quantikine, R&D Systems, Wiesbaden). Both human and murine BMP-2 give signals with the ELISA; the cross-reactivity with rhBMP-4 at a concentration of 50 ng/ml is reported to be 1.2 %[122]. RhBMP-4 is reported to be 92 % identical with rhBMP-2, and amino acids are exchanged with those of the same character (e.g. Glu to Asp)[39]. With rhBMP-5, rhBMP-6, and rhBMP-7, no cross-reactivity was reported, which can be explained by the lower structure homology with rhBMP-2 compared to rhBMP-4. The immunoassay kit is based on the sandwich technique. The well bottoms of a 96 well plate are precoated with a monoclonal antibody specific for BMP-2. In the first step, BMP-2 from the sample was allowed to attach to the murine antibody on the bottom of the well. After unbound substances had been removed by a fourfold washing step, another horseradish peroxidase-linked antibody specific for rhBMP-2 was allowed to attach to a second binding site of the protein. Excess antibodies were washed away in another four-step cleaning procedure. Subsequently, a mixture of 3,3',5,5'-tetramethylbenzidine and hydrogen peroxide was added. Depending on the concentration of rhBMP-2, different amounts of dye were produced. After addition of sulphuric acid, a sample readout at 450 nm was performed. A standard was provided with the kit and used for the generation of the calibration curve. Subsequently, a square function was fitted through all data points and used for result calculation.

After the decision on a release buffer system, the stability of rhBMP-2 in this system was to be elucidated more thoroughly. Dependency on time and concentration were investigated. Four different BMP-2 standard samples were subjected to the release conditions in absence of microspheres. From each sample, four different concentrations, i.e., 5000, 500, 50, 5 ng/ml, were prepared. The samples were exposed to

shaking stress and elevated temperature. The experimental parameters, sampling, storage and analysis are described in detail in the section 'Release Determination' (chapter 2.6.2). Constants were calculated for the decrease of BMP-2 concentration by time in the standard samples.

2.3.3 Freeze-thaw Recovery of rhBMP-2 and the Influence of Microsphere Degradation Products on rhBMP-2 Stability

During the release process *in vitro*, rhBMP-2 is exposed to several factors that may possibly influence the stability of the growth factor. Two of these are the process of freezing and thawing and the close contact with degradation products of the microspheres. In order to investigate the impact of these factors, one *in vitro* release was simulated by the use of plain microspheres. Thus, the microspheres degraded by time and reconstituted growth factor was subjected to conditions equivalent to the *in vitro* release process without the bias of its own instability in the release medium. Plain PEP 0, PEP 5 and PEP 10 microspheres were produced as described in chapter 2.4.

For each sample, 50 mg of microspheres were dispersed in 1000 µl of release medium in polypropylene vessels and tightly capped with PTFE caps. The samples were prepared in duplicate and placed on an orbital shaker with the temperature set to 37 °C. At predefined times, the samples were centrifuged (4000 rpm, 5 min). 200 µl of the supernatant were withdrawn and divided into two parts (Fig. 2.3-2): 100 µl were frozen to -20 °C and another 100 µl were stored at 4 °C. The withdrawn volume was replaced by fresh medium.

To check the influence of microsphere degradation products on rhBMP-2 stability, 10 µl of freshly reconstituted rhBMP-2 solution were added to 70 µl of each sample one week before the ELISA and the storage was carried on the same way as indicated before. As a result, the influence of microsphere degradation products on rhBMP-2 could be measured without being biased by rhBMP-2 residence time. The concentration of remaining rhBMP-2 was determined by using the ELISA kit according to the manufacturer's instructions. Details are given in chapter 2.3.2.

Residual aliquots of approximately 30 µl were kept for pH profiling (chapter 2.6.1).

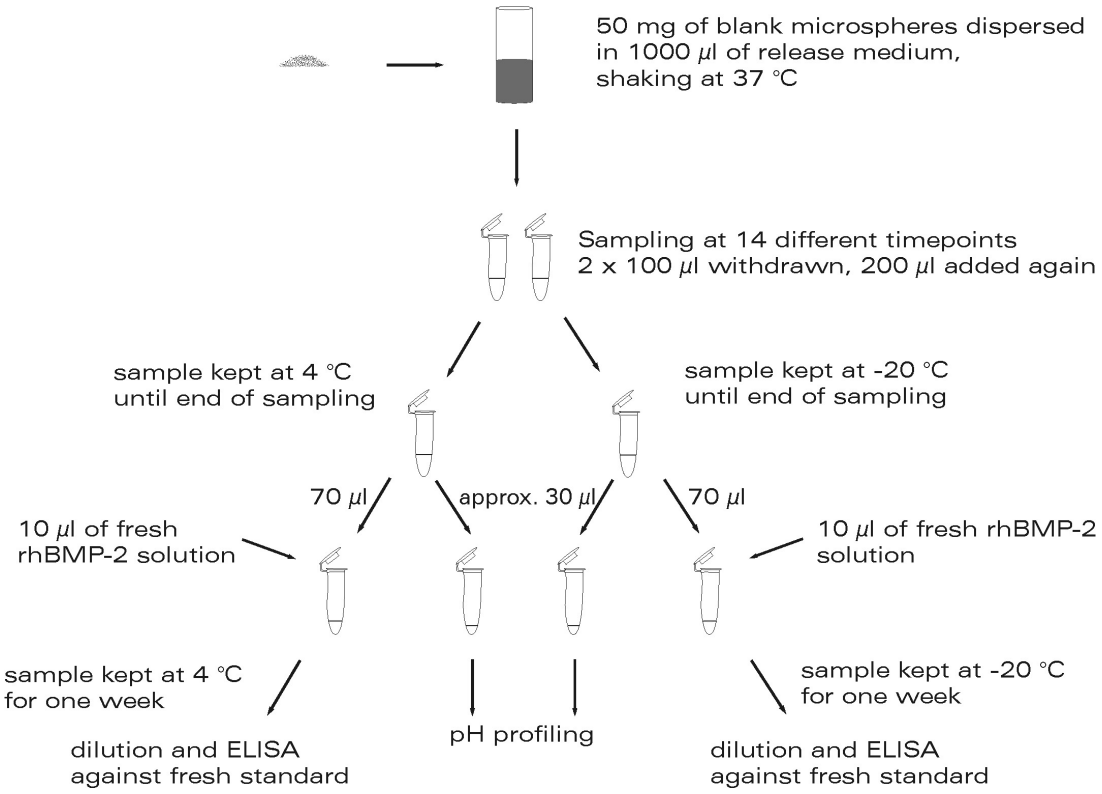

Fig. 2.3-2: Sampling regimen for freeze-thaw recovery, influence of microsphere degradation products on rhBMP-2 stability and for pH profiling.

2.4 Production of Microspheres

Polymers for microsphere production were obtained from Boehringer Ingelheim. An overview of their characteristics is given in table 2.4-1.

Table 2.4-1: Brand name, abbreviation and main characteristics of the polymers used for microsphere production.

Brand name	Abbrev.	Composition	Mw in kDa
Resomer RG 503	PEP 0	Poly(D,L)lactic-co-glycolic acid, Lactic/glycolic acid ratio 1:1	40.6 kDa[122] 31.3 kDa[123]
Resomer RGP d 5055	PEP 5	Poly(D,L)lactic-co-glycolic acid + PEG 5000 block, Lactic/glycolic acid ratio 1:1	95 kDa PLGA + 5 kDa PEG
Resomer RGP d 50105	PEP 10	Poly(D,L)lactic-co-glycolic acid + PEG 5000 block, Lactic/glycolic acid ratio 1:1	45 kDa PLGA + 5 kDa PEG

Microspheres of two PEG-PLGA diblock-copolymers (PEP 5, PEP 10) and one PLGA copolymer (PEP 0) were fabricated by a modified double emulsion-solvent evaporation technique[125] (Fig. 2.4-1). An end-capped PLGA was used because a higher inner porosity and low external porosity, as well as a lower degradation rate were expected[126].

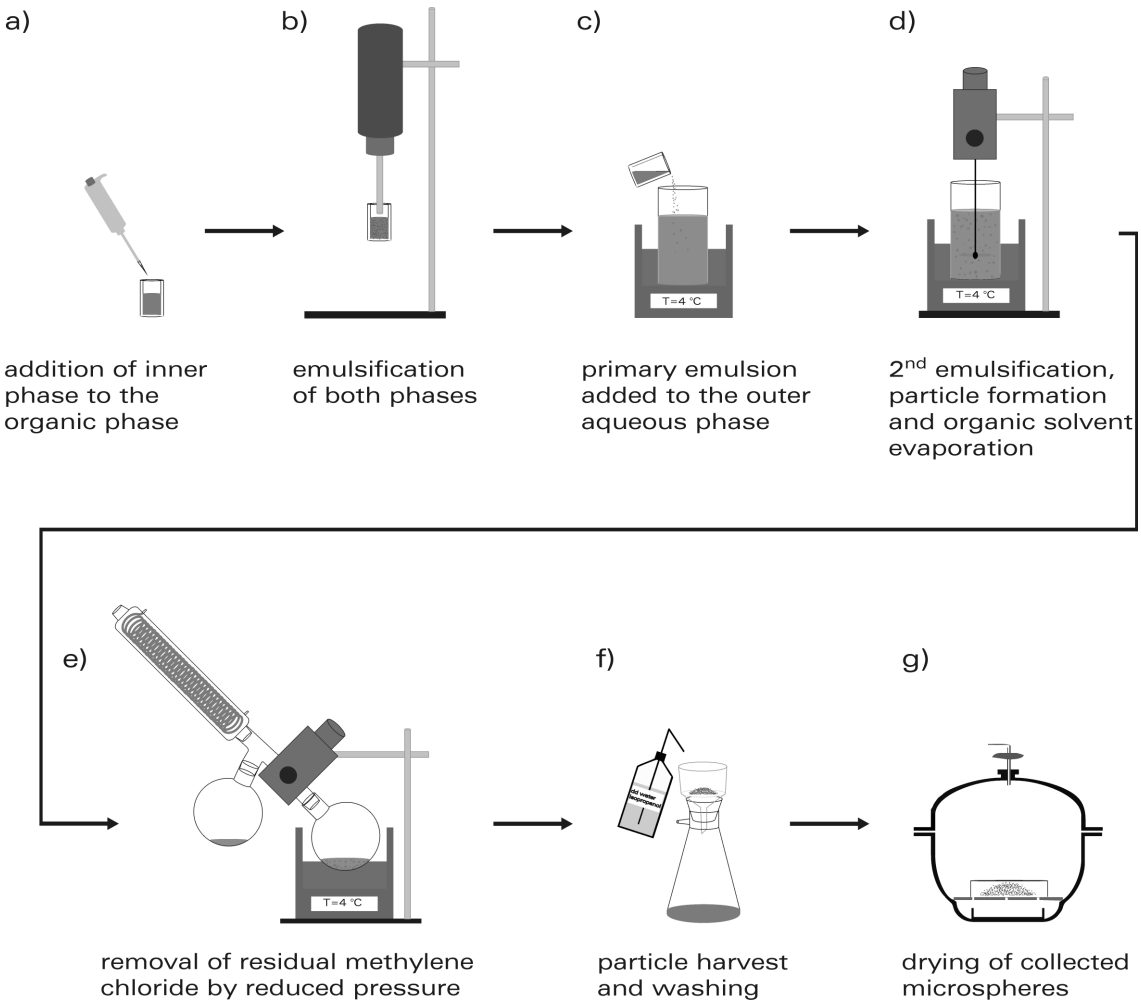

Fig. 2.4-1: Schematic depiction of the microsphere preparation process.

At first, 150 µl of rhBMP-2 (12 ± 1.5 µg/ml) in an aqueous buffer (*Ac*, *AcPEG*, or *Phos*) were homogenized with 4.0 ml of methylene chloride containing 10 % (w/v) polymer in a polytetrafluoroethylene (PTFE) beaker (step a). A pH of 4.5 (5.0 for *Phos Buffer*, respectively) was chosen because of the optimal stability of rhBMP-2[80,127] and the *in vitro* degradation rate of polyesters, which was reported to be the slowest around this pH[128]. In the beginning, the use of 300 µl inner phase and the substitution of methylene chloride was also evaluated, but found to

be inferior. A W/O-emulsion was formed by homogenization (b) for two minutes at 10'000 rpm (Ultra turrax T 18, IKA, Staufen, Germany). The emulsion was then immediately dropped into 65 ml of ice-cooled 2 % (w/v) aqueous polyvinyl alcohol (88 % hydrolyzed, 31-50 kDa) (step c). Katou et al. reported a solvent evaporation time of 40 minutes to be sufficient for the achievement of a non-aggregating microparticle slurry[129]. In this study, the solvent evaporation and hardening of the nascent particles was performed by stirring with a two-blade paddle mixer for one hour. Subsequently, residual methylene chloride was removed at a reduced pressure of 200 mbar for at least one hour (e). Due to the low glass transition temperatures of the pegylated polymers ($T_{G\ PEP\ 10}$= 29.8 °C; $T_{G\ PEP\ 5}$= 34.8 °C), the latter steps of production were conducted on ice. Finally, the microparticles were collected (f), washed three times with a mixture of isopropyl alcohol and purified water and dried under vacuum (g). After the drying process, the microspheres were collected and weighed. All samples were stored at 4 °C in the absence of light.

2.4.1 Residual Solvents

The amount of residual methylene chloride was determined by gas chromatography (HP 5890 II GC-FID, Hewlett-Packard) based on a method modified from the European Pharmacopeia[121]. 200 mg of blank microspheres were dissolved in 20 ml of N,N-dimethyl formamide. The samples were extracted for 15 minutes at 105 °C using a headspace unit (HSS 86.50, DANI Instruments S.p.A, Italy). 1 ml of the gaseous phase was withdrawn and analyzed using a Varian Factor Four column and flame ionization detection. A calibration curve of standards with concentrations ranging from 100 to 600 ppm was recorded. Nine batches of microspheres, i.e. three of each polymer, were subjected to the analysis.

2.4.2 Thermal Analyses of Polymers and Microspheres

Investigations on glass transition processes were undertaken by means of differential scanning calorimetry (DSC 200, Netzsch, Selb, Germany). Possible alterations due to the microsphere preparation procedure were studied by comparing the microspheres with the respective unprocessed polymers. Samples, either dry or pre-wet (polymer/water ratio 1:3), weighing between 10 and 15 mg, were put into an aluminium pan, tightly closed and cooled to 0 °C. After an equilibration

period, they were heated with a rate of 10 K/min to 80 °C. Subsequently, the samples were again cooled down to 0 °C and, using the same parameters, a second heating curve was recorded. This second measurement was analyzed for glass transition processes.

Thermogravimetric investigations were carried out on a TG 209 instrument (Netzsch, Selb, Germany) to obtain information on the content of water and other vaporable substances in the preparations. Between 20 and 30 mg of microspheres were placed into an open aluminium oxide pan and were heated from 20 °C to 150 °C by following a gradient of 10 K/min. The high temperature was maintained for half an hour. In another approach, samples were heated to 600 °C for a total thermal decomposition following the same parameters as described above. The weight loss was recorded online and the final values were determined when the weight of the samples remained constant.

2.5 Characterization of Drug-loaded Microspheres

2.5.1 Size Distribution

2.5.1.1 ESEM + analySIS

Environmental Scanning Electron Microscopy (ESEM; ESEM XL 30 FEG, Philips Electron Optics) was employed in order to investigate the particle surface morphology and to gain information on size distribution. For both purposes, the use of the environmental mode is beneficial, because no coating or sputtering is necessary to obtain a conducting sample. In the applied gas mode, the specimen chamber is not fully evacuated but remains at a low, vacuumized state. During the picture acquisition, the pressure was around 1 mbar to 3 mbar. The gas atoms serve as additive ionizable transmitters towards the secondary electron detector. The surface information is further processed for image creation. Microspheres were fixed on double-sided tape for investigation. Feret's diameter was measured for all particles conspicuously imaged in ESEM overview pictures (analySIS Auto, Olympus). A low magnification was chosen so that more than 100 microspheres per picture could be investigated. Usually, the diameters of around 450 particles were measured.

2.5.1.2 Laser Diffraction

The hydrodynamic diameter of the particles was determined by laser diffraction (LD; Mastersizer, Malvern). 50 mg of microspheres were dispersed in 25 ml of 0.05 % (w/v) polysorbate 20 solution and stirred for two hours. Afterwards, 5 ml of the dispersion were injected into the sample chamber and measured in quintuplicate. This step was repeated three times. Laser diffraction results were evaluated by Mastersizer 2000 software (v. 5.22, Malvern). They are dependent on the optical properties of the sample. Refractive indices for PLGA microspheres are found from 1.44 up to 1.51-1.67[130-132], typical absorption values range from 0.00 up to 0.01. For this study, measurements were made under the assumption of a refractive index of 1.50 and an absorption of 0.001. The result evaluation was performed according to Mie theory[133], because the Fraunhofer approximation tends to overestimate the number of small particles, especially in low absorbing samples[134]. The corresponding guidelines were adapted recently[135]. For comparison with microscopical data, a conversion into number weighted data was performed[136].

2.5.2 Surface Morphology

2.5.2.1 Light Microscopy

The particles were dispersed in water, put on microscope slides and investigated with a light microscope (Axiolab re, Zeiss, Jena). Microspheres were dispersed in release buffer and studied again 28 days later. Pictures were taken with a mounted digital camera (Power Shot G5, Canon, Krefeld, Germany).

2.5.2.2 Environmental Scanning Electron Microscopy

By means of ESEM, surface characterization was performed according to the sample preparation protocol reported in chapter 2.5.1. For investigations of the surface, higher magnifications than in the overview mode were used.

2.5.3 Drug Distribution

The distribution of the labelled protein within the microspheres was examined by confocal laser scanning microscopy (CLSM; LSM 510 Duoscan, Zeiss). Rhodamine B-labelled rhBMP-2-containing micro-

spheres of PEP 0, 5 and 10 were investigated. In one group, the labelled protein was dissolved in sodium acetate buffer (*Ac*). In another group, the inner phase of the microspheres consisted of one third of PEG 300 and of two thirds of sodium acetate buffer (*AcPEG*). The use of low molecular weight PEG has been reported to stabilize proteins during encapsulation in various approaches[108,137,138]. The pH was readjusted to the same conditions as above. Each of the six variations was manufactured twice and examined by means of CLSM.

Samples were dispersed in Prolong Gold mounting medium (Invitrogen). The rhodamine-labelled rhBMP-2 was excited at a wavelength of 543 nm and emission was filtered by a longpass filter at 560 nm. The pinhole was 1.35 airy units, corresponding to an optical slice thickness of less than 1.3 μm. For the samples, the detection gain ranged between 640 and 830. Negative controls were examined with a gain of 920 to 1080 for the detection of particles and with the same gain as the respective sample. Pictures were taken using Axiovision LE software (Zeiss, Jena, Germany).

2.5.4 Encapsulation Efficiency

Data were acquired by fluorescence spectroscopy, using the same method as for the labelling efficiency measurements (Chapter 2.2.2). Both the outer phase of the w/o/w-emulsion and the washing water were assessed for fluorescence intensity. Therefore, the outer phase was gathered along with the rinsing PVA solution and adjusted to a total volume of 100 ml. The microspheres were washed on an analytic filter (No. 410, VWR). The washing water was collected and evaporated, the residue was reconstituted in 10 ml of 2 % (w/v) aqueous polyvinyl alcohol and subjected to the same analytic method. The addition of both values was regarded as loss during fabrication and subtracted from the total amount to yield encapsulation efficiency.

2.6 In Vitro Release Studies

2.6.1 *In Vitro* Degradation of the Microspheres

In order to compare the results of *in vitro* degradation with *in vitro* release profiles, the studies were conducted under comparable conditions e.g. regarding buffer, temperature and sample volume.

2.6.1.1 pH Profiling

The investigations on the pH profile of the release medium during release were accomplished along with the freeze and thaw stability testing. An overview of the sampling regime is provided in figure 2.3-2 of the respective chapter. Approximately 30 µl were used for pH profiling. 10 µl of the sample were carefully pipetted onto an appropriate pH test strip according to the expected pH value (pH-Fix 6.0-7.7, 5.1-7.2, 3.6-6.1, 1.7-3.8; Macherey-Nagel). For verification of the colours of the pH strips, phosphate buffers or solutions, 20mM (chapter 6.2.4), were prepared at pH 7.3, 7.2, 7.0, 6.9, 6.7, 6.6, 6.4, 6.3, 6.1, 6.0, 5.7, 5.6, 5.4, 5.3, 5.1, 5.0, 4.7, 4.1, 3.8, 3.6, 3.5, 3.2, 2.9, 2.3, 2.0, 1.9, and 1.7. All buffers were measured with a freshly calibrated glass electrode. The pH values below 3.6 were adjusted with concentrated hydrochloric acid.

All samples were measured in duplicate. If there was any difference between both values, a third measurement was performed, preferably with another type of pH strip that was able to detect values between the steps (usually 0.2-0.3 units) of the paper used before.

2.6.1.2 ^{1}H-Nuclear Magnetic Resonance Experiments

PEP 0, PEP 5 and PEP 10 microspheres were prepared without rhBMP-2, containing blank *Ac Buffer*. 50 mg of microspheres were dispersed in 1000 µl of medium and shaken for a time period of 10 weeks at 37 °C. The medium consisted of PBS 7,4 R according to the European Pharmacopeia. Samples were prepared with deuterium oxide instead of purified water. It was not necessary to readjust the pH value. At predefined times, the samples were centrifuged (4000 rpm, 10 min). 200 µl of the medium were removed from the sample vial and replaced with 200 µl of fresh buffer. 500 µl of deuterium oxide were added to the withdrawn volume, the sample was vortexed and subjected to ^{1}H-NMR investigations (500 MHz; Unity Inova 500, Varian). Selected samples were spiked with polyester degradation products, i.e. glycolic and lactic acid. The resulting spectra were compared with unspiked spectra to determine peaks accounting for degradation products.

2.6.2 Release Determination

Twelve batches of microspheres were prepared as described in chapter 2.4, four of each polymer, PEP 0, PEP 5 and PEP 10. Half of the batches, two of each polymer, contained 33 % (v/v) of PEG 300 in the inner

phase. PBS pH 7.4 R, according to Ph. Eur. 6[121], was used as a release medium. Additives included polysorbate 20, 0.05 % (w/v); bovine serum albumin, 1 % (w/v); disodium EDTA, 0.15 % (w/v) and sodium azide 0.02 % (w/v).

50 mg of microspheres were dispersed in 1000 µl of release medium in polypropylene vessels and tightly capped with PTFE caps. The samples were placed on an orbital shaker with the temperature set to 37 °C. At predefined times, the samples were centrifuged in their release vessels (4000 rpm, 5 min). 200 µl of the supernatant were withdrawn and frozen to -20 °C for further analysis. 200 µl of fresh release medium were added again to the samples. The centrifuged microspheres were redispersed immediately when put back on the shaker. All frozen samples were thawed and subjected to concentration determination by sandwich ELISA in duplicate. The principle of the assay and its workflow is given in detail in chapter 2.3.2.

2.6.3 *In Vitro* Activity of Released rhBMP-2

2.6.3.1 Alkaline Phosphatase Assay

The induction of alkaline phosphatase (ALP) in C2C12 mouse myoblasts (DSMZ, Braunschweig, Germany) was investigated according to a modified version of a protocol reported by Hauburger et al.[139] Microspheres made from all three polymers, PEP 0, PEP 5 and PEP 10, were investigated. $4 \cdot 10^3$ fourth passage cells were seeded in each well of a 96 well plate and maintained at 37 °C and 5 % CO_2. After an incubation period of one day, the cell *culture medium* was removed. 40 mg of rhBMP-2-loaded microspheres were added to the wells and covered with *differentiation medium*. Negative controls included blank medium, cells in blank medium and empty microspheres of all three kinds. As positive control, a rhBMP-2 standard solution was used. Samples were adjusted to the same volume. After three days, the medium was removed. The wells were washed with 200 µl of PBS. Subsequently, 100 µl of *ALP buffer* containing 1 µg of Nonidet P-40 were added to the wells to induce cell lysis. After shaking for two hours, 20 µl were taken from each well and subjected to the bicinchoninic acid assay (BCA; Pierce, Rockford, US) according to the manufacturer's instructions. Further 20 µl were mixed with 200 µl of ALP buffer containing 670 µg of p-nitrophenyl phosphate. The ALP activity was measured at a wavelength of λ= 405 nm, both as kinetic determination and endpoint determination. The results were normalized for the protein content of each well, as determined by the BCA assay.

2.6.3.2 Alkaline Phosphatase Assay with Transwell Plates

Adherently growing C2C12 cells were impaired in proliferation by the presence of microspheres on the well bottom. Hence, transwell plates were applied to leave the whole bottom area for cell growth. Transwell plates are inserts for well plates usually used for cell migration assays.

50 mg of microspheres were added to each well of a transwell plate with a pore size of 5 μm (Corning Inc., Corning, United states). The transwell plate was introduced into a 96 well plate which had been seeded with $4 \cdot 10^3$ fifth passage cells one day before. RhBMP-2 was released and diffused through the transwell membrane into the wells with cells at the bottom. Subsequent analysis was accomplished as described above.

2.7 Microspheres in Scaffolds

Scaffolds are widely used in Tissue Engineering. In most cases, they are combined with cells or growth factors. Scaffolds intended for Bone Tissue Engineering purposes were prepared by Hagen Nitzsche, as published elsewhere[71,140]. Briefly, a composite material of equine collagen and nanoscaled hydroxylapatite was prefabricated according to methods of Itoh and Hu[141,142]. The composite was immersed into a dispersion of chitosan and collagen in water. During this step, PEP 0 microspheres were also dispersed in the system, followed by vigorous shaking. The suspension was filled into moulds and quick-frozen in liquid nitrogen. Afterwards, the frozen suspension was lyophilized. The obtained scaffold was examined by means of ESEM. Therefore, parameters were equivalent to those reported in chapter 2.5.2.2.

2.8 Microspheres in Gel

The tailored fabrication and implantation of scaffolds is a challenging process. In order to keep the delivery system as simple as possible, and to potentially circumvent the necessity of an implantation procedure, the combination of microspheres with viscous injectables was investigated. Microspheres were either dispersed

(I) in the sol of an *in situ*-forming implant based on chitosan and β-glycerophosphate that would turn into a rigid gel *in vivo.*

or (II) in an injectable gel based on hydrophobically modified hyaluronic acid (HHA).

Most *in vivo* experiments were performed with the chitosan system. The outcome of the *in vivo* experiments was used to select the most successful delivery system, regarding the microsphere polymer. For this system, the impact of the microsphere dispersant was tested and both chitosan and HHA were compared *in vivo* (*cf.* chapter 2.9, table 2.9-1).

2.8.1 Chitosan-based *In Situ*-Forming Implants

The *in situ*-forming implants were prepared immediately before application from three different solutions. The formed sol is known to form a stable gel when setting *in situ*. Solution A contained 1.5 % (w/v) of chitosan with a deacetylation degree of 95 % (Chitosan 95/2000/A1, batch 200-200206-01; Heppe Medical Chitosan, Halle, Germany), dissolved in 0.1 M hydrochloric acid. Solution B consisted of β-glycerophosphate (40 %, w/v) in bidistilled water. Solution C was a variable part that was used in some cases for the direct addition of rhBMP-2 to the gel. The protein was added in *Ac Buffer*. In all other cases, solution C consisted solely of bidistilled water. The three components were chilled on ice and the components A and C were mixed. Subsequently, solution B was added to a final component ratio A:B:C of 16:3:1. When microspheres were added, a fixed combination of 415 mg of microspheres in 2 ml of sol was retained. In order to see the growth factor retention of the microspheres and its effect on bone formation, gels without microspheres were produced with an equivalent concentration of rhBMP-2. The system will be abbreviated 'chitosan gel' in the following.

2.8.2 Hydrophobically Modified Hyaluronic Acid Gels

Hyaluronic acid (HA) is a natural polymer that plays an important role in physiological processes like angiogenesis and the regulation of inflammation[143]. Hence, it might be a meaningful support as microsphere dispersant in bone regeneration. Its main drawback is the low rigidity and fast degradation of formed hyaluronic acid gels. In order to circumvent this disadvantage, hydrophobically modified hyaluronic acid was used for the preparation of gels.

Native hyaluronic acid sodium salt, produced by *Streptococcus equi*, was first made soluble in dimethyl sulphoxide by conversion into its tetrabutylammonium salt. After the exchange of cations with protons (Dowex 50WX8-200) and following titration with tetrabutylammonium hydroxide solution (5 % v/v) to a pH of 8, the product was freeze-dried.

The obtained hyaluronic acid salt was linked to hexadecyl amine according to Finelli and coworkers[144], washed and again lyophilized. 40 mg of freeze-dried hydrophobically modified hyaluronic acid (HHA) were weighed into a syringe. Whilst kept in motion by a magnetic stirring bar, 4 ml of isotonic glycerol solution were added. After approximately one hour, the magnetic stirrer stopped due to HHA bulking and was removed. The mixture was homogenized by means of a spatula and left for a duration of two days to complete the bulking process. Immediately before application, 2 ml of the HHA gel were injected into another syringe containing 415 mg of microspheres and homogenized once more along with the microspheres.

2.9 In Vivo Investigation of rhBMP-2-loaded Microspheres

All animal experiments followed a protocol approved by the Animal Ethics Committee of the state Saxony-Anhalt, Germany. Male SKH-1 mice with a bodyweight between 31 and 39 g or female SKH-1 mice with a bodyweight between 24 and 28 g were housed under controlled conditions (12 h light/dark schedule, 24 °C) and received rodent pellets and tap water *ad libitum*.

2.9.1 Frequently Applied Techniques

2.9.1.1 Implant Application

In all experiments, 200 µl of liquid or sol, either with or without particles, were administered to the subcutis ventrally at the leg muscle pouches of mice. In the studies #1 to #4 (table 2.9-1), 1 ml syringes were used for gel application (conventional method). A single dose plus dead volume was loaded into the syringe. In study #5, an alternative application procedure with 5 ml syringes was performed. One complete batch of microspheres in sol was directly prepared within the syringe. The syringe was used for up to five applications. The first drops were withdrawn at each application to assure the output of constant volumes after the change of needles. This procedure is referred to as 'optimized method' in the following. In *verum* groups of studies #4 and #5, the applied rhBMP-2 dose was 1.3 µg.

Table 2.9-1: Overview of all animal experiments, their purpose, applied methods and experimental details. Abbreviations are used as follows: OI, optical imaging; CT, computer tomography; MRI, magnetic resonance imaging; HE, histological evaluation. '#' indicates the particular animal study numbers, which are used in the following.

#	Purpose of the study	n	Sex	Protein incorporated	MP polymer	Dispersant	Time	Exp. methods			
								OI	CT	MRI	HE
1	Dispersant suitability	1	m	rhoda*BMP-2	PEP 0	PBS	1 d	x			
2	Signal intensity, Dispersant suitability	1	m	Alexa 647*BSA	PEP 0	Chitosan gel	3 d	x			
		1	m	rhoda*BSA	PEP 0	Chitosan gel	3 d	x			
3	Colocalisation of implant and calcification site, Monitoring of rhoda*BMP-2 residence time, Bioactivity of rhoda*BMP-2	3	m	rhoda*BMP-2	PEP 0	Chitosan gel	4 w	x			x
		3	m	rhoda*BMP-2	PEP 5	Chitosan gel	4 w	x			x
		3	m	rhoda*BMP-2	PEP10	Chitosan gel	4 w	x			x
		1	m	rhoda*BMP-2	./.	Chitosan gel	4 w	x			x
		1	m	./.	PEP 0	Chitosan gel	4 w	x			x
		1	m	./.	PEP 5	Chitosan gel	4 w	x			x
		1	m	./.	PEP10	Chitosan gel	4 w	x			x
		1	m	./.	./.	Chitosan gel	4 w	x			x
4	Comparison between MP of different polymers and gel only	5	m	rhBMP-2	PEP 0	Chitosan gel	12 w	x	x	x	x
		5	m	rhBMP-2	PEP 5	Chitosan gel	12 w	x	x	x	x
		5	m	rhBMP-2	PEP10	Chitosan gel	12 w	x	x	x	x
		5	m	rhBMP-2	./.	Chitosan gel	12 w	x	x	x	x
		5	m	./.	PEP 0	Chitosan gel	12 w	x	x	x	x
		6	m	./.	PEP 5	Chitosan gel	12 w	x	x	x	x
		5	m	./.	PEP10	Chitosan gel	12 w	x	x	x	x
		4	m	./.	./.	Chitosan gel	12 w	x	x	x	x
5	Comparison between different dispersants	5	f	rhBMP-2	PEP 5	Chitosan gel	12 w	x	x	x	x
		5	f	rhBMP-2	PEP 5	HHA gel	12 w	x	x	x	x

2.9.1.2 Anaesthesia

For implant application, benchtop magnetic resonance imaging and optical imaging, mice were anaesthesized with a combination of isofluran and oxygen. Computer tomography was performed after intraperitoneal anaesthesia with ketamine (90 mg/kg) and xylazine (6 mg/kg).

2.9.1.3 Optical Imaging (OI)

In general, fluorescence images were acquired using the Maestro *in vivo* imaging system (CRi Inc., Woburn, US). Rhodamine B, rhodamine-labelled rhBMP-2, rhodamine-BSA and ALEXA 647-BSA were found to be monitored best with the green filterset, with excitation wavelengths between 503 nm and 555 nm. The fluorophore emission was filtered by a 580 nm longpass filter. Acquisition was carried out between 550 nm and 800 nm in 10 nm steps. Parallel measurements with 2 nm steps yielded the same results and were thus omitted with focus to higher numbers and significantly increased measure time in subsequent experiments. Investigations of calcification (BoneTag IRdye 800 CW, Licor, Bad Homburg) were executed with the NIR filterset. The dye was excited between 710 nm and 760 nm and the emission filtered by a 800 nm longpass filter. Acquisition was carried out between 780 nm and 950 nm in 10 nm steps. The obtained pictures were processed with CRI Maestro software, v. 2.10.0. Threshold pictures provided in one figure were processed in the 'compare images mode' of the software in order to visualize intensity differences between the pictures. The 'compare images mode' takes into account both the imaging time and obtained signal intensity, the images are then scaled based on the brightest image with respect to the imaging time. High signal intensities in the picture are symbolized by red colour; decreases in signal intensity are marked by a gradual change of colour from red towards yellow, green, blue and finally black.

In study 5, fluorescence imaging at 12 weeks was also performed by means of another *in vivo* imaging system (Pearl imager, Licor). Three kinds of images were acquired by using a resolution of 85 μm: at 700 nm, at 800 nm and greyscale images. The images obtained at 800 nm were compared with results from the Intas *in vivo* imaging system.

2.9.2 System Optimization

2.9.2.1 Injection of Microspheres dispersed in Liquid

The retention at the injection site was first tested for rhodamine-labelled rhBMP-2 microspheres dispersed in phosphate-buffered saline (PBS) pH 7.4 R[121]. The dispersion was administered to one mouse (study #1).

2.9.2.2 Microspheres with Rhodamine-labelled BSA and Alexa 647-labelled BSA in Chitosan Gel

The injection of microspheres in PBS proved unsuitable due to particle migration (see chapter 3.9.1). To investigate the influence of the fluorescent dye, a comparison of rhodamine with Alexa 647 was carried out (study #2). Both were purchased as conjugates to bovine serum albumine to circumvent measurement bias due to alterations in the labelling efficiency. PEP 0 microspheres were prepared according to the general preparation method described in chapter 2.4 with rhodamine-BSA or Alexa 647-BSA, respectively. In order to test the ability of an *in situ*-forming implant to retain the microspheres within a defined space, the particles were dispersed in chitosan gel and administered subcutaneously to the ventral pouches of a mouse. Rhodamine-BSA-loaded microspheres were injected at the animal's left side, Alexa 647-loaded microspheres were administered to its right side. The fluorescence spectra were recorded and the intensities were monitored over a period of three days. Intensity information was compared with data from CLSM photomicrographs of the dry microspheres.

2.9.2.3 Gel Placement and Stability

Microspheres of all three polymers, loaded with rhodamine-labelled rhBMP-2 were injected with sols prepared as described above into three sites each (study #3). Sols with non-encapsulated, labelled rhBMP-2 served as positive controls. Negative controls included all investigated systems prepared without rhBMP-2, labelled rhBMP-2 or rhodamine B.

The gel's position and shape were monitored *in vivo* for a period of four weeks. Fluorescence images were acquired at days 0, 2, 4, 8, 15, 22, 25 and at the end of the study.

2.9.3 Bone Formation Assessment in a Mouse Ectopic Model

Computer tomography (CT) and magnetic resonance imaging (MRI) were utilized for implant evaluation 12 weeks after injection. As a surrogate parameter for bone formation processes, the calcium deposition at the implant site was monitored by means of optical imaging (OI) during the experimental period.

2.9.3.1 Optical Imaging

Proof of Colocalization of Implant and Calcification Signal

The seven mice from the explorative pilot study of gel position and stability (2.9.2.3.) were investigated for the colocalization of rhBMP-2 and the resulting calcification. After 24 days, the implants were assessed for signs of calcification by means of a fluorescence-labelled calcium chelating agent (BoneTag, Licor). 100 µl of dye solution, prepared according to the manufacturer's instructions, were injected into the tail vein. One, five and eleven days after injection, fluorescence images were acquired using NIR settings of the Maestro equipment.

Proof of Calcification

Forty *in situ*-forming implants were administered subcutaneously to twenty mice as described above (study #4). The investigated groups (n=5) included gels with dispersed, rhBMP-2-loaded microspheres of all three polymers. RhBMP-2, dispersed in sols, served as positive control. Negative controls of the four investigated systems were prepared without addition of growth factor (n=4-6).

In a similar approach, the impact of the microsphere vehicle was investigated (study #5). In this study, the active ingredient was encapsulated in PEP 5 microspheres. The microspheres were dispersed in *in situ*-forming implants of chitosan or modified hyaluronic acid gels and administered to female mice (n=5 each).

In studies #4 and #5, signs of implant calcification were assessed 3, 8 and 12 weeks after injection non-invasively by OI as described above. Another image was recorded *ex vivo* when the skin around the implant region was abscised.

Two different ways of result evaluation were applied. In the 'Implant Volume Calculation Method' (I), calcified volumes were determined by

measuring the patella spectra and by separating them from the background spectra found in soft tissue areas of the mice. After this unmixing process, ectopic sites of fluorescence were regarded as calcified tissue and defined as regions of interest (ROI). Their volumes were determined by measuring the length l and width w of the ROI (fig. 2.9-1) and calculating the ellipsoid volume according to equation 2.9-1.

$$V = \frac{1}{6}\pi l w^2 \qquad (2.9\text{-}1)$$

For method (II), referred to as 'Total Signal Evaluation Method', the ROI were defined by a standard ellipse with an area covering 461 mm², assuring a full coverage of any ectopic signal. The total signal, scaled by the exposure time of the image, was utilized for result evaluation.

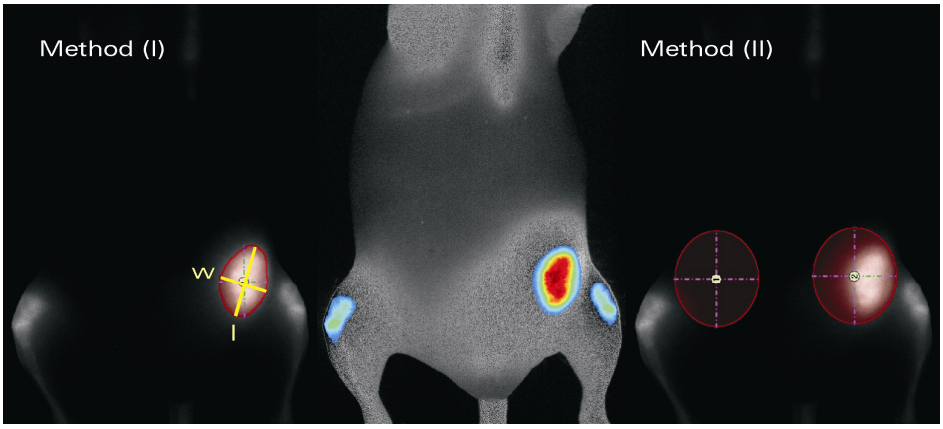

Fig. 2.9-1: Two different ways of result evaluation for OI calcification signals. Method (I), on the left, is based on the measured length and width (l and w) of the implant. The total calcification signal of standard ellipses, scaled by exposure time, was used in the second approach (II; right). For comparison, a threshold image of fluorescence intensity is provided in the middle.

2.9.3.2 Computer Tomography

The implant shape and morphology in week 12 was evaluated by means of CT (Somatron CT Scanner, Siemens). The instrument was designed for human use, so that 5 animals per run were investigated to obtain a sufficient signal. The animals were first scanned in upper the extremity mode for bone and soft tissue, then images were processed

with Syngo software. HG 300 0.6 U70u pictures were used for data acquisition and processing. Slice thickness was 600 µm and pulse frequence was set to 70 u. Bone appears bright under the used conditions, values range from 200 to 1500 units for bone, whereas darker areas (below 150 units) depict soft tissues. Bone volumes were calculated from the brightness of investigated areas. ROI were defined manually around newly-formed bone. Ectopic and orthotopic sites could easily be distinguished from one another. Within the defined ROI, the volume fulfilling the defined brightness criteria was calculated by means of the Syngo software. The volume of every ROI was calculated using length l, depth d and width w of the ROI provided by the software and regarding the implant as an ellipsoid according to equation 2.9-2.

$$V = \frac{1}{6}\pi dlw \qquad \text{(2.9-2)}$$

2.9.3.3 Magnetic Resonance Imaging

For comparison, magnetic resonance images were also acquired in the 12th week after sol administration. The images were composed of data gained with a slice width of 3 mm, slice separation of 3.5 mm, a spin echo time of 8 ms and a repetition time of 172 ms. 32 averages were recorded on a 27 mm field of view with a resolution of 64 x 64 pixels. A blinded result evaluation of the acquired data for signs of implants or ectopic bone was performed by a specialist.

2.9.3.4 Histology

All implants with *in vivo* residence times of 28 days or longer were subjected to histological evaluation. For a detailed overview of the different studies, see table 2.9-1. After excision, the implants of study #3 were frozen to -20 °C. Frozen sections were cut by means of a microtome (Jung Biocut 2035, Leica) to a slice thickness of 10 µm. During this process, photographs were taken to gain an overview of the sample composition. After the slicing process, the sections were fixed with neutrally buffered formalin solution (4 % v/v).

Implants of the studies #4 and #5 were directly immersed into the fixation solution. The specimen were rinsed in PBS-containing sucrose (6 % w/v) and dehydrated in an acetone series until the organic solvent remained clear. Subsequently, the samples were embedded in a cold polymerizing resin (Technovit 8100, Heraeus Kulzer, Wehrheim, Germany) according to the manufacturer's instructions. Sections of 5 µm thickness were prepared with the microtome.

All further processing of the samples of studies #3, #4 and #5 was accomplished in the same manner. At least two sections per sample were investigated by hematoxylin-eosin staining. The sections were rinsed in distilled water for 5 minutes and then immersed in dilute Mayer's hemalum solution (1:4, Merck, Darmstadt, Germany). After an incubation period of 60 minutes, the sections were treated with tap water for blueing. The second staining was performed by immersion of the samples in 0.1 % (w/v) eosin solution for three minutes. The sections were rinsed again with distilled water and covered with Entellan (Merck).

Calcification and bone formation were monitored in studies #4 and #5 by means of von Kossa staining. This method, first described in 1901, is based on the reaction of silver with the phosphate deposit. After washing with water, the sections were immersed in silver nitrate (5 % w/v) for one hour and rinsed with distilled water twice. The silver ions were reduced by addition of pyrogallol (1 % w/v for five minutes), subsequent fixation was accomplished by adding sodium thiosulfate solution (5 % w/v). After another rinsing step, nuclei were counter-stained for four minutes with nuclear fast red (1 % w/v in aluminium sulphate solution). Excess dye was removed with distilled water and the stained sections were covered with Entellan (Merck).

The histological evaluation of the stained sections from studies #4 and #5 was independently performed by three individuals on the basis of a scoring scheme (table 2.9-2). The samples were evaluated at different magnifications and examined for signs of bone formation, i.e., calcification and the presence of bone marrow. Four sections of each implant were investigated to gain a good overview of the whole implant. Microscopic pictures were acquired at an Eclipse 80i microscope with a connected workstation (Nikon instruments, Düsseldorf).

Table 2.9-2: Score system for the histological evaluation of the implants obtained after 12 weeks in the mouse ectopic model.

Bone Formation Score
5 predominant formation of vital bone with bone marrow
4 articulate regions of vital bone with bone marrow
3 scattered islets of vital bone with bone marrow
2 intense calcification, no bone marrow
1 traces of calcified tissue
0 no sign of bone formation or calcification

3 Results and Discussion

3.1 Extraction and Purification of rhBMP-2

Thirty years ago, the production procedure of the expression of recombinant proteins in bacteria was still not feasible[145]. Today, growth factor production by prokaryota, especially *Escherichia coli,* is very successful and by now also a common tool in biotechnology. The fruits of these achievements have been translated into many pharmaceutical preparations.

The isolation of rhBMP-2 from *E. coli* was performed according to an established protocol[110-112]. The affinity and binding of *E. coli*-derived rhBMP-2 to its receptors has been demonstrated by Keller et al. and Klages et al.[146,147] In a typical approach, 15 g of biomass yielded roughly 1.5 g of rhBMP-2 aggregates, so-called inclusion bodies. The protein was misfolded, so that a renaturation step was necessary to provide bioactive, homodimeric molecules. The dimer is regarded as the native form, because the monomers require the stabilization via an inter-molecular disulphide bond[116,148]. The six other cysteines per molecule form three intramolecular disulphide bonds and build the cystine knot[148]. It is assumed that naturally occurring, dimeric rhBMP-2 is the thermodynamically most stable form and will thus evolve over time from a provided redox system. The principle used in the renaturation step is known as redox shuffling[113]. Glutathione in its reduced and oxidized form composes the redox system within the buffer. The pH during this refolding is a critical issue, as it may prevent the shuffling process below pH 8 and lead to denaturation processes above pH 9[113]. It was shown by Hillger[110], that about 50 % had turned into the dimeric form of rhBMP-2 after 14 days, following the given protocol. Fig. 3.1-1 shows a typical outcome of the refolding control after nine days. Comparable refolding efficiencies of up to 43 % were reported by Vallejo and Rinas[113], who utilized a different refolding regime. The renaturation buffer of this protocol was also investigated for comparison but led to an irreversible precipitation of the protein.

The purification of folded, dimeric growth factor is based on the stronger binding affinity of renatured, dimeric rhBMP-2 to heparin compared to monomeric rhBMP-2[113]. The sodium chloride gradient is responsible for a good separation between the early eluting bacterial contaminants, the monomers with lower affinity and the renatured, dimeric growth factor[149].

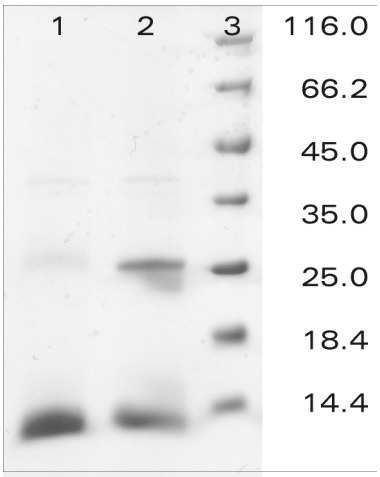

Fig. 3.1-1: Typical SDS-PAGE gel of a refolding control after nine days. Lane 1: rhBMP-2 in reducing buffer is found in the monomer range right below 13 kDa; lane 2: rhBMP-2 in non-reducing buffer reveals two articulate bands, the dimeric rhBMP-2 and its monomer; lane 3: marker. Numbers on the right represent the molecular weight of the marker bands in kDa.

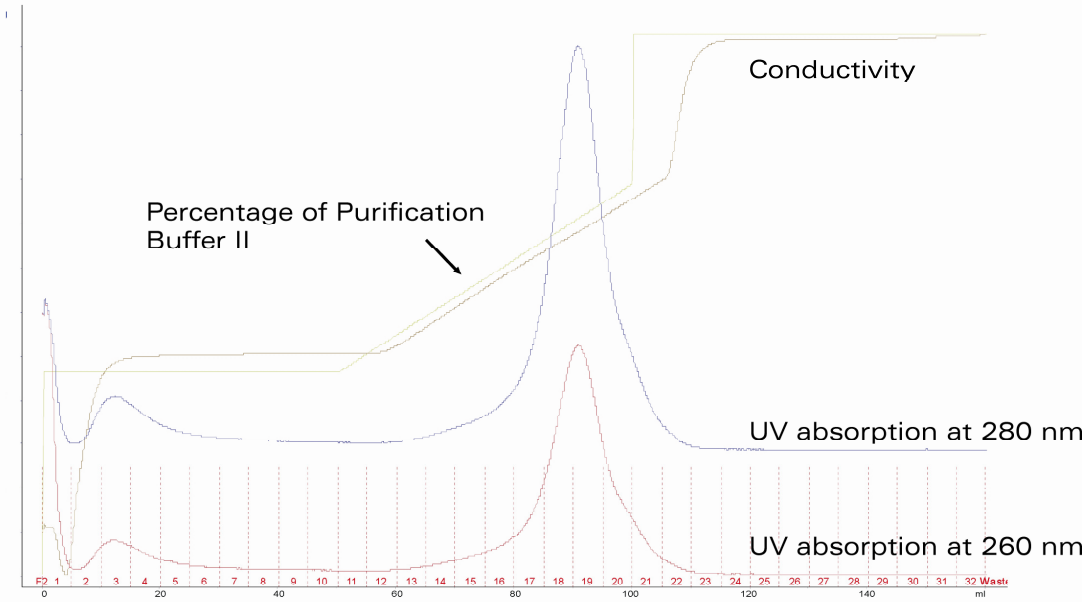

Fig. 3.1-2: FPLC chromatogram of rhBMP-2 affinity chromatography. Against the total eluation volume with the respective fractions (red numbers), the UV absorption signal at 260 nm (red graph) and 280 nm (blue graph) is depicted. Dimeric rhBMP-2 was found in fractions 15 to 22.

Sufficient concentrations of the dimeric form were usually found in fractions 18 to 21, when the sodium chloride concentration exceeded 0.6 mol/l (Fig. 3.1-2). SDS-PAGE confirmed these findings and demonstrated a high purity within the fractions (Fig. 3.1-3).

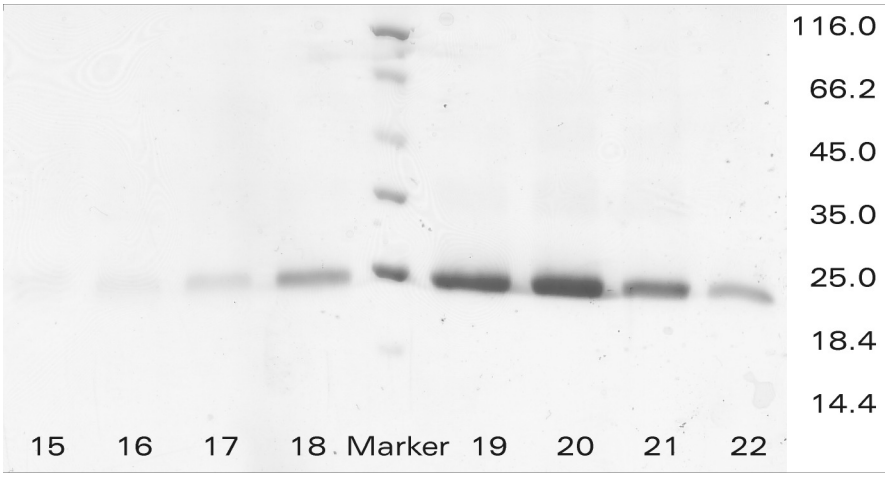

Fig. 3.1-3: SDS-PAGE gel of FPLC eluate fractions 15 to 22. In this example, fractions 18 to 21 were chosen for further processing.

A precipitation of protein was found in some of the batches during step (n) (Fig. 2.1-2), the dialysis against *Lyophilization Buffer*. It was not investigated whether the precipitation occurred directly because of misfolding or for other reasons. Physicochemical properties, such as solubility, also depend on the state of folding, as, for example, usually hidden hydrophobic moieties may be directed outwards, making the protein less soluble. Misfolded proteins exhibit different physiological output, e.g. reduced or no activity or adverse effects[150-154]. However, it is most likely that misfolding was involved, as no alterations on the refolding and purification protocol were performed except of one refolding approach according to Vallejo and Rinas[113].

One out of five standard batches and the aforementioned external renaturation buffer led to a precipitation of the protein during the final dialysis step (Table 3.1-1; Fig 2.1-2, step (n)). These two batches could not be resolubilized by dialysis and were discarded. Four batches were produced successfully and showed typical protein spectra by means of UV spectroscopy. The concentrations of the reconstitutes were determined by means of ELISA prior to further work. The batches showed different aggregation patterns after reconstitution. Details on aggregation are provided in the subchapters below.

Table 3.1-1: Batches of rhBMP-2 and their use during further experiments.

Batch	Start of Purification	Utilization
07-I	15.01.2007	Used for preliminary tests
07-II	02.02.2007	Precipitated irreversibly during step (n), discarded
07-III	04.04.2007	Modified renaturation step according to Vallejo[113], precipitated irreversibly during step (n), discarded
07-IV	11.04.2007	Used for in vitro investigations
09-I	07.01.2009	Used for in vivo experiments no. 1,2
09-II	07.01.2009	Used for in vivo experiments no. 3-5

3.2 Modification of rhBMP-2

3.2.1 Carboxyfluorescein Labelling

The encapsulation efficiency and load distribution within the microspheres were investigated with fluorescence techniques. Therefore, rhBMP-2 had to be covalently linked to a fluorescent dye.

Labelling of primary amines with NHS-activated carboxyfluorescein is a well-established method. Today, it is preferred over carboxyfluorescein isothiocyanate due to equivalent reactivity and a higher stability[155]. NHS esters preferentially react with primary amines. The nucleophilic reaction is rather specific in proteins, because its possible side products, thioesters or esters, are much less stable in an aqueous solution. The side products will hydrolyze, leaving amides as predominant products after the removal of unbound dye. The optimal reactivity of NHS ester coupling reactions is obtained within a pH range of 7 to 9. NHS-activated carboxyfluorescein is less soluble in water than the pure dye and the solubility minimum of rhBMP-2 is also described to be in this range. Consequently, an insufficient solubility of the conjugate was expected. The labelling was thus carried out at pH 6. A lower efficiency of the reaction at this pH had to be taken into consideration. After dialysis, a yellowish fluorescent liquid was found in the dialysis tube. By means of SDS-PAGE, the covalent linkage to rhBMP-2 was proven. Tests on encapsulation of the labelled rhBMP-2 into microspheres (chapter 3.5.3) showed an undesirably large overlap between the emission spectra of carboxyfluorescein-labelled rhBMP-2 and the autofluorescence of the polymers, disabling further differentiation between the two species (Fig. 3.2-1) and an insufficient fluorescence intensity of the construct. Hence, carboxyfluorescein-

labelled rhBMP-2 was disqualified for further analytical procedures. An optimization of the fabrication procedure was omitted in favour of a change of the dye. A well accessible alternative was sought and found in rhodamine B.

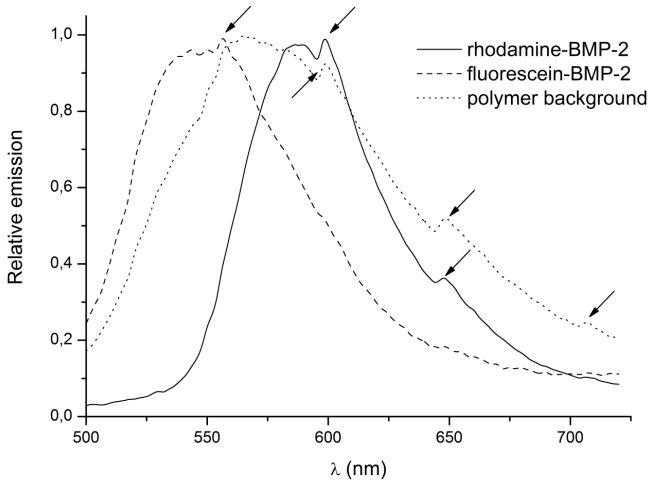

Fig. 3.2-1: Normalized fluorescence spectra of rhBMP-2 covalently linked to fluorescein or rhodamine B and background spectra of PLGA. Local maxima at 550 + 50 x nm (x= 1, 2, 3) are artefacts due to a mode hop in the liquid crystal tunable filter of the *in vivo* imaging system.

3.2.2 Rhodamine Labelling

Rhodamine was purchased in unactivated form. The dye was chosen because its fluorescence emission was easy to distinguish from the microsphere background fluorescence. The dye has a higher emission wavelength than fluorescein, ameliorating the transmission of signals from in vivo samples. Other advantages include the high quantum yield and its small size compared to many other dyes, so that the properties of rhBMP-2 were altered as little as possible. Furthermore, an overlap with the spectra of the intended calcification marker (chapter 2.9) in optical imaging could be precluded by the use of rhodamine B.

Stable NHS ester derivatives are only obtained in non-aqueous media[155]. Thus, the activation of the fluorescent dye was performed in dimethyl sulphoxide. Hydrolysis of the NHS-ester and reactivity of the amide moiety in proteins both increase with growing pH values. On the other hand, protein solubility decreases dramatically[80]. The labelling process itself was conducted in an aqueous sodium acetate, 20mM, at pH 5.5. Out of the six lysines per rhBMP-2 monomer, lysine no. 97 has the

highest probability to be amidated with NHS-activated dyes because of its ease of accessibility[116]. Consequently, the ratio of rhBMP-2 to activated rhodamine B was chosen to be 1:1.85 in order to label both of these lysines in the homodimer. The covalent linkage between rhBMP-2 was proven by means of SDS-PAGE. Fluorescent spots on the gel were compared with subsequent Coomassie staining results, and were in excellent match with them (Fig 3.2-2).

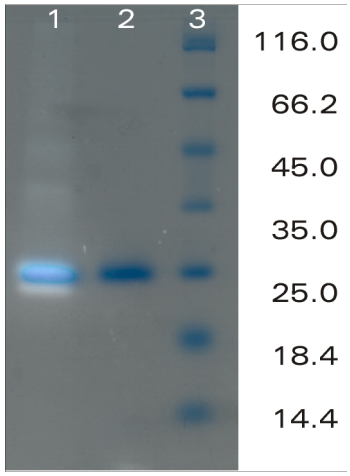

Fig. 3.2-2: SDS-PAGE - overlay of fluorescence imaging and subsequent Coomassie staining of one gel for labelling proof. Bright areas represent fluorescent protein, blue areas label stained protein. Lane 1: rhBMP-2 with attached rhodamine B-label; lane 2: unlabelled rhBMP-2; lane 3: marker

No significant increase in aggregate or oligomer fractions was detected. The labelling efficiency was found to be rather low, with values ranging from 8.8 % to 9.7 %. The low labelling efficiency is probably due to an incomplete activation of rhodamine B and the relatively low pH value (pH 5.5) during labelling. At this pH, a clear solution was obtained, but the amount of unbound rhodamine was visually detectable during dialysis. The labelled growth factor was stable at 4 °C for at least three weeks in solution.

At a higher pH, a higher percentage of free, non-protonated amino groups is available, which is beneficial for the nucleophilic substitution at the carboxylic acid group of the dye. However, a partial precipitation of rhBMP-2 at a higher pH (pH 6.5) in a preliminary test was observed during the procedure.

Excitation and emission spectra were recorded with maxima at λ_{ex}=555 nm and at λ_{em}=578 nm, respectively. The data are similar to results of pure rhodamine B reported by Rohatgi-Mukherjee and Lopez-

Arbeloa[156]. The rhodamine-labelled rhBMP-2 was used for the localization of rhBMP-2 in the microspheres and the revelation of the inner structure of the microspheres (chapter 3.5.3). It was also necessary for the determination of encapsulation efficiency (3.5.4). The residence time of labelled rhBMP-2 *in vivo* and colocalization of resulting bone formation are described in chapter 3.9.2. Rhodamine-labelled rhBMP-2 will be abbreviated rhoda*BMP-2 in the following chapters.

3.3 Analysis of rhBMP-2

3.3.1 Aggregates

Very recent work demonstrated that the term 'aggregation' is, in spite of its importance, still used differently in several groups[154]. The proposed definition of Wang et al. was that of any protein species in non-native states with a protein size at least twice as much as the native protein[154]. Due to the applied methods in this study, a differentiation between native and non-native states was not performed. Consequently, all species with a size or molecular weight of more than 1.5fold of the native protein were regarded as aggregates in the following.

Aggregation can result in activity loss or may even cause adverse effects[150-153]. In general, three different kinds of aggregates can be distinguished:

(I) defined, repetitive structures such as fibrils,

(II) native protein with decreased hydrated shell, as obtained by salting out protocols,

and (III) amorphous, denatured aggregates.

Several methods provide access to information on aggregation in protein samples. Apart from chromatographic methods, electrophoretic approaches, and mass spectrometry, also several spectroscopic methods are described[150,153].

In MALDI-TOF-MS, oligomers of up to four native dimers were detected. Calculations, carried out for comparison with the other techniques, showed diameters of up to 9 nm for these small aggregates. Diameters in this range were also calculated for AF4 measurements. In contrast, NTA and PCS both found no detectable particles in this range, presumably due to the weak scattering abilities of these small particles compared to larger ones. Bulkier aggregates with hydrodynamic

diameters of around 200 nm were found by both PCS and NTA. By dynamic light scattering, another fraction with hydrodynamic diameters of around 25 nm was detected, similar to those found in other batches. NTA was not able to track these particles, as they are smaller than the reported resolution limit for the technique[119]. Advantages, disadvantages, and results of the methods are discussed in more detail in the following subchapters.

3.3.1.1 MALDI-TOF-MS

MALDI-MS was first described in 1988 for the analysis of proteins[157]. The method is very sensitive, and the matrix can protect the analyte during the ionization process. MALDI-TOF-MS is an accurate method, but inefficient in the determination of high molecular weight molecules above 100 kDa due to lower ionization yields. Weak interactions between protein molecules, yet forming aggregates, may be underestimated because of the sample preparation, desorption and ionization process. As mentioned above, rhBMP-2 is a homodimer of two 13 kDa subunits linked by one single disulphide bond. According to the principle of the method, a monomer and a double charged dimer would result in nearly the same peak not to be unravelled. The relatively low resolution of the method[150] would impair such differentiation. Hence, (I) monomers as impurity, (II) split dimers, and (III) intact, double charged dimers will yield merely the same result. The method itself is described to yield mainly singly charged ions[158], but exceptions are also known, e.g. for bovine serum albumin, where up to 30 % of the ions can bear two or more charges[159,160]. For a final decision, further investigations on the charge uptake behaviour of rhBMP-2 would have been necessary, as no literature data on this issue is available to date.

In all investigated samples, the 26 kDa peak of native rhBMP-2 was by far the main peak. Peaks at an m/z ratio of around 39, 52, 65, 78, 91 and 104 kDa/charge, equivalent to 1.5, 2, 2.5, 3, 3.5 and 4 molecules of native rhBMP-2 per positive charge, were found (Fig. 3.3-1). The peak heights, which are a relative value of occurrence as they correspond to counts, were decreasing with growing molecular weight. Aggregates involving monomers were present to a much smaller extent. The occurrence of ‘half’ molecules may be surprising, but can be explained by double charging of the native homodimers or by monomers in the sample.

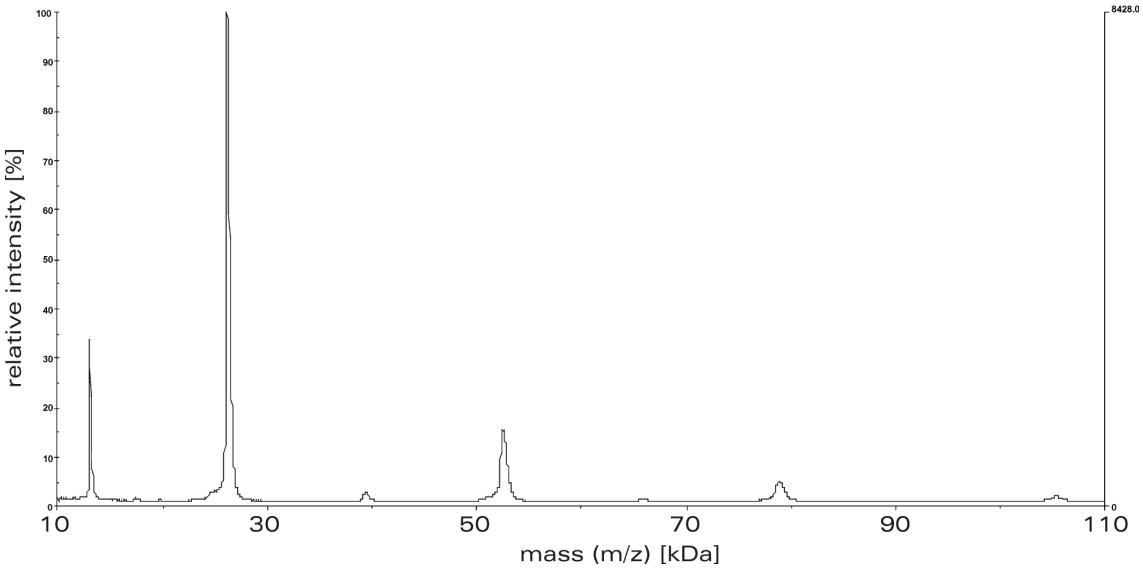

Fig. 3.3-1: Mass spectrum of a typical rhBMP-2 sample as determined by MALDI-TOF. Of special interest are the alternating peak heights every 13 kDa and the decreasing signal intensities towards higher m/z ratios.

Based on the method of desorption and ionization, a lower efficiency of MALDI-TOF-MS in the detection of fractions with very high molecular weight has to be implied. Hence, investigations were only undertaken for a range from 10 kDa (to detect possible monomers) to 110 kDa (to detect at least tetrameric aggregates of the native homodimer). Above this investigated range, aggregates were detectable by other techniques such as AF4, PCS, and NTA.

To compare the measurements with other data, the theoretical diameter was calculated using known molecule sizes of the rhBMP-2 dimer[116,161]. With the assumption of a constant water content and hence a constant volume/weight relation, a doubling of the molecular weight during aggregation causes a growth in diameter by the third root of two. Furthermore assuming a pancake-like aggregation, i.e. aggregate growth towards one dimension, the increase of molecular weight from 26 kDa to 104 kDa leads to a growth in diameter from 5.3 nm to 8.8 nm. This calculation is based on the Matthews parameter[162], which links the volume of a protein to its molecular weight. Measured in crystals, it is clear that the ratio found in aggregates should be remarkably higher. On the other hand, the interior of proteins consists of closely packed atoms[163]. Furthermore, the influence of the Matthews parameter on the calculation is rather limited due to a high initial value for rhBMP-2[116] and its influence in the third root order of magnitude, so

that an approximation based on these preconditions is reasonable. The method proposed by Erickson[163] yielded comparable results.

A less dense aggregation would yet result in diameters below 12 nm, still not detectable with NTA and difficult to find in PCS measurements. AF4 is theoretically able to give results in both molecular weight and the gyration diameter of the molecules. However, the isotropic scattering of small molecules like rhBMP-2 does not allow an angle-dependent size determination.

3.3.1.2 Asymmetric Flow Field Flow Fractionation (AF4)

With AF4, molecules of high molecular weight of as much as several megadaltons are still accessible. The accuracy is, amongst other factors, highly depending on defined flow conditions, sample stability during the measurement, proper peak separation, and the preclusion of interactions of the sample with the flow channel. With the final method described in chapter 2.3.1, four different samples of rhBMP-2, two in *Ac Buffer*, one in *AcPEG Buffer*, and one in *Phos Buffer* were investigated. All were reconstituted freshly from the 07-IV batch to concentrations of 0.5 mg/ml rhBMP-2.

Although several modifications were made to optimize the method, e.g. variation of focus flow and crossflow, very heterogeneous results were obtained. Base line separation was not achieved between the first two peaks of the samples, complicating the calculation of mass for the populations. However, errors of the Mw calculation, as given by the software, were below 0.8 % in all cases. Only a rough estimation can be made from the results, because not all samples could be investigated in triplicate. An approximate overview of the calculated molecular weights is given in fig. 3.3-2.

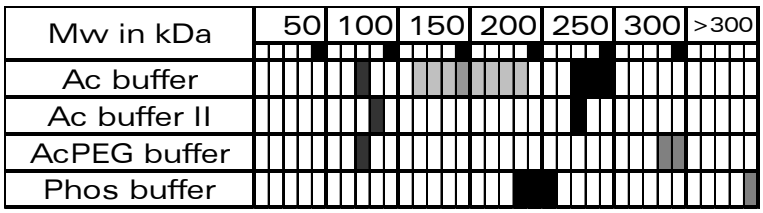

Fig. 3.3-2: Approximated distribution of molecular weight fractions of rhBMP-2 as determined by AF4. Darker colours indicate higher intensities due to a higher peak volume. Areas represent molecular weight including standard deviation.

Surprisingly, no monomers could be detected in any of the samples. Measurements with an increased crossflow had proven that no low molecular weight species were lost in the void peak. This finding contrasts with the MALDI-TOF-MS measurements, and should be handled cautiously. RhBMP-2 presumably interacts with the slightly negatively charged membrane consisting of regenerated cellulose. The heparin binding segment of rhBMP-2, a cationic moiety in the molecule, should be prone to this interaction. Potentially, the use of another, more appropriate material, e.g. polyethersulfone or polyvinyliden difluoride, might result in a different outcome. Nevertheless, interesting parallels were found for all *Ac Buffer* and *AcPEG Buffer* measurements. One species of aggregates with a molecular weight of around 85 kDa was found in all of these measurements. A second, intense area around 255 kDa was found only in the *Ac*, but not in the *AcPEG* samples. In the *AcPEG* sample, a comparable fraction was detected at a corresponding molecular weight of about 290 kDa.

When rhBMP-2 was dissolved in *Phos Buffer*, the outcome was completely different. No single molecules or low molecular weight aggregates were detectable, the main fraction was found with a molecular weight of 200 kDa. A second species was detected around 710 kDa, most likely indicating further aggregation.

In all samples, aggregation processes were detected. No free dimers with a molecular weight of 26 kDa were found. In *Phos Buffer*, the tendency for aggregation seemed to be different. The detected aggregates were larger, probably due to the less desirable pH of 6.0. Another influence could be the presence of phosphate ions, which was not cross-checked by preparation of acetate and phosphate buffers of the same pH. No reports on rhBMP-2 aggregation determination by AF4 were found, so data comparison is not possible in this case.

Diameters between 7 and 16 nm were calculated for the different oligomer species. The theoretical aggregate sizes were generated under the precondition of a certain water content and a very dense structure. Hence, it may well be possible that with a higher water content and a less dense structure, rhBMP-2 aggregates in *Ac Buffer* with calculated molecular weights of approximately 230 kDa exhibit hydrodynamic diameters of around 20 to 25 nm, as found in the PCS samples.

3.3.1.3 Photon Correlation Spectroscopy (PCS)

Another method of choice in the size determination of submicron particles is PCS. The fast optical method is based on the diffusion velocity of the measured particles. Prerequisites for accurate results are spherical particles and the knowledge of their optical properties. The obtained particle sizes have to be evaluated along with the dilution, gain and their polydispersity index (PDI). With this method, the hydrodynamic diameter of the aggregates is measured. Although the PCS data were acquired at least in triplicate, the variations in the measurements were very high in some older samples. Hence, the presented data have to be considered as rough estimates.

Immediately after reconstitution, a quite narrow distribution was found in the rhBMP-2 batches produced in 2009. For both batches, a volume weighted diameter of 25 nm was calculated. As expected, the z-average was found slightly above. Details are given in table 3.3-1.

Table 3.3-1: PCS results of two different batchs of rhBMP-2. The PDI is acceptable for this sample type with respect to a few larger aggregates.

Lot	$d_{vol\ weighted}$ (nm)	z-average (nm)	PDI
09-I	26	34	0,231
	25	34	0,223
	25	35	0,236
09-II	23	27	0,191
	22	27	0,207
	24	28	0,229

In two out of six datasets from 09-rhBMP-2, particles or molecules smaller than 20 nm were detected. Due to the low scattering ability of small particles, this may well be a hint of their presence. In a sample of 09-II, stored at 4 °C for two weeks, aggregates with a hydrodynamic diameter of around 28 nm were still detected. Additionally, a huge fraction of very high molecular weight aggregates was found, corresponding well with the visible occurrence of turbidity in this very sample.

In sample 07-IV, which had been stored in a lyophilized state at -20 °C for 15 months more than the 09-I and 09-II batches, different species were found. In addition to the peak at low hydrodynamic sizes, there

was clear evidence for high molecular weight aggregates in all measurements of this sample. Due to the resulting high polydispersity of this sample (PDI≈0.5), no meaningful mean diameter or z-average can be concluded. The question remains whether these aggregates result from long storage or whether they were present from the beginning. Previous data, derived from a freshly reconstituted sample 07-IV measured in 2008, support the latter thesis. In summary, in all samples of the 07-IV batch of rhBMP-2, high molecular weight aggregates with hydrodynamic diameters very roughly around 200 nm were found, whereas these were absent in fresh 09-rhBMP-2 batches.

3.3.1.4 Nanoparticle Tracking Analysis (NTA)

Both samples, originating from the 07-IV batch, provided similar results in spite of different storage times before the measurement. Aggregates were detected, and the mean diameter determined by the software was 183 nm and 192 nm, respectively. A monomodal distribution was observed and consequently, the highest intensity was found at hydrodynamic diameters right below 200 nm (Fig. 3.3-3). These diameters are comparable to data obtained from PCS measurements.

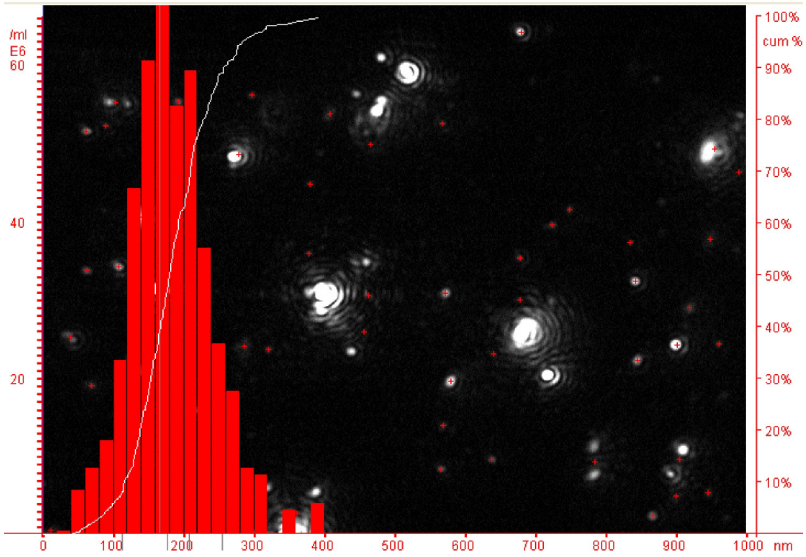

Fig. 3.3-3: Nanoparticle Tracking Analysis: Calculated particle distribution and visualization of tracked bright spots.

3.3.1.5 UV Spectroscopy

Proteins can roughly be distinguished from nucleic acids and protein aggregates due to their different UV absorption maxima. In a typical spectrum, a superposition of all three species displays the maximum of nucleic acids around 260 nm, of the tyrosin residues of proteins around 280 nm[164], and of aggregates above 300 nm. In this area, typically no other absorption would be found.

Due to the principle of the method, no quantitative aggregation data can be obtained. Nevertheless, relative estimations between different batches or between different buffer systems are possible. All three samples, though significantly different from one another, showed absorption above 300 nm (Fig. 3.3-4).

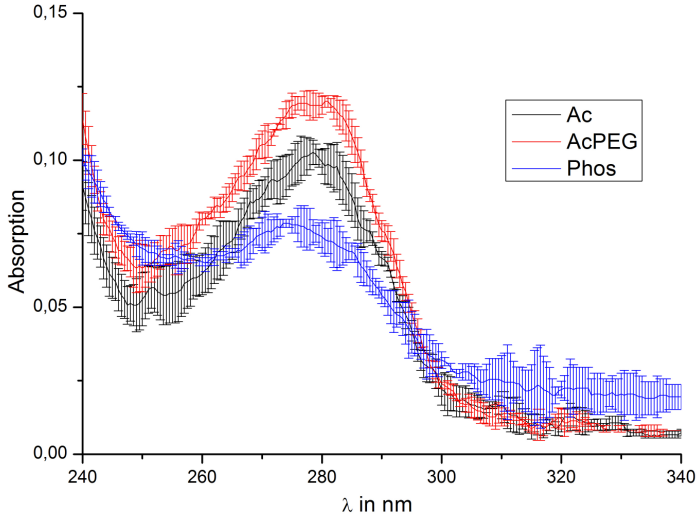

Fig. 3.3-4: UV spectra of equivalent concentrations of rhBMP-2 dissolved in three different buffers, i.e. *Ac*, *AcPEG* and *Phos Buffer*.

The amount of aggregates estimated by this method was defined as ratio of A_{300} divided by A_{280}. The ratio can be regarded as a relative number and not as an absolute ratio, because of the different molar extinction coefficients at the two wavelengths. Furthermore, the bias of possible turbidity of aggregated samples has to be taken into account when interpreting those measurements. The highest ratio of aggregates per total protein was found in *Phos Buffer* (Fig. 3.3-4, blue plot).

The absorption above 300 nm, related to aggregation, was clearly higher than in acetate buffered sample of lower pH. The local maximum around 280 nm accounting for protein absorption was notedly decreased. These data are emphasized by results reported by Luca et

al.[127], who found more and larger rhBMP-2 aggregates at pH 6.5 compared to a buffer of pH 4.5. *Ac* buffered samples showed less absorption above wavelengths of 300 nm and a more distinct maximum at 280 nm. The *AcPEG* buffered rhBMP-2 provided comparable results to the *Ac Buffer* regarding the shape of the curve, yet with higher maxima. Hence, a slightly stabilizing effect of PEG 300 on the protein unter the given conditions may be concluded.

3.3.2 Stability of rhBMP-2 in Release Media

As explained in chapter 1.2, rhBMP-2 derived from *E. coli* is less soluble in aqueous solutions than CHO-derived glycosylated protein. Additionally, pH used in release media for parenteral applications is 7.4, which has been demonstrated to be detrimental to rhBMP-2 solubility and stability[80,114,127]. Interestingly, this fact is neglected in nearly all *in vitro* release studies[52,67,165,166], which would consequently lead to an underestimation of the burst effect and total release when the solubility is exceeded. The alteration of pH in the release media by other groups[75,167] may support the stability of the growth factor in solution.

In pretests, the influence of several solubilizers, i.e. polysorbate 20, 0.05 % (w/v); polysorbate 80, 0.1 % (w/v); solutol HS 15, 0.1 % (w/v); and arginine, 0.8 M, on the detectable amount of rhBMP-2 immediately after reconstitution and after nine days of incubation in two different phosphate buffer systems was determined. A constant rhBMP-2 concentration was not found in any of the buffers. The investigated samples differed strongly not only in the outcome on day 9, but also in freshly diluted samples. After the preparation time of the ELISA, i.e. about 4.5 h, as few as 4 % to 45 % of the standard concentration were found in all samples. This result was equivalent for both PB and PBS. After nine days, however, the concentration detected in PB was three- to sixfold less than in PBS.

Low solubility is often accompanied by a high aggregation tendency. Schwartz investigated the salt concentration dependency of rhBMP-2 solubility and found similar results: an increase of ionic strength from 50 mM to 100 mM raised the rhBMP-2 solubility by factor 5[80]. The ionic strength of PB is about 50 mM, of PBS about 175 mM. It is suggested that the higher solubility of rhBMP-2 in PBS compared to PB leads to a better stability.

The use of arginine proved absolutely inadequate, although Geiger reported on good stability of rhBMP-2 in a phosphate-arginine-sodium chloride system with the same concentration and pH range[168].

Compared to blank buffer, remarkable improvements were achieved by the use of polysorbate 20 and solutol HS 15. Hence, PBS with added polysorbate 20 was selected as the most suitable, yet not ideal release buffer. Bovine serum albumine was utilized to further improve the stability of rhBMP-2 by blocking adsorption sites. EDTA-Na was employed to prevent degradation due to metalloproteinases; sodium azide served as preservative.

3.3.3 Freeze-thaw Recovery of rhBMP-2 and the Influence of Microsphere Degradation Products on rhBMP-2 Stability

The time-dependent increase in microsphere degradation products was used to investigate any influence on rhBMP-2 stability. The polymers were broken down to monomers like lactic acid, glycolic acid and polyethylene glycol remainders. An increase of short chained organic acids decreased the pH of the release medium (chapter 3.6.1). This effect increased the solubility of rhBMP-2 and possibly even stabilized the protein in solution. However, degradation products of microspheres were found not to interfere significantly with the stability of rhBMP-2 as determined by ELISA (Fig. 3.3-5).

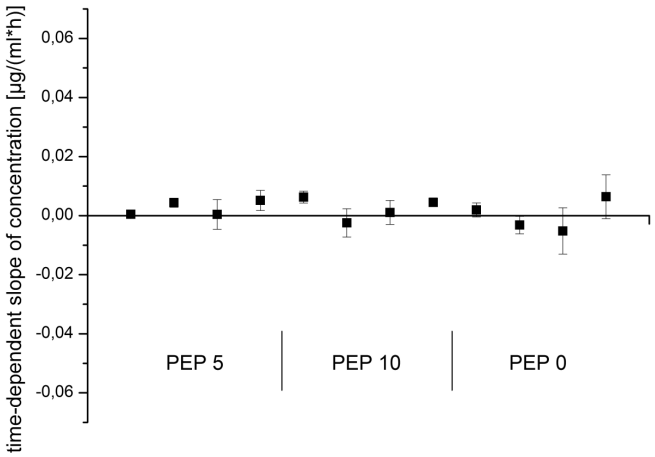

Fig. 3.3-5: Time dependent slopes of rhBMP-2 concentration as determined by ELISA. Each data point represents the increase or decrease in concentration in one rhBMP-2 sample subjected to twelve different increasing amounts of microsphere degradation products for the fixed time of one week.

Storage of one week at 4 °C did not cause considerable loss of rhBMP-2 in the supernatant of any of the three polymers. In contrast, one single freeze-thaw-cycle to -20 °C caused a loss of about one third in ELISA

detection (Fig. 3.3-6). The effect may be due to an adsorption to the vessel walls or to partial destruction of the molecule by ice crystals. The freezing of samples is a common storage method during release studies[80]. It is necessary to consider the effect in experimental design.

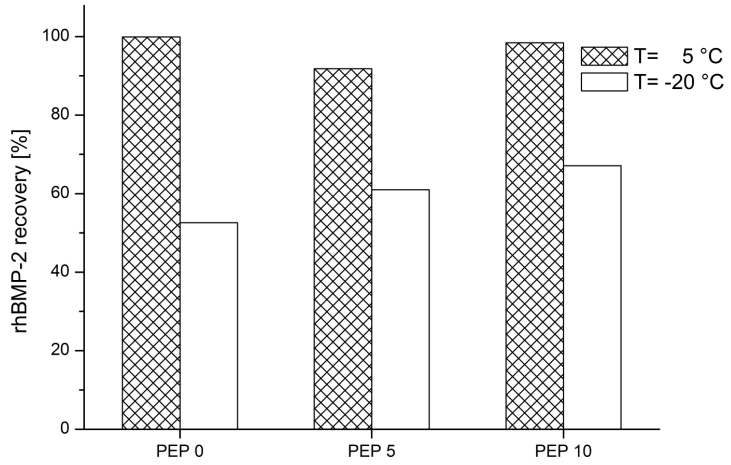

Fig. 3.3-6: ELISA recovery of rhBMP-2 after one week of storage in release buffer at different temperatures.

3.3.4 Solubility, Aggregation and Stability: Conclusion

In general, multiple aspects can contribute to a possible failure in physiological response to a protein. Protein solubility, unfolding and aggregation are closely linked and cannot be viewed apart from one another. It was not within the scope of this study to examine all of these aspects. A few relevant items were selected and investigated systematically, such as the stability of rhBMP-2 in release conditions. Others, e.g., the occurrence of aggregated protein in the samples were accomplished to gain an overview. Further work on these subjects should substantiate the outcome.

Aggregation, a process widely spread among proteins in solution, is one of the reasons for activity loss of the respective molecules[114,150-153,169] and may also be attributed to increased immunogenicity[150,154]. Aggregation may be caused by a variety of different factors, such as pH shifts, shear stress, interaction with surfaces, ions or temperature changes, to name just a few. Based on several reports on the rhBMP-2 aggregation and solubility behaviour[80,114-116,127], it becomes clear that the growth factor is relatively prone to aggregation processes. Thus, an estimation of occurring oligomerization was necessary. Five different

methods were selected to investigate aggregation. The advantage of a multi-method approach is the ability of recognition of possible artefacts due to variations in the sample preparation for the different methods. Furthermore, a full coverage of the very wide molecular weight range can be achieved. One batch, always freshly reconstituted in *Ac Buffer*, was used for all techniques. As expected, an aggregation of rhBMP-2 was found with all methods. Based on the applied method, the measured extent and pattern of oligomerization differed strongly. Based on the model of Wang et al.[154], at least six different states of a protein within an aqueous system can be found. Native, intermediately unfolded, denatured, chemically reacted protein, protein aggregates and precipitates may be found. The variety of applied methods is often feasible for detection of combined fractions of more than one species, so that the differences between the methods have to be attributed to both different measurement principles and possible alterations between samples.

It has to be noted that most methods were only accessible for a few samples, so that the remarks in this subchapter have to be regarded as estimations. Nevertheless, it can be concluded that rhBMP-2 tends to aggregate even after a relatively short period of time. It is clear that environmental conditions such as protein concentration and buffer composition have a huge impact on this behaviour. Outwardly directed hydrophobic areas and a rather small hydrophilic center of the molecule[116,161] contribute to this outcome. The solubility of rhBMP-2 was proven to be dependent on its degree of glycosylation[41], furthermore on the type of buffer used, on salt concentration, ion types and pH[80,114,168]. Information on the influence of different pH values and buffer systems were obtained from UV spectroscopy. Relative to each other, *Ac Buffer* and *AcPEG Buffer* showed higher aggregation protection than *Phos Buffer*. Schwartz[80] described a partial precipitation of rhBMP-2 in phosphate-buffered solutions. A lower rhBMP-2 recovery compared to *Ac* solutions was also found in ELISA. Furthermore, different batches tended to vary in aggregation behaviour as determined by PCS, which can be explained by slight alterations during the multi-step purification process and the biological origin. It was shown that different batches do not only exhibit different aggregation behaviours, but that the results are consistent with concentration determinations in ELISA measurements. Lowly aggregated samples showed better results in ELISA measurements compared to higher aggregated ones. To obtain a complete picture, it would have been necessary to perform all techniques with all batches. This was, however, not possible, due to time, cost and availability constraints.

According to the data presented above, the choice of PBS for release measurements appears to be not ideal. The major drawbacks of the utilized release system consist in a disadvantageous pH value and a temperature of 37 °C, which were not to be changed due to their physiological relevance. Furthermore, it was shown that salt concentration and detergent choice can influence the outcome. The most suitable combination was chosen. Hence, an acknowledged standard system for release determinations was used in spite of known stability impairments. Mathematical methods enabled a calculation of lost rhBMP-2 which was included in result evaluation of the release data.

It was demonstrated in chapter 3.3.3 that freezing and thawing will cause the loss of approximately one third of rhBMP-2 in ELISA detection. It is not clear whether this effect must be attributed only to aggregation or if other processes may occur additionally. Commercial rhBMP-2 is always delivered with the note to avoid freeze-thaw cycles. Nevertheless, the freezing and thawing was necessary during the release determination, because its time-independent effect is much more favourable for result interpretation than a slow, but continuous decomposition or aggregation in the fridge to which the samples would have been subjected for different time spans.

3.3.5 Considerations towards rhBMP-2 Encapsulation

The early formulation development for proteins is usually conducted with the investigation of a model protein, predominantly bovine serum albumin (BSA)[89,109,170-177]. From these investigations, general characteristics of the formulation and its interaction with proteins are thought to be found. On the one hand, a model protein may provide information on basic characteristics of the formulation in a fast and cheap way. On the other hand, a time-consuming second method development may be necessary and the information gained with one protein should be extremely carefully extrapolated to other proteins and their formulation.

In this study, the use of a model protein was not promising due to the very low intended protein concentrations within the microspheres and the very uncommon characteristics of rhBMP-2. The main characteristics exhibit a huge difference between rhBMP-2 and classical model proteins. BSA, for example, is an acidic protein (pI= 5.60) with a molecular weight of 66.4 kDa. In contrast, rhBMP-2 has a calculated pI of 8.21[178] and a molecular weight of only 25.8 kDa in native, dimeric form. Stability and hydropathy calculations reveal rhBMP-2 to be less

hydrophilic according to the method of Kyte and Doolittle[179] and less stable in solution[178].

Although there is a broad variety of information on protein stability during processes like freeze-drying and surface-adsorption, still very limited data have been published to this point about the process of microencapsulation[153,180]. Hitherto, information on rhBMP-2 behaviour during encapsulation is not available to date, and universal rules for the prevention or inhibition of aggregation have not yet been defined due to the diversity in the group of proteins and the multiplicity of exceptions for every parameter[154]. For example, protein adsorption processes are likely to occur at aqueous-organic interfaces leading to aggregation[153].

A general instability of proteins in microspheres prepared from PLGA was reported[153,180]. This can be attributed to adsorption processes to PLGA and to the pH decrease during particle degradation, causing aggregation and/or denaturation in most proteins. Whereas the first issue should not be neglected for rhBMP-2, protein aggregation in the sense of Crotts and Park, who identified the covalent aggregation as the predominant process for bovine serum albumine in PLGA microspheres[89], is less likely to occur in rhBMP-2 due to the lack of free thiol groups. Oldham et al. demonstrated the *in vitro* activity of rhBMP-2 released from PLGA microparticles[93]. A decrease of pH is also not likely to decrease rhBMP-2 solubility or stability due to the solubility profile of rhBMP-2. An overview of the reasons of protein instability during microencapsulation and possible prevention strategies is provided by van der Walle et al[153].

3.4 Production of Microspheres

The reproducibility of microsphere preparation is still a challenge, especially at larger scales. A variety of parameters may change the outcome of the particle characteristics. The final result of drug release will mainly be determined by these particle characteristics. The goal to develop medium-sized, dense microspheres with a non-porous surface, high encapsulation efficiency and a preferentially low burst release can be approached in various different ways. Fig. 3.4-1 gives an overview of selected key parameters and some of their influences on the final outcome. In the following subchapters, the relations between the most important parameters will be discussed in detail. Letters refer once again to the microsphere production scheme provided in chapter 2.4. The fabrication process was optimized to yield good results with all polymers. In order to guarantee a good comparability between the three

used polymers, the variation of the production process was kept as little as possible. Apart from changes in the type and volume of the inner phase, the used organic solvent was subjected to optimization.

The first step is the formation of a primary emulsion from a sodium acetate-buffered protein solution (*Ac Buffer*) as inner phase and the polymer dissolved in methylene chloride as continuous phase (a,b). The primary emulsion permits the dispersion of the active ingredients in the polymer matrix[177]. A small droplet size of the primary emulsion has been found advantageous for high encapsulation efficiencies[83]. However, an intense application of energy is necessary to achieve a small droplet size. The needed high shear might impair the protein stability[153].

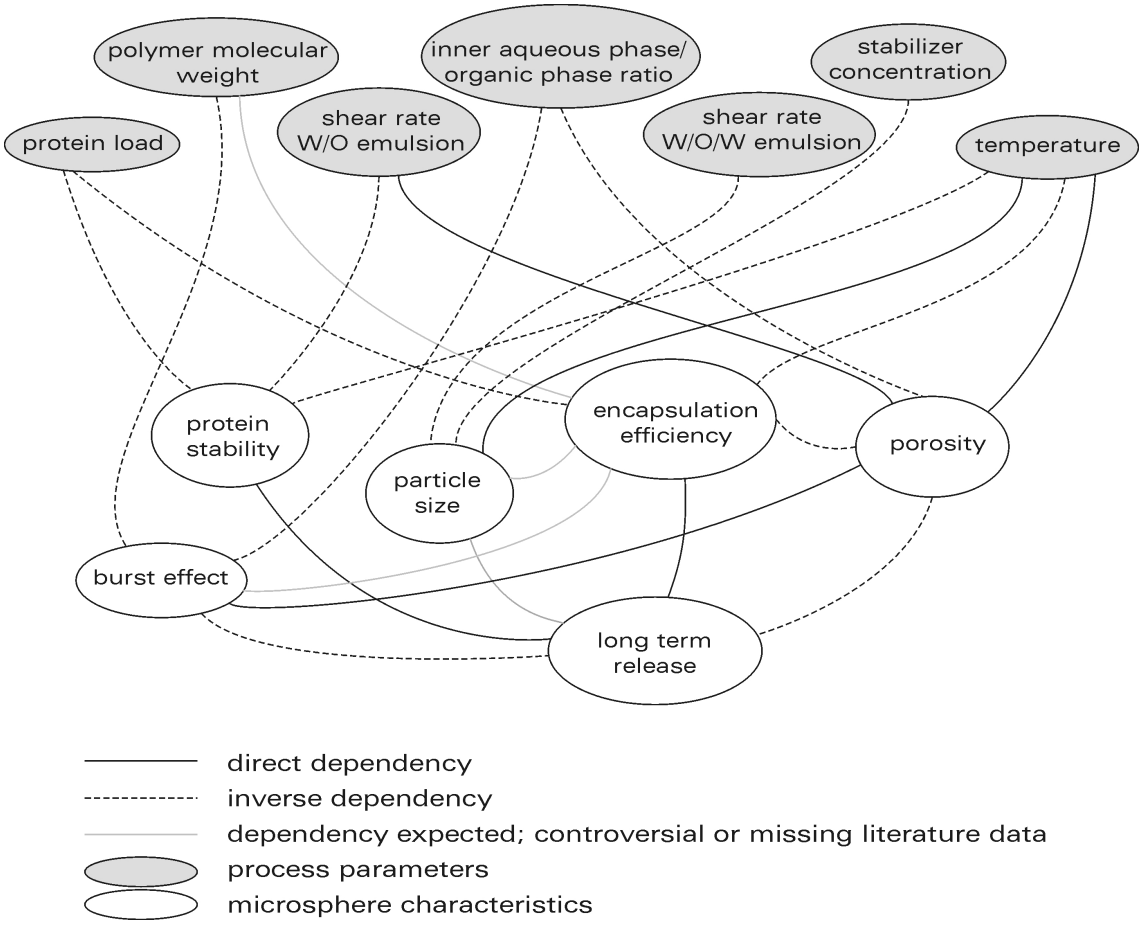

Fig. 3.4-1: Selected process parameters during particle formation and some of their impacts on resulting microsphere characteristics.

Whether the volume ratio between inner and outer phase has an impact on particle size is still controversially discussed. While some groups

reported a size decrease with an increasing organic phase volume[181,182], other groups reported no significant effects[183,184]. The impact of the volume ratio on inner phase morphology is clearer: the coalescence of aqueous droplets is more probable for higher inner phase volumes. In the beginning, microspheres were prepared with 300 µl of inner aqueous phase. However, using a volume of 150 µl proved beneficial for the inner morphology and size distribution of the particles. Compared to the amount of used polymer, the chosen concentration of rhBMP-2 in the primary emulsion was low. With low drug-to-polymer ratios, a higher encapsulation efficiency is usually found along with a less porous structure, sometimes a more uniform drug distribution and a lower burst release[77,83,185].

Protein stability can be improved by faster particle hardening[153]. Ethyl acetate (EE) increases the hardening velocity due to a higher flux to the water phase[87]. To protect the rhBMP-2 during encapsulation, the substitution of methylene chloride by EE was investigated. However, it proved unsuitable for the used particle fabrication scheme. The observed disrupted and hollow particles indicated that the particle hardening velocity was too high[87].

In another approach to stabilize the active ingredient, the codissolution of polyethylene glycol 300 and protein in the inner aqueous phase was investigated. PEG is not only flexible and hydrophilic, but also uncharged and highly hydrated, thus indwelling all basic requirements for protein rejection[186]. Malzert-Fréon and coworkers concluded that the use of PEG prevents the exposure of protein to the aqueous/organic interface[186]. The positive effects of polyethylene glycol during encapsulation were reported to be existent when PEG was either dissolved in the inner aqueous phase[108,186] or in the organic phase along with the polyester[138,186]. For each of the three polymers, at least four batches were produced with 33 % (v/v) PEG 300 in the inner phase (*AcPEG buffer*). Compared to PEG-free preparations, alterations in structure and release were found (chapters 3.5, 3.6).

The addition of antacids to the inner phase as proposed by Zhu et al.[187] was not promising due to alterations of the microsphere degradation profile, changes in release and the negative influence of a higher pH on rhBMP-2 stability[127].

The polymer concentration in the organic phase plays a key role in the predetermination of resulting particle morphology[89] (c). A higher polymer concentration in the continuous organic solution was selected, yielding denser particles. A skin is formed quickly around the nascent particle, which prevents the loss of active ingredient into the outer

aqueous phase[83]. The polymer matrix surrounds the aqueous droplets of the primary emulsion during particle formation (d). The droplets finally generate spherical, drug-containing microdomains within the particles.

The final particle size is primarily determined by the shear rate of the second emulsification. Smaller particles are obtained by faster stirring[185]. Surface active agents such as poly(vinyl alcohol) are also described to decrease the particle sizes of microspheres with increasing concentration[181,183,185], probably due to the prevention of coalescence or aggregation during hardening[177]. These beneficial effects can be explained by a decreased contact between both aqueous phases[83]. Hence, a rather high concentration of 2 % (w/v) PVA was used in the outer aqueous phase in this study.

Methylene chloride is slightly soluble in the aqueous environment, enabling the disappearance of the organic solvent from the polymer-rich organic phase into the outer phase. During this process, the polymer non-solvent, water, may also penetrate into the nascent particles[77].

In general, the used solvent evaporation technique, either with or without reduced pressure, had no important effects on encapsulation efficiency or drug release[83]. A slow and careful solvent removal process (e) at 4 °C was chosen to yield non-porous particles without a high burst release. In the washing step, the particle flowability was increased by the removal of PVA[188] (f). To keep a low porosity within the particles, they were dried under gentle conditions in a desiccator (g), but not freeze-dried.

The fabrication temperature is another important, yet widely ignored parameter to influence particle characteristics. It is clear that thermal conditions will affect not only the protein stability, but also the surface tension and viscosity of the solutions and, due to this, the emulsification process and the particle hardening velocity. The solidification rate of the nascent particles has been shown to influence the porosity of PLGA microspheres[89]. Yang and coworkers investigated the temperature impact during encapsulation of BSA either in PLGA microspheres or in PLGA microspheres blended with PEG[170,189]. They found a relatively low burst release and the highest encapsulation efficiency at a preparation temperature of 4 °C. A faster formation of the skin around nascent particles, faster polymer precipitation[87] and the formation of denser particles may account for that. Furthermore, a narrower size distribution and smaller particles were obtained at lower temperatures[170,189]. Consequently, most steps of the fabrication process in this study were also performed at 4 °C.

133 batches of microspheres were successfully produced, 62 of which were PEP 0 microspheres, 39 batches were made from PEP 5 and PEP 10 was used for 32 batches. Six different formulations were subjected to further characterization. An overview of these formulations is provided in table 3.4-1.

Table 3.4-1. Composition of formulations A through F with respect to their PEG contents. PEG 300 was used in the inner phase, PEG 5000 is linked to the polymer. Details on polymer composition are given in table 2.4-1, p. 26.

	Ac; Inner phase: 0 %	AcPEG; Inner phase: 33 %
PEP 0	A	B
PEP 5	C	D
PEP 10	E	F

For characterization, particles were divided into groups with identical properties in terms of inner phase type and volume, organic phase type and drug load. If not stated otherwise, data are provided for standard preparations of 150 µl inner phase volume without addition of PEG 300, prepared in methylene chloride.

400 mg of the respective polymer were used to prepare the microspheres. Because of the drying process and organic solvent removal, these 400 mg were considered as 100 % when calculating the yield (see 2.3.3). From all polymers, well-shaped microspheres could be obtained. Higher yields were found with no or low PEG content in the polymer, ranging around 93 % for formulation A and 89 % for C microspheres. Batches of formulation E yielded around 85 % of microspheres. Batches with *AcPEG* as the inner phase (B, D, F) showed a similar pattern. Absolute values are given in table 3.4-2.

Table 3.4-2. Yields of microsphere production. Given values represent mean ± standard deviation.

Formulation	Yield [mg]	n
A	381 ± 18	26
B	372 ± 19	3
C	376 ± 18	22
D	357 ± 19	3
E	340 ± 18	23
F	325 ± 7	3

3.4.1 Residual Solvents

A possible concern may arise from the use of organic solvents. They are necessary in many fabrication steps of pharmaceuticals. The classic double emulsion approach for microsphere production is one of these. Some methods are also trying to circumvent the application of organic solvents[77,125,180], but the success in lab scale remains limited compared to the convenient and cheap double emulsion method[83,87,177].

In spite of the necessity of their use, organic solvents bear health and environmental risks. If they cannot be abandoned, their removal has to be assured and controlled. The European Pharmacopeia categorizes organic solvents and divides them into four groups[121]: (1) Solvents to be avoided, (2) solvents to be limited, (3) solvents with low toxic potential, (4) solvents for which no adequate toxicological data are available.

Two organic solvents are used during the production process: (a) methylene chloride and (b) isopropanol. Whereas the latter is classified as of 'low toxic potential', methylene chloride is regarded as one of the 'solvents to be limited'. Effective removal of residual solvents, especially of harmful ones, is absolutely necessary for the applicability of pharmaceutical preparations. Therefore, the European Pharmacopeia has set concentration limits according to the hazard potential of the preparations[121]. The maximum concentration is 600 ppm or 6 mg per day in the case of methylene chloride (DCM) and 5000 ppm for isopropanol. Therefore, their residual concentrations in the preparations were to be tested. Gas chromatography has been shown to be a suitable method to determine organic solvents in microparticulate formulations[190,191].

In this work, the concentration of residual DCM was generally found to be below 250 ppm, less than half of the accepted maximum. PEP 0 microspheres (formulation A) contained between 142 and 237 ppm of DCM after the production process (Fig. 3.4-2).

Pegylated polymers showed less DCM retention after the same treatment, residual concentrations were below 150 ppm. Details are given in table 3.4-3. The washing and evaporation steps during microsphere production appear to be sufficient for the removal of methylene chloride in the extent required by the Pharmacopeia. Nevertheless, the removal seems to be easier in microspheres made from pegylated polymers. In this case, the DCM removal is supposed to be ameliorated by better penetrability and lower hydrophobicity of the PEP 5 and PEP 10 microspheres.

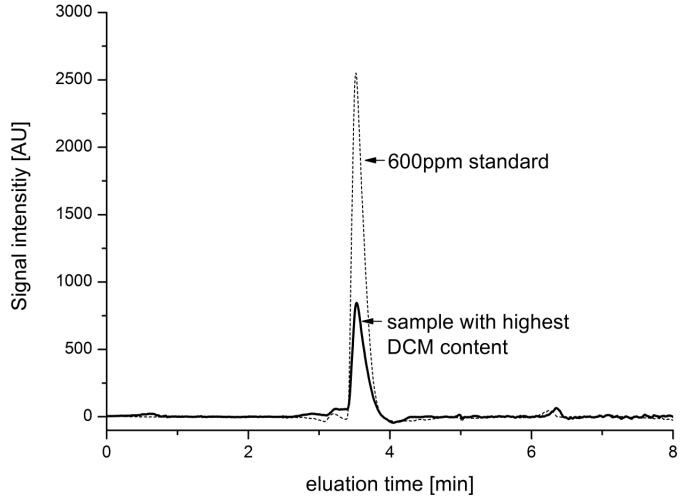

Fig. 3.4-2: GC-FID chromatograms of a 600 ppm standard and a sample of PEP 0 microspheres with the highest residual DCM content.

Table 3.4-3: Concentration of methylene chloride in nine batches of microspheres as determined by GC-FID. Formulations B, D and F were not assessed, because they showed inferior properties regarding morphology and release (chapters 3.5 and 3.6) and were thus excluded from further evaluation.

Formulation	c_{DCM} [ppm]		
A	175	142	237
C	105	87	103
E	148	95	117

In the method used, isopropanol residues would have been detected as well. The isopropanol used in combination with water during the washing process was not found in any of the samples. Hence it can be deduced that isopropanol was not retained at the microsphere surface or removed completely.

3.4.2 Thermal Analyses of Polymers and Microspheres

In amorphous solids like polymers, no melting is observed. A transformation of the substance from the amorph and glassy to a rubbery state occurs. The respective temperature range of this kinetically controlled relaxation process is referred to as glass transition temperature, T_g. The increased polymer chain segment motion accounts for the change of

state[87]. The effect depends on several factors, such as molecular weight, internal strain in the polymer and residual solvents. Water and PEG 400 act as external plasticizers on PLGA. They enhance the movement of the PLGA polymer chains by decreasing the interactions of chains with one another. PVA was reported to be a slight antiplasticizer for the same polymer[192]. This is one of the reasons for its application during PLGA microsphere hardening. It was shown by Reich that particle size, fabrication method and degree of hydration will influence the glass transition[193]. Rouse et al. demonstrated that encapsulated proteins have no significant effect on the glass transition of PLGA microspheres[192]. On the other hand, the diffusion of rhBMP-2 through the polymer matrix will be facilitated in the rubbery state. Thus, it is of great importance to characterize the polymers regarding their physicochemical state.

One standard method for determining the glass transition temperature is Differential Scanning Calorimetry (DSC). For result evaluation, the second heating curve is used, because an influence of the thermal history of the sample can thus be omitted. The obtained midpoints differed articulately between the three unprocessed polymers (Fig. 3.4-3). The PEG moiety of the polymer was found to decrease the T_g and acted as an internal plasticizer. However, a direct comparison was not accomplished due to the differing molecular weights of the utilized polymers. The results are consistent with data on PLLA–PEG–PLLA triblock-copolymers[194].

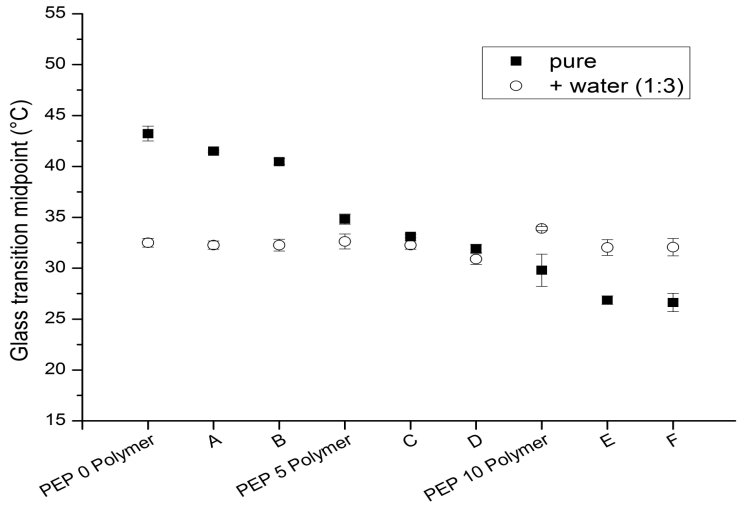

Fig. 3.4-3: DSC: Glass transition midpoints of the different formulations and the respective polymers from the second heating curve. Error bars represent standard deviations of at least three independent measurements.

The influence of the microsphere manufacturing process was comparably low, as T_g decreased only for approximately 2 K. Interestingly, the incorporation of another buffer, *AcPEG*, in formulations B, D, and F was reflected by a further decrease of about 1 K. This effect was attributed to the plasticizing potency of the incorporated PEG 300.

All polymers and microsphere formulations displayed a levelled glass transition of 32.2 ± 0.9 °C, when excess water had been added at the beginning of the measurement. It is speculated that during the first run, water ingressed between the polymer chains during their very mobile state at elevated temperatures and was then effectively acting as a plasticizer. The effect is supposed to be dominated by the interaction of PLGA and water. The PEG of the polymer chain has a higher affinity towards the surrounding water than towards the PLGA moieties and can thus no longer act as a plasticizer for PLGA.

Keeping in mind the huge effect water may display on the polymer behaviour, thermogravimetrical analyses were conducted to quantify the amount of volatile substances within the microspheres. With the precondition of almost complete removal of methylene chloride (chapter 3.4.1), the weight loss below 150 °C may be attributed to residual water, as no other incorporated substances were volatile below this temperature. The highest weight loss (0.70 ± 0.01 %) was detected for PEP 0 microspheres. It gradually decreased with increasing PEG content of the polymer chain. It is speculated that the transport of water from PEP 5 (0.56 ± 0.05 %) and PEP 10 (0.48 ± 0.15 %) microspheres was easier during drying due to the higher chain mobility of these polymers at equivalent temperatures. At temperatures above 285 °C, complete thermal decomposition of the polymers was detected. Less than 0.5 % of the initial weight was found at 600 °C.

The thermal characteristics of microsphere preparations obtained by TG and DSC are close to the unprocessed polymers, indicating a gentle production and a careful removal of methylene chloride and low residual amounts of water.

3.5 Characterization of Drug-Loaded Microspheres

3.5.1 Size Distribution

As demonstrated and discussed in chapter 3.5, a broad variety of parameters is influencing particle size. Size is an important parameter in terms of syringeability and drug release rates[77]. Berkland and coworkers

showed that the size of microspheres plays a key role in both the control of the drug release rate and the polymer degradation rate. They found a faster decrease in the molecular weight of the polymer and more internal pore formation in particles of 100 µm compared to 10 µm particles[195,196]. Higher encapsulation efficiency and more uniform drug distribution are usually achieved in smaller microspheres. This is discussed to be due to faster particle hardening and faster drug entrapment[83,88,196]. Due to all these effects, the need for a controlled particle size and a well-reproducible size distribution becomes obvious. If a uniform particle size, i.e. a narrow distribution, is not achieved, sieving is often chosen as a simple and common technique to obtain a well-defined microparticle fraction[197-200]. However, fractioning in classes of above and below 125 µm as used in other groups[199,200] was not necessary in this case due to careful choice of the production parameters. All of the particles were small enough to fit through cannulae in suspended state during injection. As determined by ESEM, the Feret's diameters were in the range of 5 to 185 µm for all microspheres. None of the particles was larger than 200 µm and only less than 2.5 % of all particles exceeded 100 µm (Fig. 3.5-1).

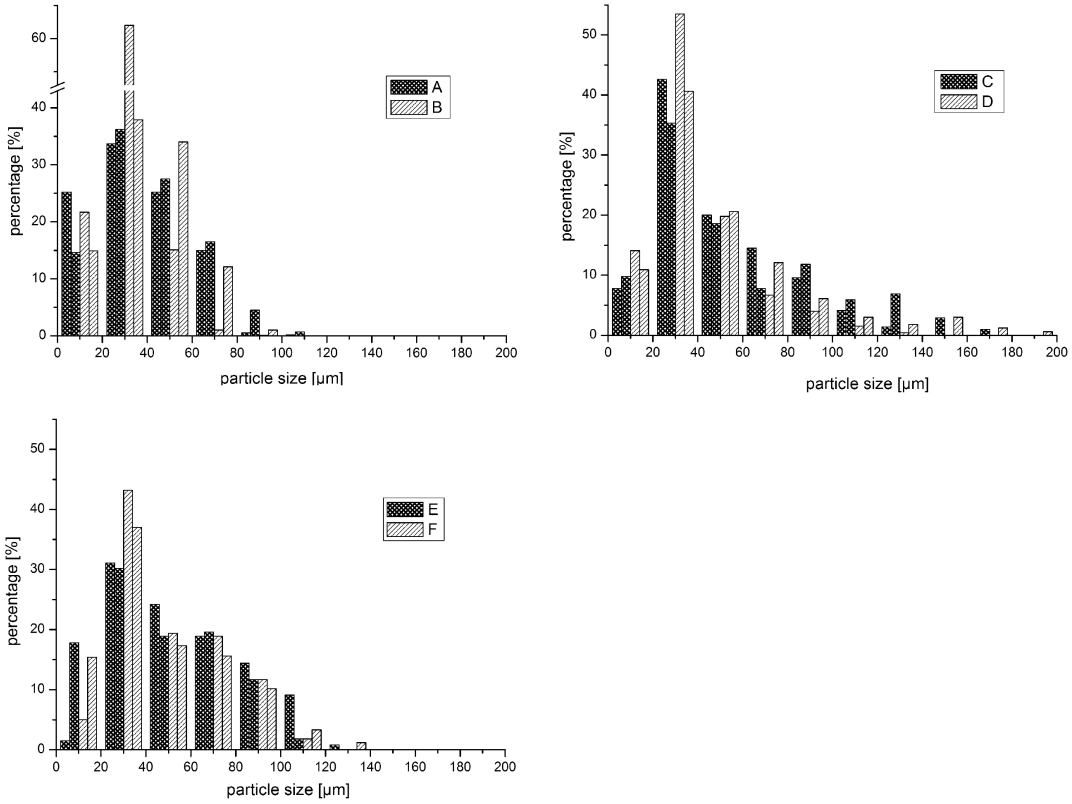

Fig. 3.5-1: Size distribution as determined by means of ESEM.

The size distribution of formulations A and B was rather narrow, with more than 80 % of the particles smaller than 60 µm. In contrast, formulations E and F showed a broad distribution with noticeable amounts of microspheres at least between 20 and 80 µm. However, the uniformity among different batches was very high.

Comparable results were obtained with laser diffraction. An overview of the results of both methods is provided in table 3.5-1. A gradual increase of particle size with an increasing PEG-polymer ratio was detectable in spite of the use of the same preparation method. This may be due to a slower microsphere hardening, providing more time for coalescence during particle formation.

Table 3.5-1: Particle sizes (number weighted mean) as determined by laser diffraction (LD) and environmental scanning electron microscopy (ESEM). Data are given batchwise for LD data and particlewise cumulated from both batches under ESEM investigation. The abbreviations w/o and n.a. refer to 'without' and 'not assessed', respectively.

Formulation	LD		ESEM	
	mean ± SD [µm]	n	mean ± SD [µm]	n
A	37 ± 7	14	39 ± 21	837
A w/o BMP	35 ± 4	8	n.a.	
B	32 ± 4	4	34 ± 16	1770
C	50 ± 9	9	51 ± 30	447
C w/o BMP	50 ± 4	5	n.a.	
D	50 ± 5	3	41 ± 26	640
E	64 ± 10	11	51 ± 27	718
E w/o BMP	67 ± 5	4	n.a.	
F	67 ± 3	3	47 ± 27	644

Free carboxyl ends are responsible for much more intense swelling behaviour than capped polymers[87]. Thus, microspheres prepared from the end-capped PEP 0 are not supposed to increase much in size after dispersion in water, which can be confirmed by a comparison of LD and ESEM measurements.

In contrast, polyethylene glycol-linked PEP 5 and PEP 10 particles possess larger diameters if measured in solution. This indicates either an alteration in optical properties and/or a different swelling behaviour of these particles[201], which is not accessible with ESEM.

By means of ESEM, a gradual decrease of the particle size in *AcPEG* (B, D, F) samples was detected compared to the respective *Ac* formulations A, C and E. In contrast, the presence or absence of PEG 300 or of rhBMP-2 in the inner phase of the particles did not alter the particle size as determined by LD. The aforementioned swelling behaviour may explain the findings.

3.5.2 Surface Morphology

The particles of different polymers varied in shape in spite of the use of one preparation technique (Fig. 3.5-2).

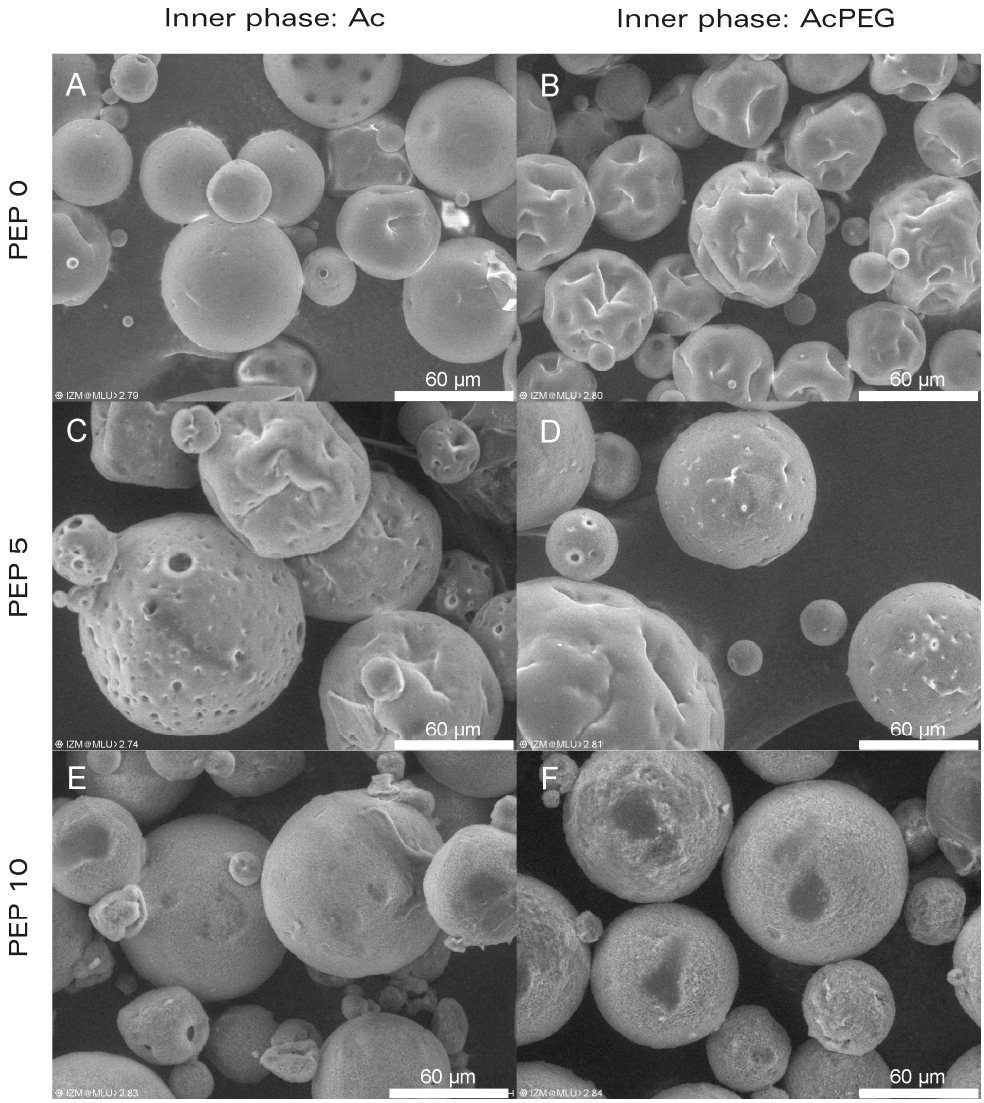

Fig. 3.5-2: Environmental Scanning Electron micrographs of microspheres prepared from formulations A–E. Differences in structure caused by the inner phase composition are most apparent between formulation A and B.

Although the use of PEG as an inner phase cosolvent (formulations B, D, F) did not alter the particle size, it caused differences in the microsphere shape of PEP 0 microspheres. Low processing temperature and low inner phase/ organic phase ratio caused a rapid particle hardening, resulting in a very smooth surface of formulation A. In contrast, a crumpled surface was usually obtained in formulation B, caused by the preparation with *AcPEG*. This crumpling may indicate a loss of volume after the primary skin formation in the nascent particle. No articulate alterations were found in the structure of PEP 5 or PEP 10 microspheres caused by the addition of PEG 300 to the inner aqueous phase. Their immanent increased hydrophilicity due to covalently attached PEG 5000 is expected to superimpose any PEG 300 effect on the surface morphology.

3.5.3 Drug Distribution

Unexpectedly, microspheres of all three polymers showed autofluorescence in fluorescence techniques although chromophores should be absent in the PEG-/PLGA-backbone. The autofluorescence was also detectable in the unprocessed substances. All three polymers exhibited the same background fluorescence spectra, so that the effect was concluded to originate from the PLGA-part of the polymer. Nevertheless, rhoda*BMP-2 was successfully detected within the microspheres. The inner cavities of the rhoda*BMP-2-loaded particles appear much brighter, giving evidence for the localization of the labelled growth factor (Fig. 3.5-3).

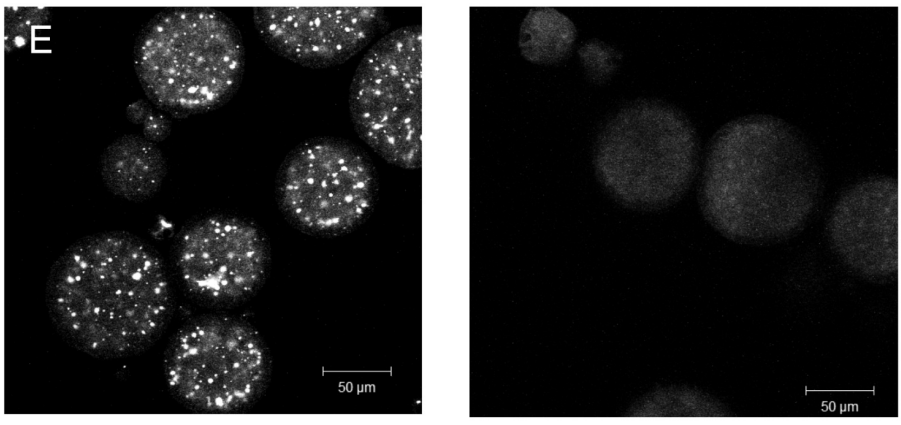

Fig. 3.5-3: Confocal laser scanning micrograph of microspheres with labelled rhBMP-2 (formulation E, left). The labelled dye is well distributed throughout all particles in spherical microdomains. For comparison, the same microspheres without rhoda*BMP-2 pictured as control (right).

The low fluorescence signal detected in the negative controls could be attributed to the autofluorescence of the polymer at a lower wavelength. A comparable distribution was reported by Ding and Schwendeman for a dye conjugated to a dextran of 10 kDa[197]. Van de Weert et al. found similar results for the lysozyme distribution in PLGA microspheres following a cutting and staining approach[202].

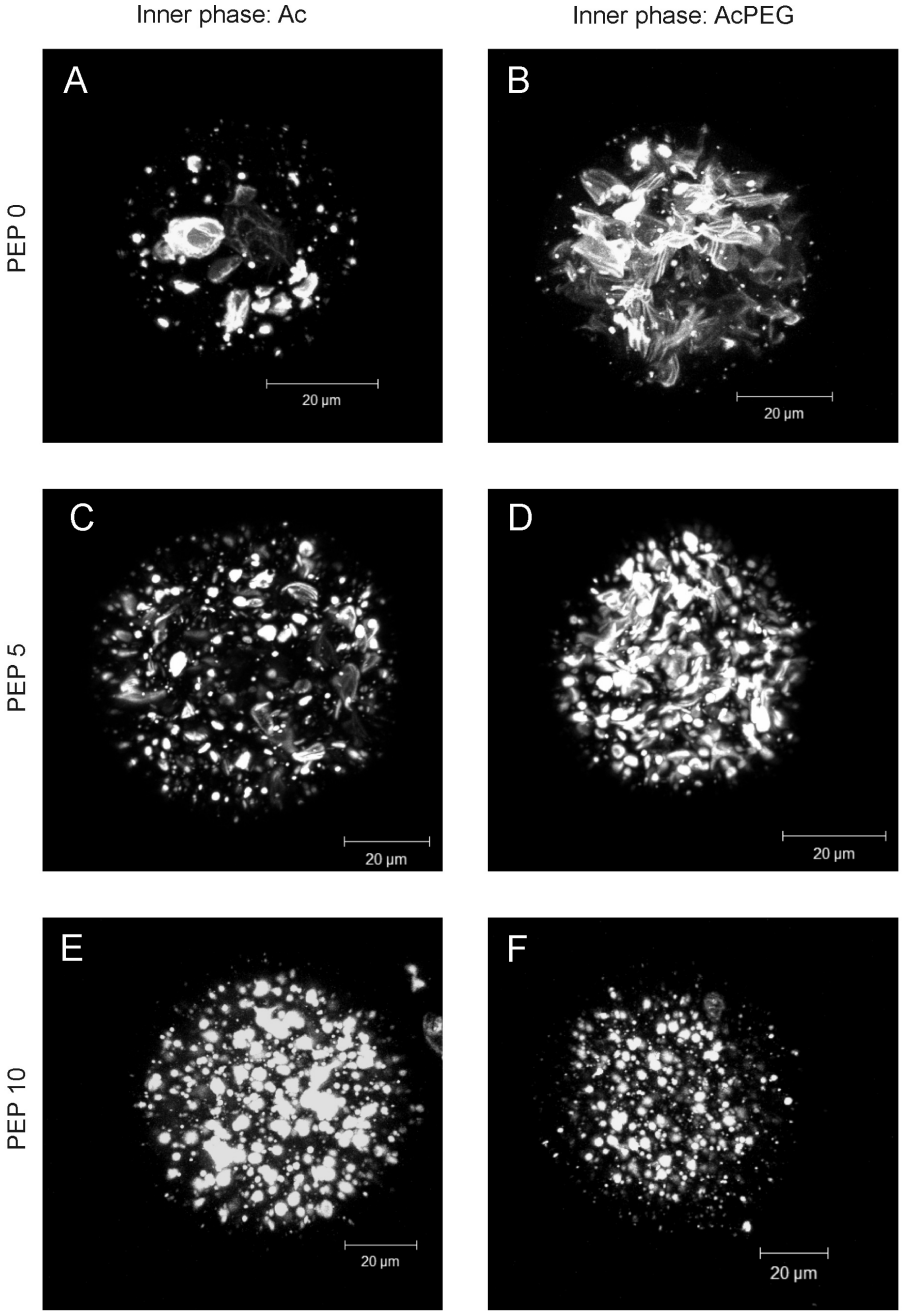

Fig. 3.5-4: Confocal Laser Scanning micrographs of single microspheres loaded with rhoda*BMP-2. Particles consisted of formulations A – F (table 3.4-1). With a lower content of PEG 5000 in the polymer matrix, the influence of PEG 300 on the inner structure increased dramatically.

The influence of PEG on particle morphology and drug distribution was dependent on the combination of the two application modes of PEG, either covalently bound to the polymer backbone or simply added to the primary emulsion. Covalently attached PEG in formulations C and E did not alter the inner phase morphology (Fig. 3.5-4).

In contrast, microspheres with an inner phase comprised partly from PEG (B, D, F) exhibited a rather blurred distribution of the labelled growth factor within the particle. This effect is negligible in preparation F and most apparent in formulation B. Here, and to some extent also in formulation D, the use of *AcPEG* led to a partial loss of the spherical microdomains. It is hypothesized that PEG 300 interferes with PLGA chains during emulsification and particle formation as it may also be used as solvent for PLGA in higher concentrations[109,203,204]. Moreover, it has been reported that the local accumulation of PEG near the aqueous/organic interface can enhance interfacial turbulences[205], which may be reflected by the structural changes in the microspheres visualized by confocal laser scanning microscopy. Malzert-Fréon and coworkers reported an unwanted spontaneous formation of an emulsion at the DCM/water interface after the dissolution of PEG 2000 in water. The authors concluded that this might influence the formation of a stable primary emulsion[186], which may also contribute to the alterations of inner phase morphology reported in this study. It is obvious that these structural changes contribute to variations in drug release, which will be elucidated in chapter 3.6.

3.5.4 Encapsulation Efficiency

The encapsulation efficiency is an important parameter for the quality of the microsphere fabrication process. A very low encapsulation efficiency may render an otherwise successful and effective treatment uncompetitive due to a dramatic increase in costs for active ingredients lost during fabrication. One advantage of double emulsion techniques is the usually high encapsulation efficiency into PLGA[86].

One common method for the determination of entrapment rates is the measurement of radioactively labelled protein[91], which requires special equipment besides environmental concerns. Dissolution and extraction of the particles in organic solvent/ sodium dodecylsulphate mixtures may also be used[206,207]. Several different alkaline approaches can be applied[208], but due to the untypical solubility and stability profile of rhBMP-2, none of these techniques was promising. Furthermore, the complete digestion of PLGA microspheres with aqueous sodium

hydroxide in the presence of sodium dodecylsulphate is very destructive down to the primary structure of the protein[89]. An acidic degradation of the polyester would also be reasonable to break down the polymer and release and quantify the entrapped protein. However, a good stability of PLGA was found between pH 3 and pH 7, and the acid-catalyzed saponification of PLGA under harsh conditions for proteins (pH 1.6) was reported to be much slower than with alkaline approaches[209,210]. A few reports can also be found on enzymatic degradation of polyesters[211,212], but the use of enzymes did accelerate the polymer decomposition rate only marginally. Besides the need for standardization of the enzymatic activity and protection of the entrapped growth factor, the incompleteness of degradation within a short period of time renders this approach not promising.

Encapsulation efficiency data obtained with different techniques vary considerably. Wischke et al. described an encapsulation rate of 78.7 ± 5 %[172] for bovine serum albumin into small PLGA microspheres, measured with UV spectroscopy in the supernatant after dissolving the microspheres. Choi and Park[206] found an encapsulation rate of 86.9 % for G-CSF in RG 502 H particles. For rhBMP-2 encapsulation into PLGA microspheres, only few data are available. Kempen et al. estimated 85 % of rhBMP-2 to be encapsulated into PLGA microspheres by a radiolabelling approach[91]. Ruhé et al. found comparable results (78 ± 9 %)[90]. Shi et al. reported to have encapsulated more than 90 % without further specification[74]. High values, ranging from 72 to 99 %, have also been reported for other pegylated polyesters[194]. The only approach based on fluorescence spectroscopy was published by Isobe and coworkers, who found 91 % of initially used rhBMP-2 entrapped in their microcapsules[92].

In this study, the amount of encapsulated rhBMP-2 was calculated from remaining fluorescence activities in the outer phase of the double emulsion and the washing water (2.2.2; 2.5.4). Mean encapsulation values are given in table 3.5-2.

Table 3.5-2. Rhoda*BMP-2 encapsulation efficiencies into microspheres of different formulations. Data are shown as mean ± standard deviation.

Formulation	Encapsulation Efficiency [%]	n
A	95.0 ± 4.7	6
C	97.1 ± 1.5	6
E	97.5 ± 0.6	5

The outer phase contained between 0.9 and 11.7 % of rhoda*BMP-2. In the washing water, 0.3 to 4.8 % of the initial rhoda*BMP-2 concentration were found. The reported encapsulation efficiency data are in the higher range compared to the literature, but it has to be kept in mind that data determined by differential methods tend to be higher compared to extraction measurements. Sah described an underestimation of encapsulation with extraction techniques because of protein loss during the extraction process and incomplete extraction steps[208]. The propensity of rhBMP-2 to interact non-specifically with hydrophobic surfaces may also decrease the loss into a second aqueous phase and will thus favour both high encapsulation and lower extraction.

3.6 In Vitro Release Studies

Release determinations from microparticulate delivery systems are more complicated than conventional delivery systems. Methods defined by the European Pharmacopeia are not applicable. The *in vitro* release of protein entrapped in PLGA microspheres does not necessarily correlate well with the *in vivo* response[89], because numerous factors may change the outcome[77,89,197,213]. Those factors include:

(I), the utilized PLGA (molecular weight, composition, endcapping, residual amount of metallic catalyst, possible modifications),

(II) the kind of protein (protein molecular weight, amino acid composition, isoelectric point),

(III) the formulation (size, size distribution, surface and internal morphology of microspheres, protein encapsulation efficiency, addition and type of excipients and residual moisture content of the microspheres),

(IV) experimental factors (volume and buffer capacity of incubation medium, amount of microspheres in the incubation medium, use of sink or non-sink conditions, release temperature, type of agitation, method of sampling for released protein, type of sample storage and method of protein quantification),

and (V) protein stability (covalent aggregation via thiol oxidation, non-covalent aggregation by hydrophobic interaction, non-specific protein adsorption onto polymer surface, ionic interaction between PLGA and protein, peptide hydrolysis, deamidation, oxidation).

Pretests showed that rhBMP-2 of lower concentrations in glass containers led to almost immediate adsorption of the protein to the container wall, whereas polypropylene vessels caused less problems. Sah described a protecting effect of 0.5 % BSA in ovalbumine and in lysozyme solutions[214]. However, the precoating of the release vessels with 1 % BSA did not protect the protein against adsorption. Consequently, uncoated polypropylene vessels were used during the following experiments.

3.6.1 *In Vitro* Degradation of Microspheres

The *in vitro* degradation of PLGA and PEG-PLGA has been investigated by numerous groups and techniques[107,197,215-217]. The saponification of polymeric ester bonds occurs randomly throughout the particle with higher probability in more acidic regions[128], resulting in an autocatalytic process in the core. Emerging monomeric acids accumulate within the PLGA microspheres[107,197,218]. The introduction of PEG results in a faster water penetration into the polymer, thus enabling a fast exchange of hydrophilic molecules between the polymer and the dispersant. Polymer degradation and erosion occur initially faster, but in more linear kinetics than with PLGA. The fate of pure PLGA systems is characterized by a slow degradation onset and by a delayed yet very intense particle erosion when the polymer becomes water soluble due to the decrease in its molecular weight. Both processes show articulately non-linear kinetics in PLGA microspheres. The molecular weight loss of the polymer can be monitored by means of size exclusion chromatography[196,212,218], and mass loss of larger devices may be investigated gravimetrically[218,219]. As the degradation products of polyesters are acidic, a pH profiling is also useful to obtain information on the development of the degradation process. In contrast to PEG-PLGA, the diffusion through PLGA is less facile for monomeric and oligomeric degradation products, so that a lower pH decrease in the surrounding medium may be expected in the first weeks.

3.6.1.1 pH Profiling

The pH profiles of the release medium exhibited a large drop of the pH value in both pegylated formulations and much less pronounced for the PEP 0 microspheres (Fig. 3.6-1). Within four weeks, the pH of the buffered release medium had dropped to less than 4 in both PEP 5 and PEP 10. The decrease to pH 5.8 in PEP 0 microspheres is in good

accordance with values determined for comparable polymers by Witschi and Doelker[125]. Incorporation of acid-base indicators, or fluorescent dyes, as well as EPR measurements have been utilized to monitor the pH inside PLGA microspheres[88,107,215-217]. In all approaches, a considerable accumulation of acidic products was detected over time. The particle degradation may be accelerated in larger particles compared to smaller ones due to acidic degradation residues, even in the microsphere scale investigated in this study[77,196]. The diffusion rate of polymer degradation products through the polymer phase decreases with increasing molecular weight of the used polymer[77]. However, microspheres can be expected to degrade much more homogeneously compared to larger devices of PLGA, because of the shortness of diffusion distances[220].

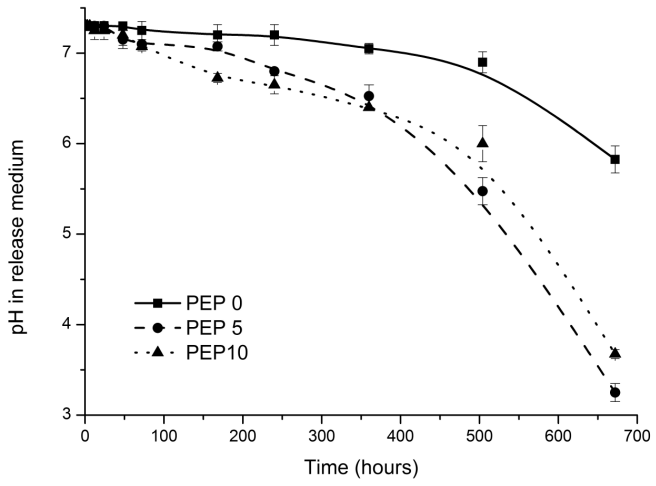

Fig. 3.6-1: Time dependence of the pH in the medium under *in vitro* release conditions (for details, see chapter 2.6.2). The pH decrease in the release medium was significantly higher with pegylated polymers.

PEG-blended polymers have been reported to yield microspheres with less intense acidification during degradation[197]. Kissel et al. found a faster degradation onset and a slower degradation rate *in vitro* for microspheres of PEG-PLGA triblock polymers compared to microspheres made from PLGA of comparable molecular weight[194]. It is assumed that a better transport through the more hydrophilic pegylated particles PEP 5 and PEP 10 may enable a faster removal of acidic degradation products out of the particle into the release medium. Due to the low volume, the buffer capacity was not sufficient in this case to compensate the pH drop.

3.6.1.2 ^{1}H-NMR Experiments

^{1}H-NMR data were acquired in deuterium oxide, because a very low solubility of the polymers and degradation products of higher molecular weight is known in this medium. Consequently, the non-detection of a high percentage of polymer hydrogen atoms will enhance the probability to detect the well-soluble monomeric acids that emerge during the degradation process. The main drawback of the applied method is the peak of oxygen-bound hydrogen, which is dominant due to a fast exchange of acidic protons with the deuterium ions of the solvent. The oxygen-bound hydrogen peak also impedes the detection of the hydroxyl groups that would arise during saponification. The carboxylic hydrogen of monomers is virtually undetectable due to its acidic nature. In general, four different kinds of hydrogen atoms can be existent in the samples (Fig. 3.6-2). Depending on the shielding intensity of surrounding electrons, different chemical shifts can be expected. Highly shielded, electron dense groups will have a low chemical shift and are referred to as upfield. In figure 3.6-2, the letters besides the hydrogen atoms, beginning with a, symbolize growing chemical shifts. The characteristic effect of spin-spin-coupling alters the appearance of a single peak according to the number of its surrounding, resonant neighbours and therefore enables conclusions on the molecule structure.

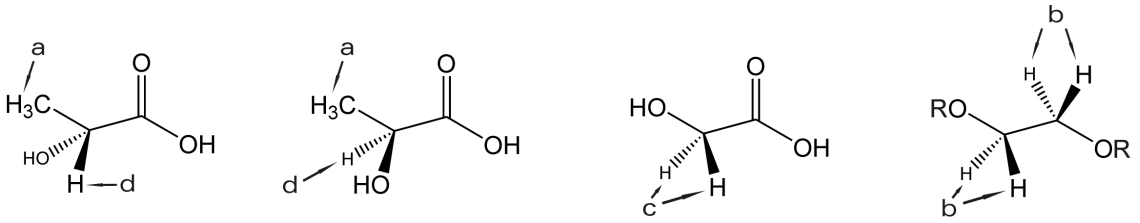

Fig. 3.6-2: Depiction of the four different expected species of hydrogen in ^{1}H-NMR spectra.

In spite of plenty of information available for other solvents, few data can be found of the relevant functional groups of PLGA or PEG-PLGA in deuterium oxide[221-225]. The observed chemical shifts and peak splittings corresponded well with the literature data (table 3.6-1). Polyethylene glycol as an ether is expected to be stable under the given conditions, so that a breakdown into ethylene glycol monomers was improbable. However, besides the larger PEG singlet at δ 3.70 ppm, which has been

described by several other groups[221,223,224], a smaller peak shifted highfield was detected (Fig. 3.6-3).

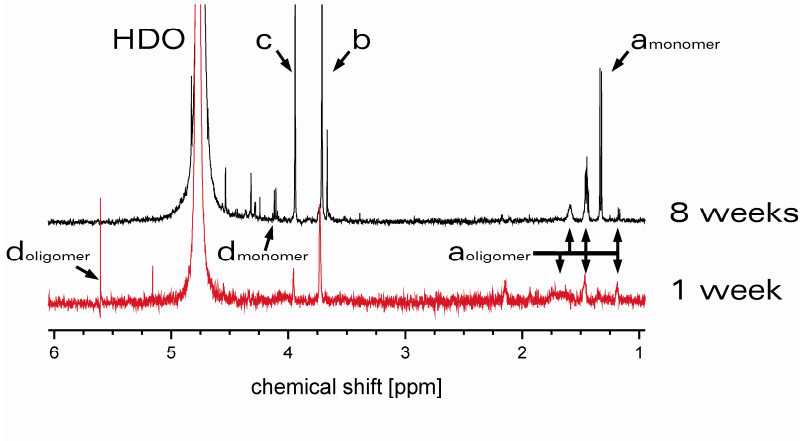

Fig. 3.6-3: Typical NMR spectra of PEP 5 microspheres after one and after eight weeks of incubation under release conditions.

Table 3.6-1: Chemical shifts of the four different species depicted in figure 3.6-2 as measured in the monomer and attributed to oligomers.

Hydrogen species	Peak form in the monomer	Chemical shift		
		Monomer	Oligomers	Literature data
a	doublet	1.37	1.17; 1.44; 1.65	1.2-1.5; 1.43, 1.55, 1.6
b	singlet	3.70	3.70	3.65; 3.68; 3.7; 3.70
c	singlet	3.94	3.94	
d	quadruplet	4.21	5.57	5.2

This peak may be explained by PEG still linked to polyester parts. Data were acquired for all three polymers, PEP 0, PEP 5 and PEP 10. There were, except of the expected intensity difference of peak b, no articulate variations between the different formulations, so that the results are discussed below for all three species together.

Hydrogen atoms originating from PLGA or its degradation products were found in the expected range, their identity was proven by spiking samples with the respective monomers. Articulate shifts between monomeric and oligomeric degradation products were found in hydrogen atoms of lactic acid. The presence of two different peaks or peak series can sometimes be attributed to different species of one group. Heald et al. describe a double doublet of the methyle group in PEG-PLA at around δ 1.43 and δ 1.55 ppm and explain this peak formation with the presence of both isomeric forms of lactic acid in the

block polymer[224]. Both peak formations were detected in the samples, but neither of these doublets was found to increase in intensity after spiking with D,L-lactic acid.

A third doublet around δ 1.37 ppm, appearing after incubation in the release medium, showed superposition with the methyle group of a lactic acid standard. This third doublet was hence regarded as the methyle group in lactic acid monomers (a). First traces of this peak were detectable after 8 days of incubation, which may be regarded as rather fast. As expectable, the doublet area kept increasing until the end of the experiment after eight weeks. Even at this date, however, the peak area of the monomer was smaller than the peak area sum of the oligomer peaks in all three polymers.

The *in vitro* degradation is usually slower than decomposition processes *in vivo*, which may be explained by enhanced plasticity and contribution of enzymatic degradation *in vivo*[87]. Furthermore, shear stress of different intensities may be applied to the implant depending on the application site. An aggregation of microspheres and the tissue retention of acidic degradation products and a consequential increase of autocatalytic processes was proposed as another reason for faster *in vivo* degradation[219]. Particle aggregation may be minimized by dispersion in a viscous dispersant, as performed in this study, which should ideally provide a buffering environment.

3.6.2 Release Determination

PLGA microparticle release times are described from 1 week up to 4 months, with the majority of examples ranging from 4 to 6 weeks with polymers like PEP 0[87]. Hence, *in vitro* release profiles were assessed for a period of 28 days. No specifications are made for the release determination of long time release microspheric systems in the European or American pharmacopeiae[87,219]. Usually, the use of *in vitro* systems with sink conditions is propagated[87,213,226]. However, non-sink conditions close to the solubility maximum have been shown to have a negligible influence on the release outcome[183]. In this study, sink conditions were not desirable due to the low *in vivo* solubility of rhBMP-2 and the limited volume of the *in vivo* administered gel (chapter 3.9) to which the growth factor was supposed to be released first[219]. Lagarce and colleagues also omitted sink conditions due to the nature of their microspheric system dispersed in chitosan gel or other gel systems[227]. The addition of polysorbate 20 to the release medium was not only beneficial for the stability of rhBMP-2 in the release medium,

but also mimicking *in vivo* conditions where a multitude of surface-active substances can be found[87,195].

The quantification of released growth factor is often performed by means of radioactive labelling and detection of the marker over time[57,58,76,90,91,228-235]. However, this approach was not chosen for the study because of known limitations regarding sensitivity to changes of protein conformation or aggregation. A further limitation is the possible detachment of the radioactive tracer from the growth factor[91]. Uludag reported fractions of up to 10 % which were not precipitable by trichloroacetic acid and thus have to be regarded as not linked to protein[39]. It remains unclear whether rhBMP-2 linked to radioactive iodine represents bioactive rhBMP-2. The release data of ^{125}I do most likely reflect a mixture of both bioactive and bioinactive rhBMP-2, rendering the gain of information on released bioactive growth factor merely impossible. Mathematical models to predict release rates have also been developed and were shown to work well for small molecules and model compositions[236-238]. However, the number of necessary assumptions is rather high. It has been shown by means of confocal laser scanning microscopy, that the microspheres in this study did not contain the growth factor randomly dispersed, but in spherical microdomains (chapter 3.5.3), which does not match the preconditions of the modelling protocol. A fluorimetric estimation of release of purified native BMP-2 was reported by Isobe et al.[92], but has basically the same bottlenecks as the iodine labelling approach. Enzyme-linked immunosorbent assays may provide much more information on the release pattern and will be able to detect at least more intense alterations in the protein structure. The used ELISA kit is based on the sandwich method, so that at least two epitopes of rhBMP-2 had to be linked together, to be intact and still exposed, thus artefacts can be largely excluded[239]. The specificity data provided by the manufacturer did not show any significant crossreactivity with relevant members of the TGF-β superfamily. Even with rhBMP-4, the protein with the highest structural homology, as little as 1.2 % of crossreactivity was observed[122]. It can therefore be assumed that all detected signals were derived from incorporated and released rhBMP-2. The cellular responses *in vitro* and *in vivo* (chapters 3.6.3 and 3.9.2) provide final information on the bioactivity of the released molecule.

For the release calculation, the dilution factor, the weight of the microspheres, the protein stability as determined above and the dilutions due to the sample taking regime were taken into consideration. All release profiles appeared more or less biphasic. In an initial burst phase, about one third of the amount found during the investigated

period was released within the first 24 hours. A second increase in the release rate was detectable after approximately ten days (Fig. 3.6-3). It is very likely that a noticeable amount of rhBMP-2 was not detected by ELISA because of the freeze-thaw loss demonstrated in chapter 3.3.3.

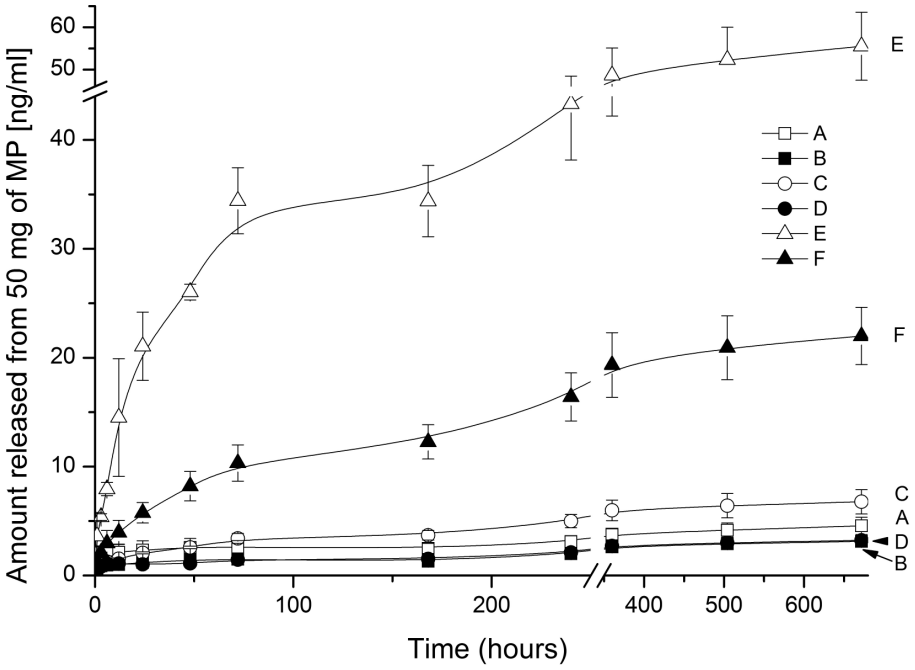

Fig. 3.6-4: Release profiles of microspheres as determined by ELISA and corrected for a loss constant of rhBMP-2 in release medium. Error bars represent standard deviation.

Profiles with an initial burst release and lower release rates after several hours are very frequently found[58,67,74,89,177,240,241]. In most cases, a burst release is undesired, although other views have been stated[52,59]. Smaller particles have been shown to yield higher release rates during the first hours, attributed to the tremendously increased surface area[177]. Boury and coworkers postulated that the burst effect of a protein released from PLGA microspheres is not to be explained with adsorption to the surface but is due to the leakage of protein from regions bordering the surface[177]. This appears logical with the background of less than 5 % of rhoda*BMP-2 removable in the intense washing process. The very low solubility of the incorporated rhBMP-2 in the polymeric phase will impair its diffusion through this phase[88]. The diffusion of the growth factor through water-filled pores is thought to be a major drug release mechanism in PLGA microspheres[77,242]. Hence, both the formation of water-filled pores and the release of protein from the microspheres will be dependent on polymer degradation.

The release profiles were comparable to findings reported by Kempen et al.[231] Interesting differences were found between the release rates of the three polymers. A higher PEG content in the polymer matrix, such as 10 % in PEP 10, was found to yield significantly higher release rates than lower PEG contents in the polymer matrix. PEP 5 is intermediate with regard to the slight increase in the release rates compared to PEP 0. The use of *AcPEG* instead of *Ac* as the protein solvent generally led to a decrease of protein release, especially during the first hours. The profile shapes did not differ apparently, whereas the total amount released was decreased by 30 to 60 % compared to the respective formulation without incorporation of PEG 300. These findings are consistent with data reported by Dorati et al. for coencapsulation of ovalbumine and PEG 400[243]. Out of 225 ng of rhBMP-2 detectable per release batch, between 3 and 60 ng were found during release measurements. This may appear low compared to the data reported by other groups, but it has to be taken into account that most release measurements were performed with radioactively labelled rhBMP-2[57,58,76,90,91,228-235] with all the limitations mentioned above.

An incomplete release of protein from PLGA or triblock PEG-PLGA is very common[89,137,244-246]. It was attributed at least in part to the higher polymer/ inner phase ratio[77] among general instability issues[180]. It has also been supposed that a higher molecular weight of PLGA may be a reason for a lower and incomplete release[76]. Duggirala et al. described that rhBMP-2, which is adsorbed tightly to PLGA, will not be released as long as the polymer is not degraded. The authors were able to quantify the amount of protein which was entrapped in those microspheres and found 98 % of the expectable rest still in the particles[247]. After four weeks, rhoda*BMP-2 was still detectable *in vivo* (chapter 3.9-2), indicating a slow release due to dense microsphere composition going along with microsphere degradation.

Higher release rates of PEP 10 may result from a faster degradation onset. Furthermore, the shorter polymer chain and the presence of a PEG block in the polymer both increased the permeability of the spheres and possibly retained a less hydrophobic environment during microsphere formation. The high molecular weight PEP 5 still shows slightly higher release rates than PEP 0, supporting the idea of increased permeability in the presence of a PEG block. In contrast, the addition of PEG 300 to the inner phase during microsphere formation appears to be unfavourable for rhBMP-2 stability, yielding lower release rates and less defined drug distributions within the microspheres.

Lagarce and coworkers showed that the burst release of a small molecule, baclofene, can be effectively reduced by mixing microspheres with dispersants of higher viscosity, such as polyvinyl alcohol solutions or chitosan gel systems[227]. Although not tested explicitly in this study, it is most likely that the release rate of rhBMP-2 from the microspheres will be slowed down further by the higher molecular weight of the growth factor. Furthermore, a lower diffusion coefficient for rhBMP-2 in the gel matrix is expected compared to baclofene.

3.6.3 *In Vitro* Activity of Released rhBMP-2

For the determination of rhBMP-2 effects, the quantification of alkaline phosphatase induction is an ideal surrogate: Alkaline phosphatase is the most prominent marker enzyme for osteogenic differentiation. Thus, the differentiation into the osteoblast lineage can easily be monitored by following the induction of alkaline phosphatase, an enzyme which is regarded as an early marker for osteoblast differentiation[248].

The C2C12 mouse myoblasts used in this study grew adherently on the well bottoms. The addition of microspheres results in a decrease in growth area for the cells. Approaches with the direct insertion of microspheres into the wells were not successful. Transwell plates were used to circumvent the limitation of growth space, so that the cells were not impaired in growth by particles or scaffolds on the well ground[166,231].

In all investigated samples, bioactive rhBMP-2 was successfully encapsulated. Interestingly, the amount of bioactive rhBMP-2 released from the various microsphere formulations differed not as much as determined by ELISA. Again, PEP 10 yielded better results than PEP 5, causing an ALP induction of 0.85 $dEmin^{-1}\mu g^{-1}$ at an equivalent concentration of 2.6 nM. Surprisingly, the ALP induction with rhBMP-2 released by PEP 0 microspheres did not differ significantly from the PEP 10 value. An overview is provided in table 3.6-2.

Table 3.6-2: Rates of alkaline phosphatase induction.

Formulation	ALP induction [$dEmin^{-1}\mu g^{-1}$]
A	0.96
C	0.52
E	0.85

The induction of alkaline phosphatase was in the expected range for the pegylated microspheres but surprisingly high for the non-pegylated polyester PEP 0. Due to the instability of rhBMP-2 in the release medium and the loss due to freezing and thawing, the obtained equivalent concentration for PEP 0 is slightly higher in the cell assay than the calculation from the release study. It is hypothesized, that the microspheres made of pegylated polymers may release to some extent rhBMP-2 which is still detectable by ELISA in spite of being not bioactive anymore. However, a full answer to bioactivity shall be given by the *in vivo* investigations.

3.7 Microspheres in Scaffolds

Microspheres offer great opportunities for the combination with several devices and systems used in Bone Tissue Engineering. In this work, the combinability of microspheres with scaffolds as well as with injectable systems was tested. The ESEM pictures revealed a good distribution of the microspheres within the scaffold. Microspheres were dispersed throughout the whole scaffold matrix (Fig 3.7-1).

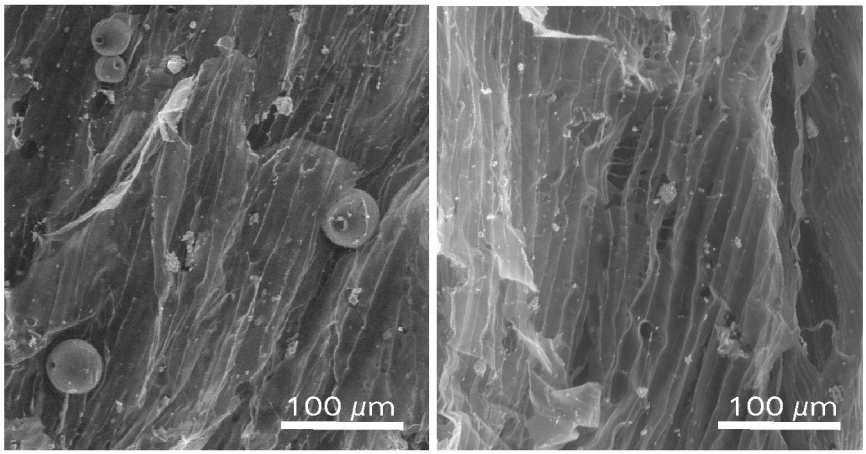

Fig. 3.7-1: Environmental Scanning Electron micrographs of PEP 0 microspheres dispersed within a scaffold prepared from collagen, chitosan and hydroxylapatite (left) and of a similar scaffold without microspheres (right).

A slightly higher amount of microspheres was found near the outer rim of the construct, probably due to the forces during shaking and/or shock-freezing. The physical stability of the obtained construct was

rather poor[71,140] and the standard method used for stability improvement (145 °C; 6 h, 9 mbar) was not applicable. High temperatures would harm both polymer and protein. Further attempts to improve the scaffold stability with incorporated microspheres should involve enzymatic crosslinkers like transglutaminase, which have been successfully tested with pure scaffolds[140]. The structure of the scaffold was virtually unaltered by the addition of microspheres. By means of ESEM, no changes could be found in the microsphere structure. Alterations of the release behaviour due to the freeze-drying process and the surrounding scaffold matrix appear most likely. They have to be investigated thoroughly in the further development of this combined drug delivery system. Nevertheless, the principle of microsphere incorporation was shown to be applicable for the studied scaffold fabrication method.

3.8 Microspheres in Gel

Combinations of microspheres with two different gel systems, (I) chitosan-based *in situ*-forming implants, and (II) hydrophobically modified hyaluronic acid gels, were characterized.

3.8.1 Chitosan-based *In Situ*-forming Implants

Chitosan is a safe and biodegradable material[249,250]. It is usually obtained from crab or shrimp chitin by N-deacetylation[250,251]. Its use is well-established in tissue engineering, e.g. as carrier for stem cells, for articular cartilage repair or as scaffold component in bone tissue engineering[74,250,252-256]. Chitosan gels are excellent materials for the growth and proliferation of various cell types including chondrocytes[250] and osteoblasts[257]. Moreover, chitosan has been shown to be osteo-inductive itself[253,258]. Oliveira et al. showed the engineering of bone through endochondral bone formation on the basis of chitosan scaffolds seeded with chondrocytes[259]. Chitosan has been used in combination with rhBMP-2 before. Park et al. demonstrated enhanced cell attachment of MC3T3 mouse osteoblasts and BMP-2-coated chitosan membranes compared to chitosan alone[257]. Engstrand et al. described superior osteoinduction of BMP-2 in chitosan/heparin compared to BMP-2/ collagen type I combinations[253]. This may be explained by a better retention of rhBMP-2 in a heparin-containing matrix[114,149,260]. On the other hand, heparin and derivatives have been shown to reduce the number of osteoblasts, to decrease the collagen synthesis *in vitro* and

to increase bone resorption[260-262], so that the superiority of chitosan/heparin over collagen type I in the reported data is likely due to chitosan effects alone. Immobilization of rhBMP-2 to a chitosan membrane was shown to be beneficial for the attachment, growth and differentiation of osteoblasts[257].

The gel formation process of chitosan–β-glycerophosphate mixtures is not fully elucidated yet. The group of Leroux surmised it to be a process based on the electrostatic interaction of cationic chitosan moieties with anionic β-glycerophosphate (βGP). Subsequent hydrogen bonding between the less repulsive chitosan chains after neutralization of the chitosan solution by βGP and hydrophobic interactions between chitosan chains[263] are supposed to contribute to gel formation. Chitosan gels were reported to be formed depending on concentration and temperature. Other parameters contributing to gelation are the degree of chitosan deacetylation, the molecular weight of the macromolecule and the type of anions present in the sol[264,265]. Sols containing chitosan with higher deacetylation degrees are reported to have a faster and less temperature-dependent gelation. Ruel-Gariepy et al. reported that gelation also occurred in highly deacetylated samples within one day when kept at room temperature[263]. The chitosan used during this study had a deacetylation degree of 95 %, so that the combination of chitosan and βGP was refrained from until 20 minutes before application. The combination of sol and microspheres was challenging in terms of homogeneity, applicability and microsphere loss. Low microsphere injection rates were achieved in study #4 when the weighed particles were mixed with the sol components in the reaction vessels and transferred into 1 ml syringes. A caking of the microspheres in the syringe was seen during injection (Fig. 3.8-1). About one fifth of the initial dose reached the implant site. Consequently, the preparation mode was altered. In the optimized method (abbreviated ‘opt’), microspheres were directly weighed into a 5 ml disposable syringe with removed piston. Into this syringe, the freshly prepared chitosan-βGP sol was injected and both components were thoroughly mixed. Before application and after needle change, a minor amount of gel was ejected to fill the needle prior to injection. Now, neither caking nor deposition of microspheres in the tip region were detected and the injections could be carried out without further loss and with high dose accuracy. During the *in vitro* investigations, a high gel rigidity after setting was observed with the chitosan gels.

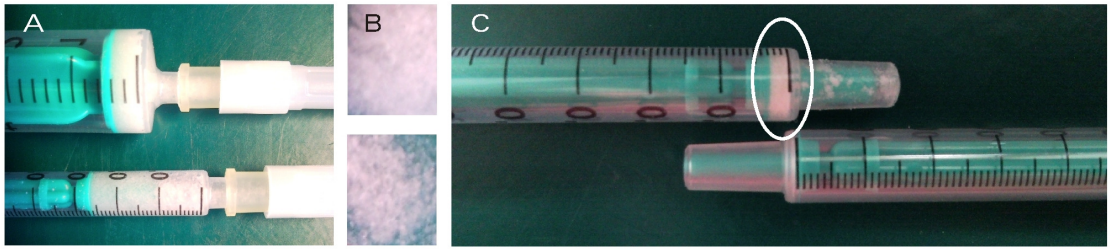

Fig. 3.8-1: Comparison of 'standard' and 'optimized' application procedure. Different syringes used for the application of the drug delivery system (A). Whereas a complete delivery of microspheres was achieved with the 5 ml syringe (B), the decreased microsphere concentration in the ejected gel fraction of the 1 ml syringe was visually detectable. The small piston of the 1 ml syringe produced a cake of microspheres (C).

3.8.2 Hydrophobically Modified Hyaluronic Acid Gels

As an alternative to chitosan-based implants, modified hyaluronic acid (HA) gels were investigated. HA has been crosslinked and/or hydrophobically modified to overcome its low *in vivo* stability and fast degradation in the native state[144]. Problems with crosslinking arise from unwanted side products, the retention of crosslinking agent within the matrix and its possible leaching therefrom[266]. HA-based BMP-2 delivery systems have been used previously in bone tissue engineering with heterogeneous results[51,267-271]. While Maus and coworkers did not find any beneficial effect after application of non-modified HA with rhBMP-2 in sheep femoral defects[267], Kim and Valentini reported good *in vitro* results with scaffolds prepared from hydrophobically modified hyaluronic acid (HHA)[269]. Itoh and coworkers described an enhancement of orthotopic bone formation in a non-defect model when rhBMP-2 and HA were combined on a titanium carrier and compared to rhBMP-2 immobilization on the titanium carrier alone[270]. The most promising results were published recently by Luca et al[271]. The authors reported superior results for high doses of rhBMP-2 delivered in hyaluronic acid compared to a chitosan gel.

In this study, the HHA gels loaded with microspheres were applied by using the modified method described in chapter 3.8.1. Microspheres were easily incorporated to obtain homogeneous, well-applicable mixtures which were. HHA gels tended to be softer than chitosan gels in *in vitro* handling, thus they could be syringed when swollen and appeared to be less rigid.

3.9 In Vivo Investigation of Loaded Microspheres

In vitro measurements are capable to define the influence of a single or of few parameters in a model environment. The complexity of interactions between the drug and the delivery system on the one hand and the organism on the other hand makes the *in vivo* evaluation the most meaningful step in the development of a drug delivery system. Due to the expected bone-inductive effect of the incorporated active ingredient, the use of surrogate parameters was not necessary. Bone formation has been studied in various models, ranging from rodents to larger mammals, and by a multitude of different systems, including ectopic bone formation[167,259], orthotopic non-critical[272,273] and critical size defects[3,41]. The creation of critical size defects and the assessment of their healing is closest to the clinical situation[3]. However, ectopic bone formation is frequently found to be more difficult and less extensive than in orthotopic sites[37,91], so that a good outcome in an ectopic model renders a clinical success very likely. An ectopic site allows the studying of the osteoinductive potential of the delivery systems without interference of osteoconduction or periosteal bone formation. A mouse ectopic model was selected, because the efficiency of the treatment can be demonstrated well in this model[167,259,274], and no surgical procedures were necessary.

3.9.1 Injection of Microspheres dispersed in Liquid

The PEP 0 particles were easily dispersed within the physiological saline (2.9.2). The administration of the suspension was facile. Unfortunately, the microspheres were not detectable by OI *in vivo* in spite of the incorporated rhoda*BMP-2. Two explanations are considered. Either the intensity of the rhoda*BMP-2 fluorescence signal was not sufficient, or the particles diffused too fast from the site of injection, so that an initially sufficient local intensity diminished too quickly. Consequently, both issues were addressed in the second animal experiment. The fluorescent dye was changed, and the particles were dispersed in an *in situ*-forming implant to slow down the diffusion of the microspheres.

3.9.2 Injection of Microspheres dispersed in Gel

After dispersion in a more viscous medium (gel), both rhodamine-BSA and Alexa 647-BSA microspheres were traceable for three days. The rhodamine-labelled BSA was slightly better detectable, so that no further alterations in the labelling procedure of rhBMP-2 were

necessary. The chitosan gel retained the microspheres well. They were found within the implant *ex vivo* after three days. A comparable test was not performed for HHA gels. Nevertheless, a retaining effect of HHA gels can be assumed due to the higher viscosity compared to water and the decreased degradation rate compared to conventional hyaluronic acid.

3.9.2.1 Gel Placement and Stability

Chitosan gels withstood the forces applied *in vivo* very well. The rhBMP-2-loaded chitosan gels showed a gain or loss in volume depending on the formulation used and its bone formation abilities (see next paragraph), but all (n=25) were found after 12 weeks *in vivo* without any sign of migration. RhBMP-2 free chitosan gels slowly diminished and were not found in four out of twenty cases in the control side. The gels were well tolerated. No signs of inflammation or non-tolerance were observed for any implant in the chitosan group, neither with nor without microspheres (n=61). After three weeks, however, inflamed areas around the implant site, which healed within the next week, were observed in two mice of the HHA group (n=5).

3.9.2.2 Bone Formation Assessment in a Mouse Ectopic Model

Proof of Colocalization of Implant and Calcification Signal

During experiment #3 (table 2.9-1), signals from rhoda*BMP-2 were traced for an observation period of four weeks. While the rhoda*BMP-2 signal diminished very fast when the dye-linked protein was dispersed in chitosan gels, it even increased over time in the microsphere formulations (Fig. 3.9-1). The effect was detected in all three microsphere types. This may be explained by a decreased quantum yield caused by quenching effects in high local concentrations of the dye within the particles. The degradation of parts of the gel surrounding the microspheres may also have decreased the shielding effect of the gel on the fluorescence intensity, which would result in a signal increase. Furthermore, changes in polarity or local pH may have altered the fluorescence intensity and/or spectra emitted from the labelled growth factor.

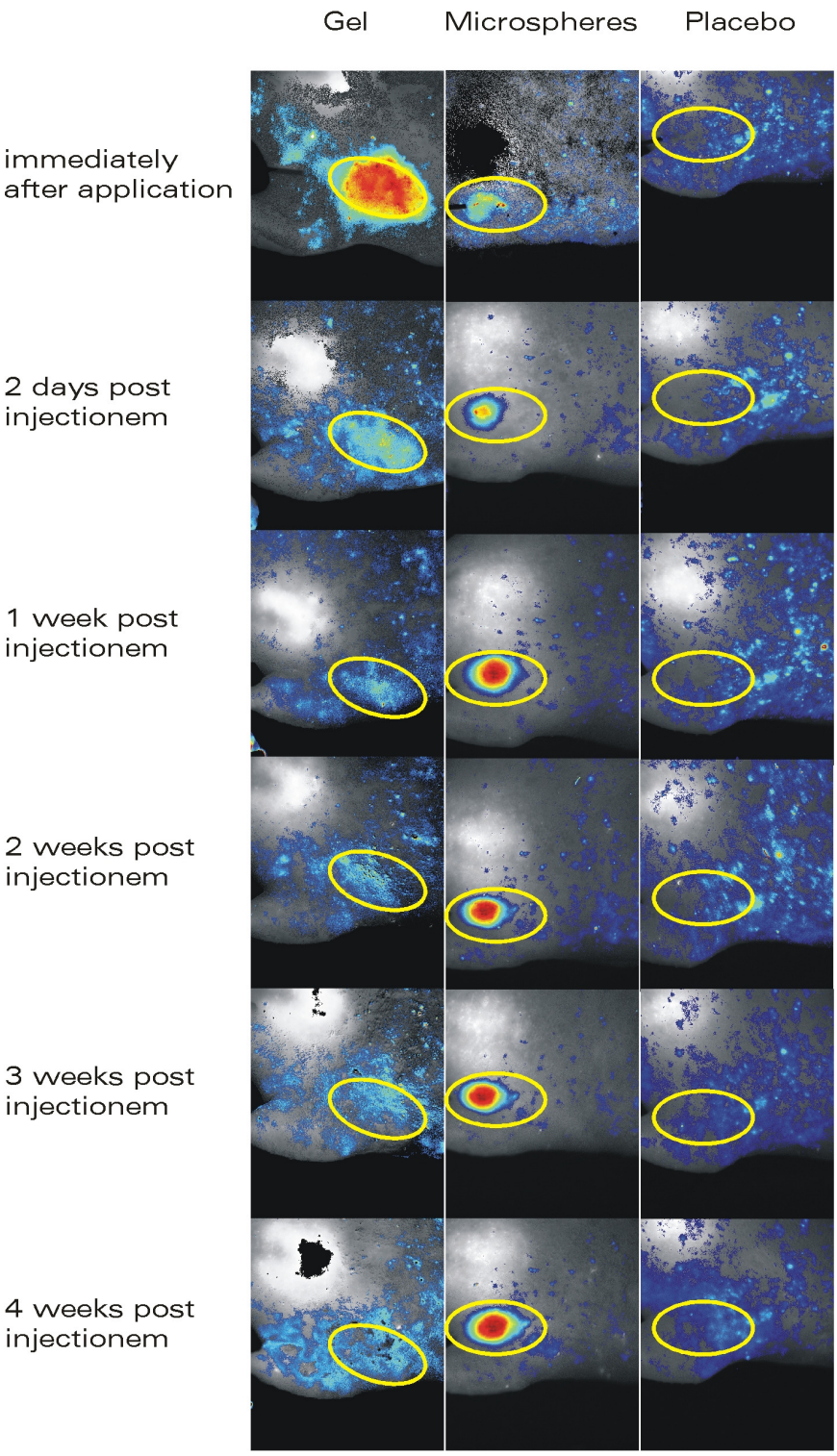

Fig. 3.9-1: Optical imaging: Intensity weighted false colour images of rhoda*BMP-2 loaded gels and rhoda*BMP-2 loaded microspheres dispersed in gel in the first four weeks *post injectionem*. High signal intensities are symbolized by red colour. Decreases in signal intensity are marked by a gradual change of color from red towards yellow, green, blue and finally black. Implant regions are circled with a yellow ellipse.

Heterotopic ossification in surrounding tissues was reported in the clinical use of rhBMP-2[101,275,276]. Hence, it is of great importance to prevent a leaking of the growth factor from the implant site and to demonstrate the colocalization of cause and effect. The calcification signal, generated by a chelator-linked fluorescent dye, was detected after four weeks in the same spot where the rhoda*BMP-2 had been injected (Fig. 3.9-2).

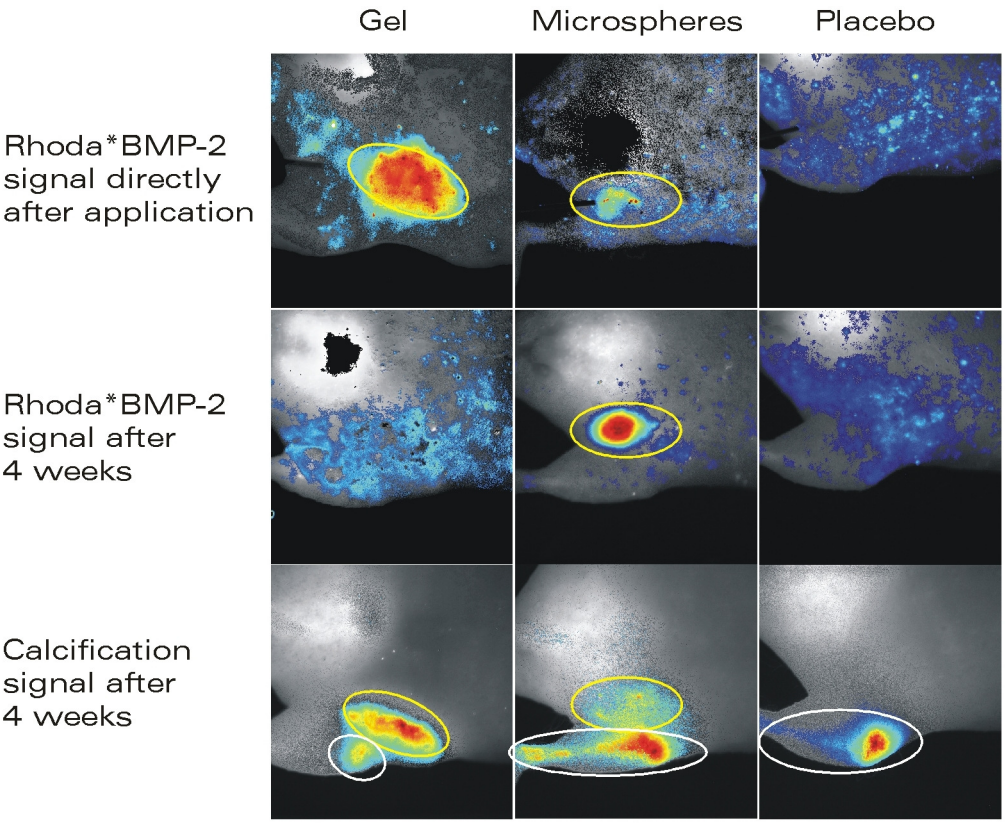

Fig. 3.9-2: Colocalization of cause and effect: OI images of rhoda*BMP-2 (upper and middle row) or calcium chelator accumulation (lower row). Regions of interest are encircled in yellow. White circles represent signals obtained from endogenous bone.

Keeping in mind the low doses applied and its microencapsulation, a high probability for the non-leakage of rhBMP-2 from the implant site is proposed. Furthermore, it was demonstrated that the rhoda*BMP-2 was still bioactive after labelling and microencapsulation, leading to calcium deposition at the implant site.

Proof of Calcification

Calcification processes may be assessed by several different methods, including ultrasonography, dual-energy X-ray absorptiometry and radiography[277]. In this study, the *in vivo* assessment of calcification was performed by non-invasive optical imaging 3, 8, and 12 weeks after implant application. After 12 weeks, the OI data were confirmed *in vivo* using CT (Fig. 3.9-3) and MRI (Fig. 3.9-4) and at the end of the study histologically *ex vivo*. A brief overview of the data is provided in table 3.9-1. It has to be kept in mind that the different techniques yield different information, e.g. calcification signals or relaxivities of tissues and their spatial distribution. The presence of vital bone can only be verified by histological evaluation (HE).

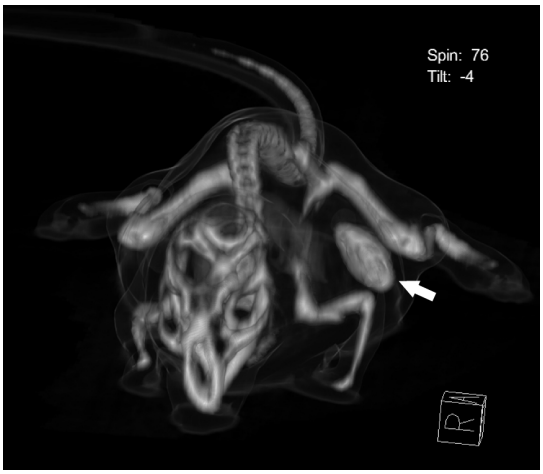

Fig. 3.9-3: CT derived picture of a single mouse (study #5) 12 weeks *post injectionem* clearly shows the ectopic nature of the newly-formed bone (arrow) in one of the two application areas. The contrast is generated by differences between low and high absorbing tissues.

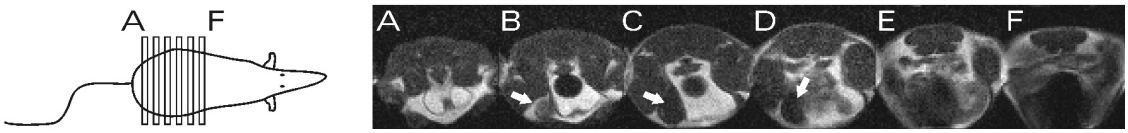

Fig. 3.9-4: BT-MRI images of transverse sections of a mouse (study #5) after 12 weeks. Typical magnetic resonance images of a mouse display the structure of the left implant in slides B to D (arrows), where it was expected, whereas the right implant was not detected. The contrast is due to different relaxation times of hydrogen atoms.

Table 3.9-1: Signals accounting for bone formation. HE abbreviates histological evaluation. PEP 5 opt refers to the optimized application procedure described in chapter 2.9.1, PEP 5 HHA were PEP 5 microspheres dispersed in the hydrophobically modified hyaluronic acid gel. Results are indicated as: +, positive; o, tendencies towards positive; -, negative; n.a., not assessed. Optical Imaging results were determined after 3, 8, and 12 weeks (w) and *ex vivo* (ex).

Formulation	Mouse #	Optical Imaging				CT	MRI	HE
		3 w	8 w	12 w	ex			
PEP 0	M 1	+	+	+	+	+	+	+
PEP 0	M 2	-	-	-	-	-	-	-
PEP 0	M 3	-	-	-	-	-	+	o
PEP 0	M 4	-	-	-	-	-	-	-
PEP 0	M 5	-	-	-	+	-	-	+
PEP 5	M 1	+	+	+	+	+	+	+
PEP 5	M 2	+	+	+	+	+	+	+
PEP 5	M 3	+	+	+	+	+	+	+
PEP 5	M 4	+	+	+	+	+	+	+
PEP 5	M 5	+	+	+	+	+	+	+
PEP 5 opt	M 1	+	+	+	+	+	+	+
PEP 5 opt	M 2	+	+	+	+	+	+	+
PEP 5 opt	M 3	+	+	+	+	+	+	+
PEP 5 opt	M 4	+	+	+	+	+	+	+
PEP 5 opt	M 5	+	+	+	+	+	+	+
PEP 5 HHA	M 1	-	-	-	-	-	-	-
PEP 5 HHA	M 2	-	o	-	-	-	-	-
PEP 5 HHA	M 3	-	o	-	-	-	-	-
PEP 5 HHA	M 4	-	o	-	-	-	-	-
PEP 5 HHA	M 5	-	-	-	-	-	-	-
PEP 10	M 1	-	-	-	-	-	-	-
PEP 10	M 2	-	-	-	-	-	-	-
PEP 10	M 3	-	-	-	-	-	-	-
PEP 10	M 4	-	-	-	-	-	o	-
PEP 10	M 5	-	-	-	-	-	-	-
ChitoGel	M 1	+	+	+	+	+	+	+
ChitoGel	M 2	+	+	+	+	+	+	+
ChitoGel	M 3	+	+	+	+	+	-	+
ChitoGel	M 4	+	+	+	+	+	n.a.	+
ChitoGel	M 5	+	+	+	+	+	n.a.	+

The blinded interpretation of MRI data yielded the same results as the majority of other techniques in 43 out of 46 implant sites. Four implant sites (chitosan gel group, 2x verum, 2x placebo) were not assessed by means of MRI, because the size of two animals exceeded the size of the MRI resonator. Calcified tissue was found in one out of five mice in the PEP 0 group by means of OI. Only after removal of covering tissues, another small calcified area was detected and proved by histology. A third animal was found positive in MRI evaluation. Histologically, only a minimal calcium deposition was found in one of four sections of this OI-negative implant. Growth factor-loaded chitosan gels and PEP 5 microspheres in chitosan gel showed, independent of the application procedure, a calcium deposition after three weeks. Interindividual differences in the respective groups regarding implant volume were detectable, but not dominant. Various possible reasons for interindividual differences were found: The mice, although being a rather homogeneous population at the beginning, started to gain weight during the experiment to a different extent. At the end of the study, the body weight ranged from 36 g to 50 g in male and from 33 g to 35 g in female animals. As an optical method, fluorescence imaging is prone to alterations in sample thickness that might be caused by increasing subcutaneous fat. In male mice, an accumulation of the calcium-chelating dye in the testes was detected. This phenomenon has been described before[278]. Furthermore, differences in the clearance of the calcium-chelating dye were detected. Especially one day after application, no comparable data were accessible. The bladder areas of some mice showed high signal intensities, whereas in other animals excessive dye had been cleared from the organism. Consequently, the detected intensity two days after injection of the calcium chelator was used for result evaluation.

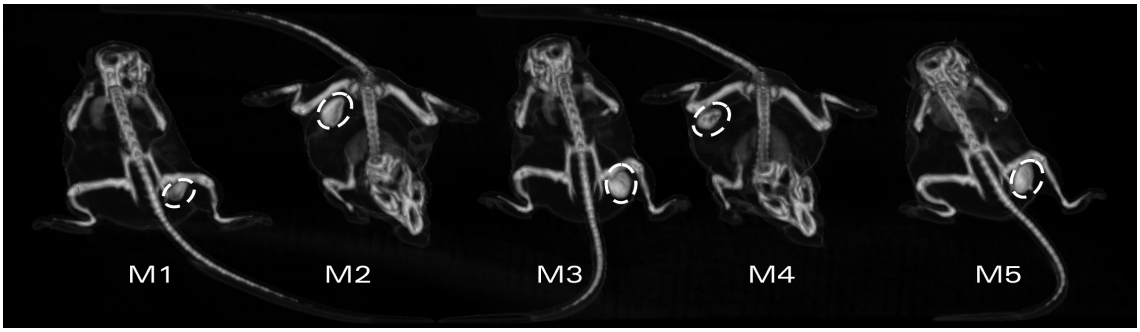

Fig. 3.9-5: CT images of calcification in one group of mice (study #5) as determined 12 weeks *post injectionem*.

In CT, the interindividual differences were not that dominant (Fig. 3.9-5). No signals were detected in any negative control and, surprisingly, in any implant of the PEP 5 HHA and the PEP 10 group. One single finding by MRI in the PEP 10 group could not be verified histologically.

Monitoring of Implant Volume Increase

The time course of implant volume was estimated by means of optical imaging. In general, implant volumes were found to increase over time. Many researchers evaluated bone formation after three or four weeks[49,80,92,253,279]. In contrast, a growth in signal intensity was detected throughout the whole investigation period of twelve weeks (Fig 3.9-6), suggesting a calcium deposition in two waves. In an early phase of up to three weeks, between 35 % and 70 % of calcium deposition were found. No or little increase was detected between week 3 and week 8, whereas further deposition of 30 % to 65 % of calcium took place in the late phase of the experiment until week 12 (Fig 3.9-7).

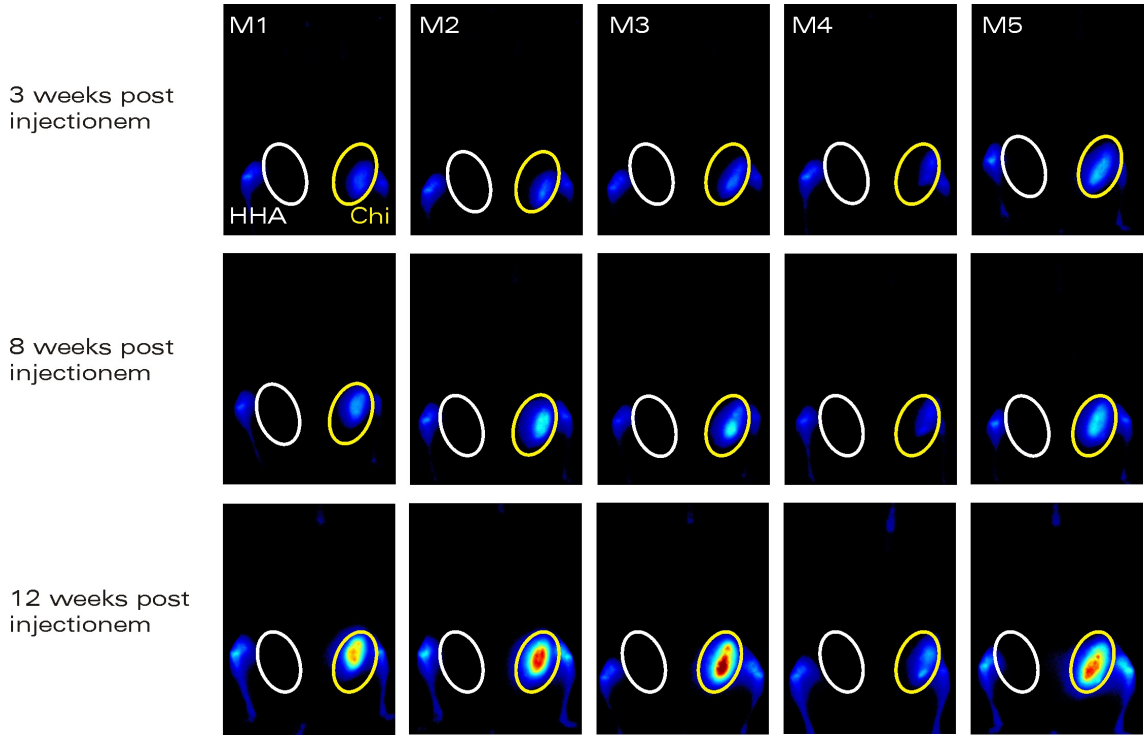

Fig. 3.9-6: OI images of one group of mice (study #5; n=5) 3, 8 and 12 weeks after implant administration. The pictures show the difference between HHA (white circles, left) and Chito carriers (yellow circles, right) with dispersed rhBMP-2-loaded PEP 5 microspheres in the time course.

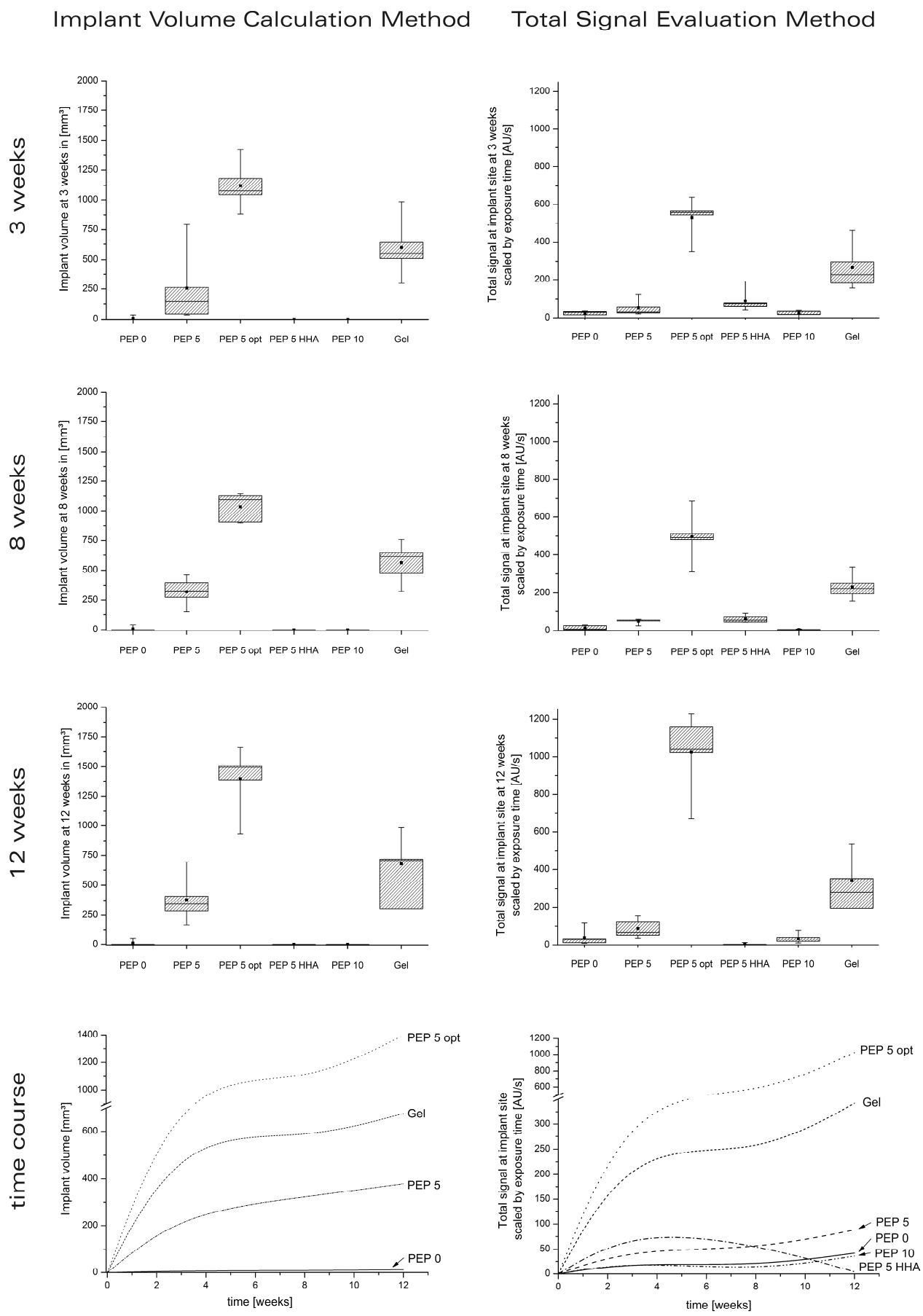

Fig. 3.9-7, explanatory notes on p.102.

Fig. 3.9-7 (p. 101): OI results on calcification intensity as obtained by the two different result evaluation methods described in detail in chapter 2.9.3. With the signal intensity-based data (method II, right column), a more differentiated picture was obtained than with the volume-based approach (method I, left). PEP 5 HHA and PEP 10 showed no detectable implant; their display was omitted in the time-dependent volume graph. Negative controls are not depicted, as implant volume was not calculable due to lack of a sufficient signal. In the boxplots, the data range from 5 to 95 % (whiskers), percentile 25/75 (box), maximum and minimum (upper/lower line), median (line within box) and mean (black quadrat) are depicted.

It is speculated that the second wave of calcification was due to the degradation processes of the implants and of the microspheres, releasing the entrapped rest of rhBMP-2. The effect was well characterized by both OI evaluation methods described in chapter 2.9.3. The volume calculation method, however, led to a strong overestimation of the calcified tissue in groups with high signal intensities. An overassessment of up to the tenfold implant volume was obtained compared to CT or conventional measurement of the implant after harvesting (Fig. 3.9-8). The CT data are regarded as the most exact in this comparison. The explant sizing with a calliper rule is based on the assumption of a completely monolithic, perfectly ellipsoid structure which did not occur in the specimen.

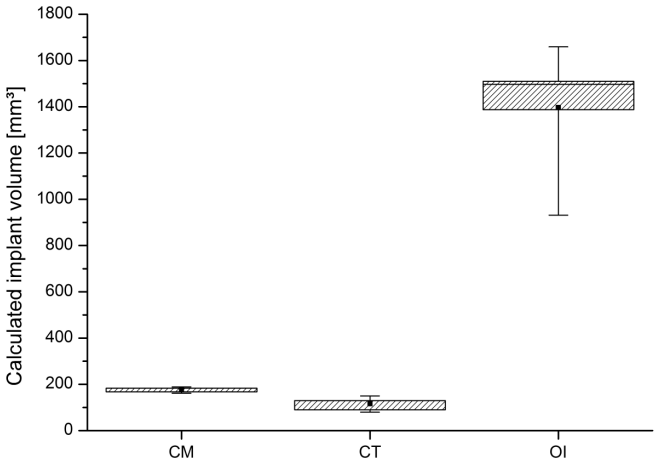

Fig. 3.9-8: Quantification of implant volume (PEP 5 opt), based on CT, OI and conventional measurement of the explant by means of a calliper rule (CM).

It is suggested that in OI, strong signals scattered intensely towards circumjacent tissues and produced false positive areas which were then included in the volume calculation. In contrast, signals with low fluorescence intensity, like those in the PEP 0 group, could not be differentiated clearly from the background. Consequently, no implant area was defined and these samples were underestimated. A more reliable method was found when comparing the signal intensities of the implant areas. Besides a lower error between the measurements, especially the low absorbing samples were described better (Fig. 3.9-7). However, total signals below 30 AU/s at the implant site were obtained for all negative controls, so that this value was defined as the background cut-off. PEP 0 and PEP 10 microspheres were detected at background level at 3 weeks and at 8 weeks. Only at 12 weeks, the total signal slightly exceeded 30 AU/s.

In study #5, the optimized application procedure was performed. The most promising microspheric delivery system according to the previous experiment, PEP 5, was chosen to test the impact of both the application procedure and the microsphere dispersant on *de novo* bone formation. With the optimized method, an increase in calcium deposition was visually evident in the false colour images (Fig. 3.9-9). The reduction of particle loss during injection yielded a further increase in bone formation potential compared to the conventional method.

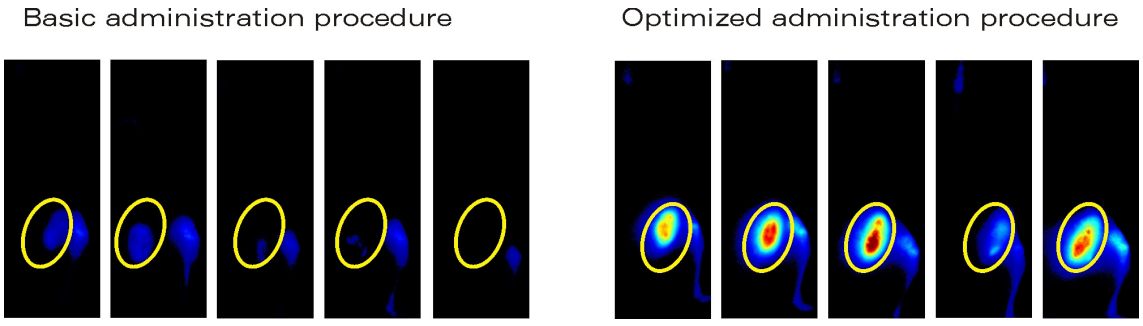

Fig. 3.9-9: OI calcification results of similar microsphere preparations after 12 weeks. The particles (PEP 5 with rhBMP-2) were administered with the conventional method (n=5; left row) and with the optimized application procedure (n=5, right row), which clearly demonstrates increased injection efficiencies with the optimized method.

Unexpectedly, the application of the same PEP 5 microsphere batch to the same group of mice did not show any sign of calcium deposition or bone formation when the particles had been dispersed in hydrophobically modified hyaluronic acid (HHA) gels instead of chitosan-based systems. After 8 weeks, however, a minimal signal in OI was detectable in three out of five implants of this group (see also Fig. 3.9-7). However, the calcification maps obtained by OI at 12 weeks show no signal at the HHA side. It may be speculated that the detected calcified tissue was not robust and possibly resorbed within the following four weeks. At 3 weeks, a swelling and redness was observed in the HHA side (n=5) of two mice. These two implants and a third one in another animal showed the formation of a fibrous capsule in the histological evaluation. The other two mice of this group did not show any remaining implant after 12 weeks (Fig. 3.9-10). Nevertheless, tissue samples from the expected implant area were excised.

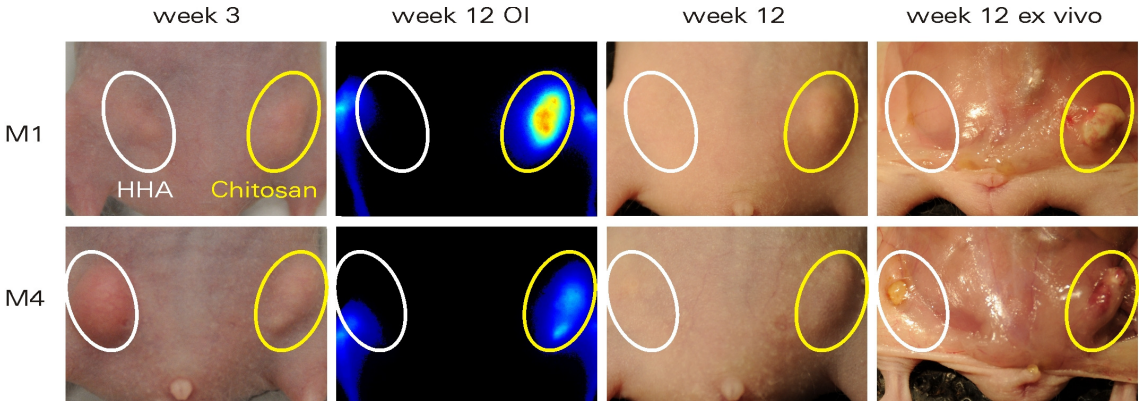

Fig. 3.9-10: Effect of microsphere carrier. RhBMP-2-loaded PEP 5 microspheres dispersed in hydrophobized hyaluronic acid (HHA; white circles, left) and chitosan carriers (yellow circles, right), 3 and 12 weeks *in vivo post injectionem*, and after 12 weeks *ex vivo*. A yellowish, non-fluoresceing remnant was found in three mice of the HHA group (lower row, right, white circle).

Overall, the reported bone formation was localized and increased with time. Saito et al. reported a robust bone formation 3 weeks after application of 10 µg of rhBMP-2 in PLA-PEG implants in mouse orthotopic and ectopic models[279]. The authors detected remnants of the implant at the end of the investigation period at three weeks. The same group monitored the healing of non-critical defects in rabbit ulnae after eight weeks[280]. The main drawback of the reported system was,

however, the application temperature of 60 °C to obtain an injectable system. The group of Mori and Isobe tested PLGA microcapsule delivery systems in combination with gelatin hydrogels[92]. In an early approach, they used 1.4 mg of BMP in a rat ectopic model and detected bone formation including bone marrow 3 weeks after application of the very high dose[92]. Later, they applied their system with a lower dose (12 µg per site) to a rabbit segmental defect, finding a continuous regeneration within a 24 week observation period[273]. One of their final conclusions was, however, that the use of the beneficial system of microparticles should be combined with a more suitable carrier, which was now conducted by the use of chitosan gels. Furthermore, the use of smaller microspheres that enable syringing and the application of better polymeric carriers in terms of release profile reveal huge advantages of the systems described in this study. The *in vivo* answer on the released protein was robust in spite of the very low dose used.

Implant Quality

While the time course of bone formation was monitored by means of optical imaging, the implant quality was assessed by means of CT 12 weeks *post injectionem*. CT enabled a better detection of differences regarding shape and structure. Furthermore, the CT allowed a better differentiation between calcified tissue and non-calcified tissue, which is reflected in a lower calculated volume in all cases. This may have three explanations:

(I) CT images have a higher contrast and no scattering effects compared to OI images;

(II) hollow structures are detected and therefore not included into the calculation of the implant volume, whereas they are not found by means of OI;

(III) in some areas, the calcium accumulation was obviously not sufficient to generate a signal defined as bone in CT measurements, whereas these areas had been detectable in the more sensitive OI. However, it has to be kept in mind that these low signals were just slightly above the background fluorescence in these specimens.

The implant volumes detected by CT at 12 weeks after application of 1.3 µg of rhBMP-2 ranged from 0 mm^3 to 116 ± 30 mm^3. Compared with the initially applied volume of 200 mm^3, a replacement of 58 ± 15 % of implant by CT active calcified tissue was achieved

(Fig. 3.9-11). This can be regarded as very effective. Kempen et al. studied a rhBMP-2 delivery system consisting of PLGA microspheres and polypropylen fumarate scaffolds within a gelatine surrounding. In an ectopic rat model, they found a bone volume of 5 mm^3 eight weeks after application of 6.5 ± 0.4 µg of rhBMP-2[91]. In the same study, the authors demonstrated that the bone formation was much more effective in orthotopic sites. In a rat femoral defect, an average new bone volume of 42 mm^3 was detected after 56 days. Lee et al. found comparable results after application of 2.5 to 20 µg of rhBMP-2 on collagen sponges ectopically and in rat calvarial defects[37]. However, they reported a dose dependency only in the ectopic sites. In orthotopic sites, even the lowest dose of 2.5 µg was sufficient to heal the created defects after 8 weeks. Hence, it may be assumed that the delivery system investigated in this study may show further increased formation of new functional bone in orthotopic sites, where an osteoconductive milieu or a periosteal bone formation can be expected.

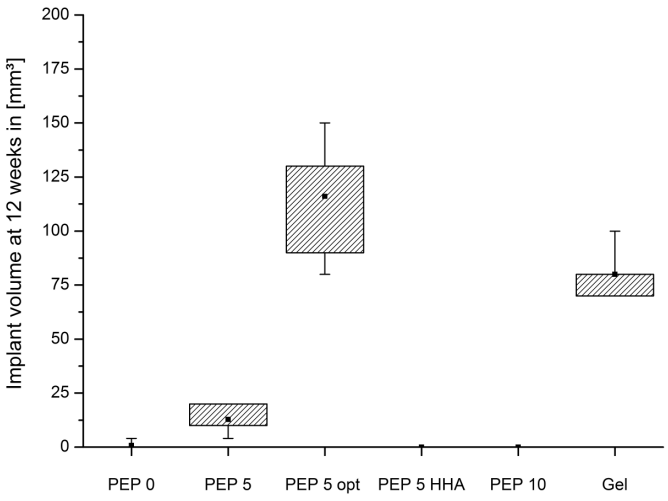

Fig. 3.9-11: Bone formation as monitored non-invasively by CT. Display of completely calcified volume at 12 weeks.

At the end of the experiment, the implants were extracted. In some placebo sites and in two animals of the PEP 5 HHA group, no implant was found. In the case of PEP 5 HHA, the tissue of the application area was taken and subjected to histological evaluation. Differences in size and calcification were detectable even before histological evaluation (Fig. 3.9-12). However, histological data are necessary to draw final conclusions.

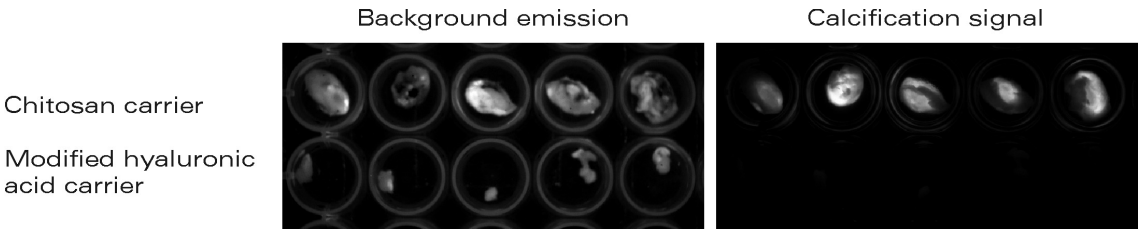

Fig. 3.9-12: Explant size and degree of calcification as determined by optical imaging. The pictures show the difference between chitosan (upper row) and hydrophobized hyaluronic acid (HHA; lower row) carriers with dispersed rhBMP-2-loaded PEP 5 microspheres. Explants in the HHA side were considerably smaller (left image) and did not show any detectable sign of calcification (right). n=5 in each group.

Histology

De novo formation of vital bone was seen in several of the investigated delivery systems. In study #4, chitosan-based delivery systems have been evaluated. Chitosan gels, PEP 5 microspheres and, to some extent, PEP 0 particles were capable of producing vital bone (Fig. 3.9-13).

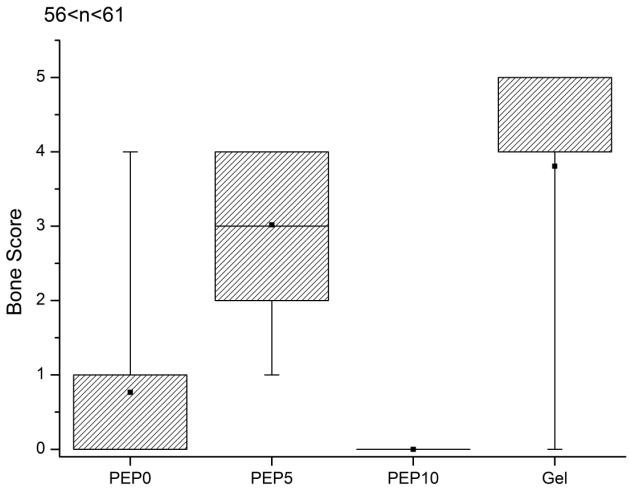

Fig. 3.9-13: Histological score (as defined in table 2.9.2, p. 43) of chitosan-based delivery systems evaluated after 12 weeks.

In contrast, no sign of calcification or even bone formation was detected in PEP 10 microspheres or in any of the negative controls. This outcome was unexpected, as neither the *in vitro* release data nor the cell differentiation assay had suggested an inferiority of PEP 10 particles. The explants obtained from the chitosan gel group appeared capsule-like. A bony region surrounded scattered gel remnants and other cells, such as fibroblasts. It may be speculated that the chitosan gel was persisting longer than necessary, possibly building a cell penetration border immediately after injection. High deacetylation degrees of chitosan are known to decrease its biodegradation velocity[249]. RhBMP-2 leaching from the gel may have been acting right at the border of the *in situ*-forming implant. Articulate interindividual differences were found especially in the gel group. In contrast, a lower score but a more homogeneous result was found for the PEP 5 group. The bone formation was found to occur in several islands within the implants, only in some cases bordering outward tissues. Here, a slower release is assumed to result in the turnover of the process towards the right direction: first, cells invaded the implants, and second, local growth factor delivery led to bone formation.

Residual microspheres were not found in the samples. Compared to microsphere-free implants, no further characteristic structure accounting for microspheres or microsphere remnants was detected. It has been shown histologically that PLGA microcapsule systems neither impaired remodelling at the defect site nor increased adverse tissue reactions[273]. Remnants of PLGA microspheres were found by day 63 after implantation by Visscher and coworkers[281]. 35 days *post injectionem,* the authors reported the microspheres to be still intact. Isobe et al. did not find any remnants of large and thus very quickly degrading microspheres after three weeks[92].

The more intense bone formation of the *in situ*-forming implants alone can be explained with incomplete administration of microspheres in study #4, as discussed in chapter 3.8.1. In study #5, with the optimized application procedure from the larger syringe, a dramatic increase in the amount of new bone was found for PEP 5 microspheres (PEP 5 opt) compared to the conventional application (PEP 5). The bone score was articulately higher than in PEP 5 and in the chitosan gel group (Fig. 3.9-14).

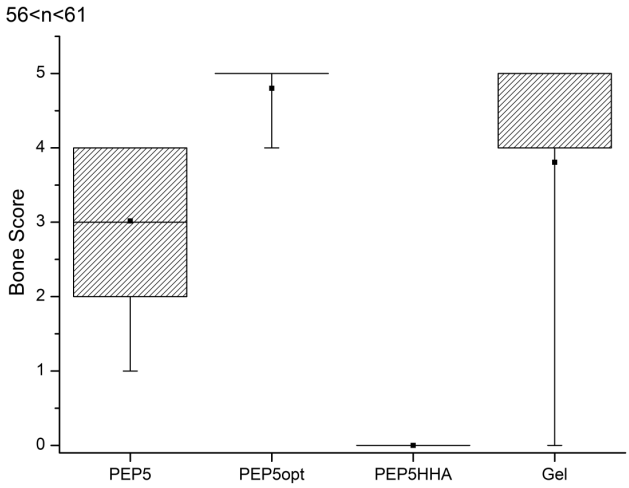

Fig. 3.9-14: Histological score of PEP 5 microspheres applied by the optimized method, dispersed either in the chitosan sols (PEP 5 opt) or in hydrophobically modified hyaluronic acid (PEP 5 HHA), evaluated after 12 weeks. Previous data from PEP 5 microspheres applied by the conventional method (PEP 5) and from the chitosan gel (Gel) are provided for comparison.

Whereas PEP 5 and, to some extent, PEP 0 exhibited an islet-like calcification process, the chitosan implants showed von Kossa-positive areas predominantly at its borders (Fig 3.9-15). Strong calcification was also detected in the PEP 5 group with optimized application (PEP 5 opt). Here, not only bordering regions but also the inner part was found positive in von Kossa staining. However, a gradually decreasing intensity of black staining towards the inside was still detectable. The use of hydrophobically modified hyaluronic acid as microsphere dispersant (PEP 5 HHA) was found to be inappropriate in the investigated model. No sign of calcification was detected in any implant of the whole group, in spite of the use of the same microspheres (PEP 5) in the same group of mice (contralateral implant site). Fibrous capsules were found in three out of five animals, possibly caused by the reported inflammation processes (Fig. 3.9-15; PEP 5 HHA).

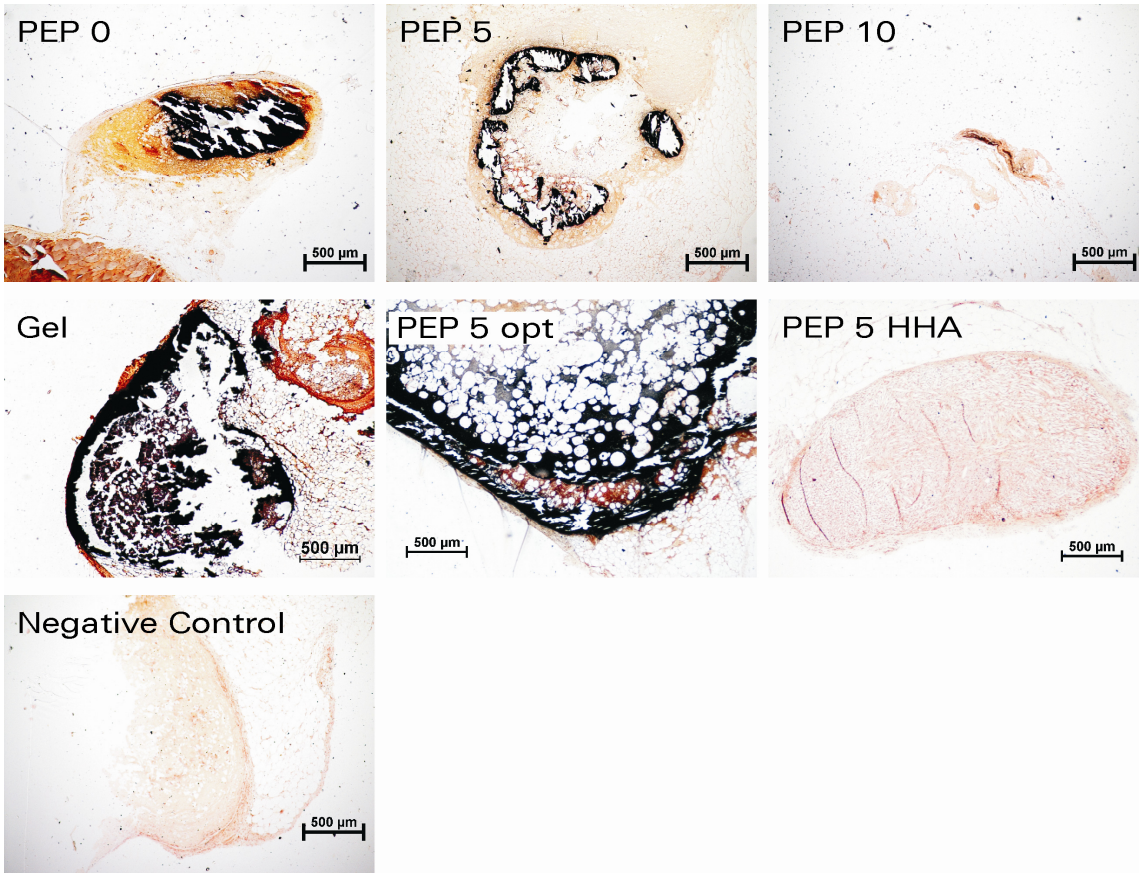

Fig. 3.9-15: Photomicrographs of explant sections after von Kossa staining. Black areas represent phosphate deposits, accounting for calcification.

4 Synopsis and Conclusions

The objective of this study was the development and characterization of a novel controlled delivery system for rhBMP-2. The growth factor was produced by and purified from *E. coli*. An established protocol was utilized for the refolding and purification process to obtain the active protein conformation. During the purification process, single batches were affected by irreversible aggregation. A thorough optimization of the conditions which lead to an enhanced solubility of rhBMP-2 was not in the scope of this study. Nevertheless, four batches of the growth factor in high purity were successfully produced. Compared to eukaryote-derived or human BMP-2, the recombinant prokaryote-derived protein lacks glycosylation, which may be regarded both as advantage and as drawback. On the one hand, the solubility of rhBMP-2 is further impaired and aggregation tendencies were found to be high, complicating the characterization articulately. On the other hand, the growth factor is supposed to achieve a higher retention at the site of implantation, suggesting the possibility of a further dose decrease due to longer presence in the intended area of action.

Few investigations have been published on the stability of eukaryote-derived rhBMP-2 in release media and in solution[80,127]. In this study, the tendency of prokaryotic rhBMP-2 to form aggregates was monitored by means of five different methods. It was expected that possible artefacts of one method may be recognized by the use of another approach. Consequently, a full coverage of the very wide molecular weight range was achieved. It has to be noted that the data on aggregation are based on a comparably low number of samples. Hence, the reported effects should be recognized as an estimation. As expected, an aggregation of rhBMP-2 was found with all methods, however, the extent and pattern of aggregation differed. Alterations between the methods were attributed to the formation of artefacts and the detection of inhomogeneous species, such as intermediately unfolded, denatured or chemically reacted protein, protein aggregates and precipitates. The oligomerization of rhBMP-2 started after a relatively short period of time, but did also increase continuously. It was demonstrated by means of UV and ELISA that the aggregation of rhBMP-2 is dependent on the type of buffer and its pH. Acetate ions and lower pH were found to be preferable conditions and were thus also used during the formulation development. These results were consistent with those reported for CHO-derived rhBMP-2[80,127].

For the controlled delivery of rhBMP-2, a broad variety of delivery systems was taken into consideration. A microspheric system was chosen because of its compatibility with classic approaches like gels, *in situ*-forming implants and scaffolds. Combinations with liquid or viscous dispersants may open opportunities to having the implantation procedure performed in a minimally invasive manner. Closed fractures may be treated percutaneously[38,282]. Furthermore, microspheres provide a protection against rapid clearance of the encapsulated growth factor and, as in the case of the used polyesters, a well-tailorable release. One conventional PLGA and two PEG-PLGA copolymers were utilized for microsphere fabrication. Polyethylene glycol has been reported to increase the stability of proteins during microencapsulation, if covalently bound to the protein, linked to the entrapping polymer or codissolved in the inner or outer phase[108,109]. For the first time, pegylated poly(lactic-co-glycolic) acid diblock copolymers were utilized for the encapsulation of rhBMP-2. In this study, the effect of PEG 5000 as one component of a PEG-PLGA diblock and the coencapsulation of PEG 300 were investigated both by themselves and in combination. Effects of PEG coencapsulation have not been investigated for rhBMP-2 so far.

A double emulsion-solvent evaporation method was modified to enable the fabrication of microspheres from the three different polymers with one set of parameters. The process development was challenging due to the low glass transition of the diblock copolymers. Even the processing at room temperature resulted in clotting with PEP 10 microspheres. Consequently, the preparation steps were performed on ice so that a well reproducible process was assured. In spite of the difficulties to remove volatile substance at low temperatures, a very low content of residual solvent was proven. Less than half of the maximum methylene chloride concentration accepted by the European Pharmacopeia was detected; isopropanol was not found at all.

133 batches of microspheres were produced in good quality and with high yields. Further yield improvement was achieved by the introduction of PTFE beakers during the first steps of fabrication. The shape of the microspheres was investigated by means of ESEM. In all six formulations, the desired round shape and negligible porosity was shown. The particle size distributions were investigated by means of ESEM and with laser diffraction. Both methods resulted in comparable sizes. From the differences between the dry measurement (ESEM) and the size determination in solution, an increased swelling tendency of the pegylated polymers was detected, which is in agreement with the literature[218].

RhBMP-2 was incorporated in the different microsphere formulations. Conventional methods for the determination of entrapment efficiency were not promising, so that a differential fluorescence approach was designed. Therefore, rhBMP-2 was covalently linked to rhodamine B for the first time. The successful linking was proven by means of SDS-PAGE and optical imaging. Both a high encapsulation efficiency and a well-defined drug distribution were shown by means of fluorescence techniques. For the first time, insights in the drug distribution of rhBMP-2 in a microspheric delivery system were gained. The labelled growth factor was detected in distinct areas, termed spherical microdomains, in high concentrations and in negligible amounts elsewhere in the particles. Explanations for the very efficient encapsulation were found in the fast skin formation at low temperatures and the high polymer/drug ratio. PEG was shown to interfere with the microsphere structure. Whereas a PEG-linkage of the polymer did not apparently change the inner structure of the polymer, the addition of PEG 300 to the inner phase for microsphere preparation led to a decrease in the number of spherical microdomains. The effect was dependent on the PEG content of the polymer itself. It was suggested that PEG 300 was more likely to interact with covalently attached PEG 5000 in the polymer than with the PLGA part. Hence, the least effect of PEG 300 addition was found in PEP 10 microspheres, made from the polymer with the highest inherent PEG content. In contrast, even a complete loss of microdomains was detected in PEP 0 particles in the presence of PEG 300.

Release profiles were recorded for six formulations by means of ELISA. The conditions applied during *in vitro* release should reflect the *in vivo* situation as closely as possible. It is beyond question that the applied conditions such as pH 7.4, 37 °C and continuous shaking were unfavourable for the stability of rhBMP-2 in solution. Consequently, the stability of the growth factor in release buffer was assessed. It was demonstrated that the growth factor recovery by ELISA follows an exponential decrease over time. The recovery results were included in the calculation of release profiles. Furthermore, the loss in ELISA recovery after freezing and thawing was tested. Storage of one week either at 4 °C or at -20 °C revealed a loss of 30 % in ELISA detection when the growth factor was frozen for one cycle, whereas the cold-stored rhBMP-2 did not show any articulate decrease in the detectable growth factor concentration compared to a freshly reconstituted standard. These data set novel implications for the accomplishment of release determinations of rhBMP-2.

Polymeric degradation products may interact with the growth factor during its release. A microsphere degradation study was performed and the influence of polymer decomposition products on rhBMP-2 recovery was investigated. The degradation processes of microspheres were monitored under release conditions *in vitro* by means of NMR and pH profiling. After eight days, first monomers were detectable from PLGA degradation by means of NMR. A pH decrease in the release medium was already detected after three days in PEP 5 and PEP 10 microspheres, indicating a better transport of small molecules, such as short-chained acidic degradation products, out of the microspheres. Similar results have been published for comparable blockcopolymers. Any contact of rhBMP-2 with degradation products of the microspheres did not interfere with the ELISA recovery. A controlled release was shown for all six formulations. An increasing PEG content linked with the polymer heightened the release rate. In contrast, the loss of spherical microdomains and the smearing of the growth factor within the microspheres after addition of PEG 300 to the inner phase was found to result in a decrease of the release rate. Furthermore, the addition of PEG was reported to decrease the encapsulation efficiency into PLGA microspheres[90].

The release profiles of rhBMP-2 were determined for 28 days. A later release during the complete degradation of the microspheres is expectable, but its positive impact on bone regeneration may be questioned. The ideal release profile and total release time are still very controversially discussed. However, due to the low release rates and the low overall recovery from these formulations, preparations containing PEG 300 in the inner phase were excluded from further evaluation. The bioactivity of rhBMP-2 released from microspheres was assessed *in vitro* by means of alkaline phosphatase induction in a C2C12 mouse myoblast cell line. The alkaline phosphatase was used as a surrogate marker for osteogenic differentiation, as this enzyme is only expressed in mouse myoblasts when they are driven into an osteogenic lineage. An osteogenic response was found in all three investigated formulations, justifying an *in vivo* evaluation.

The microspheres were incorporated into liquids, gels, *in situ*-forming implants and into recently developed scaffolds[140]. A nearly homogeneous distribution of particles in the scaffold matrix was proven by means of ESEM. However, injectable systems were preferred in the *in vivo* investigations. They are superior in defect fitting due to their viscous nature in application and open up the opportunity of minimally invasive percutane application. The performance of the microspheres was tested in an ectopic mouse model. Advantages were the easy

identification of newly-formed bone, the omission of surgery and a higher significance of the bone induction ability of the applied system due to the absence of an osteogenic environment. An extensive comparison with other reported delivery systems was considered inappropriate due to varying physicochemical carrier properties, growth factor origin, different delivery schemes and doses as well as diverse species and defect models[54].

Non-invasive analytical methods were established for the monitoring of rhBMP-2 fate and for the evaluation of bone formation *in vivo*. In a first approach, rhodamine B-labelled rhBMP-2-loaded microspheres were dispersed in PBS and injected subcutaneously into one mouse. The non-detectability was attributed either to insufficient fluorescence intensity or too rapid diffusion from the site of injection. Consequently, the dispersant was changed in the second experiment to a chitosan-based *in situ*-forming implant. The signal intensity of the dye in the first experiment was compared with the outcome of another dye, which turned out not to be superior. Both dyes, encapsulated in microspheres, were well-detectable for three days *in vivo*. It was shown that the signal loss in the first experiment was due to a fast migration of the particles in the subcutaneous area. The third animal study was focussed on monitoring the fate of rhodamine B-labelled rhBMP-2 over a period of four weeks and the attempt to colocalize cause and effect of bone formation induction. Rhodamine B-labelled rhBMP-2 was either dispersed in the sol matrix of the *in situ*-forming implant or encapsulated in PEP 0, PEP 5 or PEP 10 microspheres which were also dispersed in a chitosan-based sol. Within two weeks, the fluorescence signal had merely disappeared in the gel group, whereas even an increase in signal intensity was found in microsphere-loaded gels. It is speculated that the dequenching effects due to the release of the growth factor and the decreased scattering way between dye and detector due to the degradation of the gel enhanced the signal. After four weeks, a calcium-chelating agent linked to another fluorescent dye was injected intravenously. As far as known, the dye, intended for the use in cancer models, was used for the first time to monitor ectopic bone formation. The excitation and emission spectra of both dyes differed strongly, so that an energy transfer between them was unlikely. Signals accounting for calcification were detected in many ectopic sites, demonstrating the bioactivity even of the rhodamine-labelled rhBMP-2. The signals of rhoda*BMP-2 and calcification were colocalized, so that an excessive leaching of growth factor from the implant was precluded.

The *in vivo* response on four different rhBMP-2 delivery systems was monitored for 12 weeks. Groups of five animals were investigated per

delivery system. The respective contralateral sides of the animals served as negative control after application of the same system without any growth factor. For the assessment of implant changes, three different non-invasive methods were applied. OI was employed 3, 8 and 12 weeks *post injectionem*, CT and MRI evaluation were conducted additionally after 12 weeks. At the end of the study, the explants were investigated histologically.

Two different methods of OI result evaluation were developed. One method was based on the calculation of the fluoresceing volume, another monitored the intensity of calcification signals. The key outcomes of both were comparable to CT at 12 weeks. A more differentiated description of samples with very low signal intensity was achieved by the second OI method. However, the volume calculation from OI data was found to yield unrealistically high results. Signal scattering to circumjacent tissues resulted in an overestimation of calcified volume, as confirmed by means of CT and calliper rule sizing. CT was performed with an instrument designed for human use. With the measurement of five animals in one run, good results regarding resolution and comparability were obtained. The software enabled the calculation of ectopically formed bone based on 3D information, so that hollow areas within implants were also detected. Changes in relaxation time due to bone formation were seen in MRI measurements. A blinded evaluation was performed by a MRI specialist (n=46). His evaluations matched the results of a subsequent histological evaluation in more than 93 % of the cases. The method was found capable to detect changes associated with calcium deposition and bone formation, although the result evaluation needs some practice.

The incorporated rhBMP-2 was found to effectively induce bone formation. PEP 5 microspheres and ChitoGel were found efficient, PEP 0 particles showed moderate bone formation. A wavelike increase in signal intensity and calcified volume was detected for the implants by means of OI. After 3 weeks, between one and two thirds of the total OI signal at 12 weeks were detected. No or only slight increases were detectable between week 3 and week 8, suggesting a low release rate in rhBMP-2 during this period. It is speculated that a further increase in the amount of calcified tissue until week twelve was caused by degradation of the microspheres and release of the residual entrapped growth factor. Furthermore, a degradation of the *in situ*-forming implant may have increased the calcification signal and may also have ameliorated the formation of new bone tissue in evolving spaces. It is widely accepted that a very rapid occurring degradation of the implant may favour the encroachment of fibrous tissues, which should be

precluded to promote the formation of an osteogenic microenvironment. Implant remnants were detected histologically 12 weeks after application. A prolongation of the investigation period is suggested to study the maximum residence time of implant remnants in the host site.

No calcified tissue was found after application of PEP 10 microspheres and, expectedly, in any of the negative controls. The inability of PEP 10 particles to induce ectopic bone formation in the investigated system cannot be explained by low release rates or insufficient performance in cell culture. PEP 5 microspheres, with medium PEG content and longest polymer chain, were found to be most successful amongst the particulate-based systems. Unexpectedly, the microsphere-free chitosan implants with dispersed rhBMP-2 yielded significantly higher calcification extents than microsphere-based systems. It was concluded that a separation of the well-mixed sol-microsphere combination was responsible for a loss of microspheres during injection. The effect was shown in a subsequent experiment and another application method was developed. With this method, using a larger syringe but the same gauge size needle, a loss of microspheres could be precluded. This method was applied in animal study #5, in which the use of hydrophobically modified hyaluronic acid as an alternative microsphere dispersant was characterized. Hyaluronic acid/rhBMP-2 has recently been reported to be superior compared to a chitosan/rhBMP-2 system[271], although controversial opinions have been published to date[51,267-271]. With the hypothesis of a better bone growth due to the optimized application, the most successful microsphere formulation from the previous study, PEP 5, was selected for the comparison of the two microsphere dispersants. The animal model, group size, concentrations and analytical methods were the same as in the previous study. RhBMP-2-loaded particles were either dispersed in HHA or chitosan gels and then injected with the optimized method (Fig. 2.9-1, p. 41). Interestingly, HHA gels did not show any sign of calcification in a single case. Furthermore, adverse reactions to the implants and capsule formation were detected. It was shown that the investigated HHA system was not capable of inducing bone formation in the examined model. The calcification signals were significantly higher in the chitosan-dispersed PEP 5 microspheres with the optimized application method than in all other systems, including the gel alone.

At the end of studies #4 and #5 (table 2.9-1, p. 37), a histological evaluation was performed. A histological score was developed and four sections were scored by three independent individuals concerning the presence or absence of typical bone characteristics like calcification and bone marrow. The results of the evaluation were consistent with CT, OI

and MRI. The significantly highest amount of newly-formed bone was found in the drug delivery system consisting of rhBMP-2 in PEP 5 microspheres dispersed in chitosan-based *in situ*-forming implants.

This study contributes to a characterization of E. coli-derived rhBMP-2 regarding its behaviour during handling in pharmaceutical development. Various different drug delivery vehicles for the controlled delivery of rhBMP-2 have been designed and characterized. Structural peculiarities of these systems were analyzed by means of several methods, some of which were newly developed for this purpose. The safety and effectivity of the drug delivery systems were demonstrated *in vitro* and *in vivo*. Novel approaches for the determination of calcified tissue were designed and evaluated. One of the investigated drug delivery systems was selected and proposed for further optimization.

Further conceptual work is suggested to focus on the interaction of non-glycosylated rhBMP-2 with PLGA, PEG-PLGA and the chitosan-based *in situ*-forming implants as well as on the long-term stability of the cytokine within these systems. The use of chitosan with lower deacetylation degrees may bear some potential for the alteration of the gel degradation rate, which is regarded as slightly too low. Here, the best balance between rigidity, gel formation and degradation rate is still to be found. A longer *in vivo* release study may provide clear information on the total residence time of the encapsulated rhBMP-2 within an organism. From a translational perspective, the optimization of the suggested system in a large animal model should be focussed on next. Weight bearing defects will need the assistance of a supportive container, such as the 'lumbar tapered fusion device' used in combination with commercially available rhBMP-2/ collagen systems. A strong species-specific dose-response of rhBMP-2 administration with less efficiency in humans compared to all other species has been reported[95]. This is hypothesized to be due to a mismatch of regeneration velocity and growth factor disappearance in existing delivery systems. On the way towards clinical use, further optimization regarding rhBMP-2 dose, and safety as well as efficiency of production processes should be addressed.

5 Abstrakt in deutscher Sprache

Unphysiologisch hohe Dosen des Wachstumsfaktors rhBMP-2 sind derzeit noch nötig, um beim Menschen klinische relevante Effekte zu erzielen. Der Hauptgrund für die geringe Effizienz der Behandlung wird in einer unzureichenden Freigabekontrolle des *in vivo* kurzlebigen Wachstumsfaktors gesehen. Ziel der vorliegenden Arbeit war es, Systeme zur kontrollierten Freigabe rhBMP-2 zu entwickeln und zu charakterisieren.

Nach der Isolation, Faltung und Aufreinigung wurde rhBMP-2 in Mikropartikel formuliert. Orientierende Arbeiten zur Stabilität von rhBMP-2 unter Verwendung von MALDI-TOF-MS, AF4, UV-Spektroskopie, NTA und PCS wurden durchgeführt. Mikropartikel aus verschiedenen PLGA-Derivaten wurden hinsichtlich ihrer Morphologie (ESEM), ihrer Größenverteilung und ihres Quellungsvermögens (ESEM und LD), Abbauverhaltens (^{1}H-NMR und pH), etwaiger Lösungsmittelrückstände (GC-FID), ihrer Wirkstofffreigabe (ELISA) und ihrer *in vitro*-Aktivität (ALP-Assay) charakterisiert. Nach kovalenter Fluoreszenzmarkierung wurde die Verteilung von rhBMP-2 in den Partikeln in Abhängigkeit der Formulierung untersucht (CLSM). Der Einfluss von PEG 300 auf o.g. Parameter wurde evaluiert. Die Kombinierbarkeit der Mikropartikel mit Gerüstmatrices und Gelen wurde nachgewiesen. Ausgewählte Formulierungen wurden *in vivo* in einem Mausmodell hinsichtlich ihrer Fähigkeit ektoper Knocheninduktion getestet. Zur Verfolgung der Calcifizierung wurden erstmalig Fluoreszenztechniken und BT-MRI angewendet. Die erzielten Ergebnisse wurden mittels CT und histologischer Evaluierung der Explantate bestätigt. Es wurden mehrere kontrollierte Freigabesysteme für rhBMP-2 entwickelt und erfolgreich *in vitro* und *in vivo* getestet. Es konnte gezeigt werden, dass die Kombination von PEP 5-mikroverkapseltem rhBMP-2 mit chitosanbasierten, sich *in situ*-bildenden Implantaten ein sehr effektives Freigabesystem darstellt und damit einen Beitrag zur Verringerung der benötigten rhBMP-2-Menge leisten kann.

6 Appendices

6.1 List of Abbreviations

Ac	*see List of Media and Buffer Solutions*
AcPEG	*see List of Media and Buffer Solutions*
AF4	Asymmetric Flow Field Flow Fractionation
AI	Active Ingredient
ALP	Alkaline Phosphatase
Asp-338	Asparagine #338
BCA	Bicinchoninic Acid
BMP	Bone Morphogenetic Protein
BSA	Bovine Serum Albumin
CCD	Charge-coupled Device
CHO	Chinese Hamster Ovary
CLSM	Confocal Laser Scanning Microscopy
CM	Calliper Rule Measurement
CT	Computer Tomography
D	Diffusion coefficient
DCM	Dichloromethane, methylene chloride
DNA	Deoxyribonucleic acid
DSC	Differential Scanning Calorimetry
DTT	Dithiothreitol
Dvr	Decapentaplegic Vg-related protein
E.coli	*Escherichia coli*
e.g.	*exempli gratia*
EDTA	Ethylenediaminetetraacetic acid
EDTA-Na	Ethylenediaminetetraacetic acid, sodium salt
EE	Ethyl Acetate
ELISA	Enzyme-linked Immunosorbent Assay
EPR	Electron Paramagnetic Resonance

ESEM	Environmental Scanning Electron Microscopy
Fig.	Figure
FPLC	Fast Protein Liquid Chromatography
GC-FID	Gas Chromatography with coupled Flame Ionization Detection
G-CSF	Granulocyte colony-stimulating factor
GDF	Growth and differentiation factor
GP	Glycerophosphate
HA	Hyaluronic acid
HE	Histological evaluation
HHA	Hydrophobically modified hyaluronic acid
HS	Hydroxystearate
i.e.	*id est*
IB	Inclusion bodies
LD	laser diffraction
MALDI	Matrix-assisted Laser desorption - Ionization
MRI	Magnetic Resonance Imaging
MS	Mass spectrometry
NHS	N-hydroxysuccinimide
NIR	Near Infrared
NMR	Nuclear Magnetic Resonance
NTA	Nanoparticle Tracking Analysis
OI	Optical Imaging
OP	Osteogenic protein
PB	Phosphate Buffer
PBS	Phosphate-buffered saline
PCS	Photon correlation spectroscopy
PDI	Polydispersity index
PEG	Polyethylene glycol
PEP 0, 5, 10	PLGA-PEG diblock with 0, 5 or 10 % PEG

PLA-PEG	Polylactic acid-polyethylene glycol diblock copolymer
PLGA	Poly(lactic-*co*-glycolic acid)
PLLA-PEG-PLLA	Poly-L-lactic acid-polyethylene glycol triblock copolymer
PTFE	Polytetrafluoroethylene
PVA	Polyvinyl alcohol
rhBMP	recombinant human Bone Morphogenetic Protein
rhoda*BMP-2	rhodamine B-labelled recombinant human Bone Morphogenetic Protein 2
ROI	Region(s) of interest
SDS	Sodium dodecylsulphate
SDS-PAGE	- Polyacrylamide gel electrophoresis
TG	Thermogravimetry
TGF-β	Transforming Growth Factor β
TOF	Time-of-flight
UV	Ultraviolet
β-GP	β-glycerophosphate

6.2 List of Media and Buffer Solutions

6.2.1 Isolation and Purification of rhBMP-2

IB Isolation Buffer I, pH 7.0:	100 mM Tris/HCl, 1 mM EDTA
IB Isolation Buffer II, pH 7.0:	60 mM EDTA, 6 % Triton X 100, 1,5 M NaCl
IB Isolation Buffer III, pH 7.0:	100 mM Tris/HCl, 20 mM EDTA
IB Solubilisation Buffer, pH 8.5:	100 mM Tris/HCl, 6 M GdmCl, 5 mM EDTA
Renaturation Buffer, pH 8.3:	100 mM Tris/HCl, 1 M L-arginine, 5 mM EDTA, 5 mM GSSG, 2 mM GSH
Renaturation Buffer according to Vallejo and Rinas, pH 8.5:	50 mM Tris/HCl, 500 mM GdmCl, 750 mM CHES, 1 M NaCl, 5 mM EDTA, 1 mM GSSG, 2 mM GSH
Purification Buffer I, pH 5.9:	6 M urea, 100 mM Tris, 5 mM EDTA, glacial acetic acid *q.s.*
Purification Buffer II, pH 5.9:	6 M urea, 100 mM Tris, 1 M NaCl, 5 mM EDTA, glacial acetic acid *q.s.*
DTT Removal Buffer, pH 3-4:	5 M GdmCl, 10 mM acetic acid
Arginine Removal Buffer, pH 7.5:	100 mM Tris/HCl, 1 mM EDTA
Lyophilization Buffer, pH 4.5:	20 mM ammonium acetate

6.2.2 SDS-PAGE

Resolving Buffer, pH 8.3:	25 mM Tris/HCl, 0.1 % (w/v) sodium dodecylsulphate, 187 mM glycine
Stacking Gel Buffer, pH 6.8:	125 mM Tris/HCl, 0.1 % (w/v) sodium dodecylsulphate
Resolv. Gel Buffer, pH 8.85:	750 mM Tris/HCl, 0.1 % (w/v) sodium dodecylsulphate
Resolving Gel:	6 ml acrylamide/bisacrylamide (29:1), 3.75 ml resolving gel buffer, 5.25 ml purified water, 120 µl ammonium persulphate (10 % w/v), 50 µl N,N,N',N'-tetramethyl-ethylenediamine
Sample Buffer:	12.5 % (w/v) stacking gel buffer, 2.5 % (w/v) sodium dodecylsulphate, 0.1 % (w/v) bromophenol blue, ± 5 % (v/v) β-mercaptoethanol
Staining Solution:	1 g/l Coomassie Brilliant Blue R 250, 10 % (v/v) glacial acetic acid, 40 % (w/v) ethanol
Destaining Solution:	10 % (v/v) glacial acetic acid, 40 % (w/v) ethanol

6.2.3 Microsphere Fabrication Standard Buffers

Inner Phase, Ac pH 4.5:	20 mM sodium acetate/ glacial acetic acid
Inner Phase, AcPEG pH 4.5:	20 mM sodium acetate/ glacial acetic acid, 33 % (v/v) polyethylene glycol 300
Inner Phase, Phos pH 5.0:	20 mM potassium dihydrogen phosphate/ phosphoric acid

6.2.4 *In vitro* Release and Stability

Release Buffer, pH 7.4:	Phosphate Buffered Saline pH 7.4 R[121], supplemented with 0.05 % (v/v) polysorbate 20, 1 % (w/v) bovine serum albumin, 0.15 % (w/v) disodium EDTA, 0.02 % (w/v) sodium azide
Phosphate Buffers for pH calibration, 20 mM:	Disodium hydrogen phosphate dodeca-hydrate, potassium dihydrogen phosphate, phosphoric acid in varying ratios

6.2.5 *In vitro* Activity Assay

Cell Culture Medium:	RPMI 1640 medium (PAA Laboratories, Cölbe, Germany), supplemented with 10 % v/v fetal bovine serum
Differentiaton Medium:	RPMI 1640 medium (PAA Laboratories, Cölbe, Germany), supplemented with 2 % v/v fetal bovine serum
ALP Buffer, pH 9.6:	100 mM glycine/ Na^+, 1 mM zinc chloride, 1 mM magnesium chloride

7 References

1. Haidar ZS, Hamdy RC, Tabrizian M. Delivery of recombinant bone morphogenetic proteins for bone regeneration and repair. Part A: Current challenges in BMP delivery. Biotechnol Lett 31[12], 1817-1824. 2009.

2. Reddi AH. BMPs: From bone morphogenetic proteins to body morphogenetic proteins. Cytokine Growth Factor Rev 16[3], 249-250. 2005.

3. Hollinger JO, Kleinschmidt JC. The critical size defect as an experimental model to test bone repair materials. J Craniofac Surg 1[1], 60-68. 1990.

4. Westerhuis RJ, van Bezooijen RL, Kloen P. Use of bone morphogenetic proteins in traumatology. Injury 36[12], 1405-1412. 2005.

5. Gründer JWL. Geschichte der Chirurgie von den Urzeiten bis zu Anfang des achtzehnten Jahrhunderts. Breslau: Trewendt und Granier; 1859.

6. Longacre J, de Stefano G. Reconstruction of extensive defects of the skull with split rib grafts. Plast Reconstr Surg 19[3], 186-200. 1957.

7. Urist MR, O'Connor, BT, Burwell, RG (Eds.). Bone grafts, derivatives, and substitutes. 1st ed. Oxford: Butterworth-Heinemann; 1994.

8. Lieberman JR, Friedlaender GE (Eds.). Bone Regeneration and Repair Biology and Clinical Applications. 1st ed. Totowa, NJ, US: Humana Press; 2005.

9. Senn N. On the healing of aseptic bone cavities by implantation of antiseptic decalcified bone. Am J Med Sci 98[3], 219-247. 1889.

10. Mowlem R. Cancellous Chip-Bone Grafts. A Report on 75 Cases. Lancet 244[6328] 746-748. 1944.

11. Mowlem R. Bone and cartilage transplants: Their use and behaviour. Brit J Surg 29[114], 182-193. 1941.

12. Zalavras CG, Marcus RE, Levin LS, Patzakis MJ. Management of open fractures and subsequent complications. J Bone Joint Surg Am 89[4], 884-895. 2007.

13. Geiger M, Li RH, Friess W. Collagen sponges for bone regeneration with rhBMP-2. Adv Drug Deliv Rev 55[12], 1613-1629. 2003.

14. Winn SR, Uludag H, Hollinger JO. Sustained release emphasizing recombinant human bone morphogenetic protein-2. Adv Drug Deliv Rev 31[3], 303-318. 1998.

15. Urist MR. Bone: formation by autoinduction. Science 150[698], 893-899. 1965.

16. Urist MR, McLean FC. Osteogenetic potency and new-bone formation by induction in transplants to the anterior chamber of the eye. J Bone Joint Surg Am 34-A[2], 443-476. 1952.

17. Van de Putte KA, Urist MR. Osteogenesis in the interior of intramuscular implants of decalcified bone matrix. Clin Orthop Relat Res 43, 257-270. 1965.

18. Reddi AH, Kuettner KE. Vascular invasion of cartilage: correlation of morphology with lysozyme, glycosaminoglycans, protease, and protease-inhibitory activity during endochondral bone development. Developmental Biology (US) 82[2], 217-223. 1981.

19. Sampath TK, Reddi AH. Dissociative extraction and reconstitution of extracellular matrix components involved in local bone differentiation. Proc Natl Acad Sci USA 78[12], 7599-7603. 1981.

20. Wozney JM, Rosen V, Celeste AJ, Mitsock LM, Whitters MJ, Kriz RW, Hewick RM, Wang EA. Novel regulators of bone formation: molecular clones and activities. Science 242[4885], 1528-1534. 1988.

21. Langer R, Vacanti JP. Tissue engineering. Science 260[5110], 920-926. 1993.

22. Kim HK, Shim WS, Kim SE, Lee KH, Kang E, Kim JH, Kim K, Kwon IC, Lee DS. Injectable In Situ-Forming pH/Thermo-Sensitive Hydrogel for Bone Tissue Engineering. Tissue Eng A 15[4], 923-933. 2009.

23. Stevens MM, Marini RP, Schaefer D, Aronson J, Langer R, Shastri VP. In vivo engineering of organs: The bone bioreactor. Proc Natl Acad Sci USA 102[32], 11450-11455. 2005.

24. Betz OB, Betz VM, Nazarian A, Pilapil CG, Vrahas MS, Bouxsein ML, Gerstenfeld LC, Einhorn TA, Evans CH. Direct percutaneous gene delivery to enhance healing of segmental bone defects. J Bone Joint Surg Am 88[2], 355-365. 2006.

25. Rengachary SS. Bone morphogenetic proteins: basic concepts. Neurosurg Focus 13[6], e2. 2002.

26. Bessa PC, Casal M, Reis RL. Bone morphogenetic proteins in tissue engineering: the road from the laboratory to the clinic, part I (basic concepts). J Tissue Eng Regen Med 2[1], 1-13. 2008.

27. Reddi AH. Regulation of cartilage and bone differentiation by bone morphogenetic proteins. Curr Opin Cell Biol 4[5], 850-855. 1992.

28. Termaat MF, Den Boer FC, Bakker FC, Patka P, Haarman HJT. Bone morphogenetic proteins. Development and clinical efficacy in the treatment of fractures and bone defects. J Bone Joint Surg Am 87[6], 1367-1378. 2005.

29. Ten Dijke P, Fu J, Schaap P, Roelen BAJ. Signal transduction of bone morphogenetic proteins in osteoblast differentiation. J Bone Joint Surg Am 85-A Suppl 3, 34-38. 2003.

30. Tsumaki N, Yoshikawa H. The role of bone morphogenetic proteins in endochondral bone formation. Cytokine Growth Factor Rev 16[3], 279-285. 2005.

31. Rosen V. BMP2 signaling in bone development and repair. Cytokine Growth Factor Rev 20[5;6], 475-480. 2009.

32. Bostrom MP, Lane JM, Berberian WS, Missri AA, Tomin E, Weiland A, Doty SB, Glaser D, Rosen VM. Immunolocalization and expression of bone morphogenetic proteins 2 and 4 in fracture healing. J Orthop Res 13[3], 357-367. 1995.

33. Reddi AH, Reddi A. Bone morphogenetic proteins (BMPs): From morphogens to metabologens. Cytokine Growth Factor Rev 20[5;6], 341-342. 2009.

34. Smith DM, Cooper GM, Mooney MP, Marra KG, Losee JE. Bone morphogenetic protein 2 therapy for craniofacial surgery. J Craniofac Surg 19[5], 1244-1259. 2008.

35. Allen RT, Lee Y, Stimson E, Garfin SR. Bone morphogenetic protein-2 (BMP-2) in the treatment of pyogenic vertebral osteomyelitis. Spine 32[26], 2996-3006. 2007.

36. Arnander C, Westermark A, Veltheim R, Docherty-Skogh A, Hilborn J, Engstrand T. Three-dimensional technology and bone morphogenetic protein in frontal bone reconstruction. J Craniofac Surg 17[2], 275-279. 2006.

37. Lee JH, Kim CS, Choi KH, Jung UW, Yun JH, Choi SH, Cho KS. The induction of bone formation in rat calvarial defects and subcutaneous tissues by recombinant human BMP-2, produced in Escherichia coli. Biomaterials 31[13], 3512-3519. 2010.

38. Seeherman H, Li R, Wozney J. A review of preclinical program development for evaluating injectable carriers for osteogenic factors. J Bone Joint Surg Am 85-A Suppl 3, 96-108. 2003.

39. Uludag H, D'Augusta D, Palmer R, Timony G, Wozney J. Characterization of rhBMP-2 pharmacokinetics implanted with biomaterial carriers in the rat ectopic model. J Biomed Mater Res 46[2], 193-202. 1999.

40. Bessa PC, Casal M, Reis RL. Bone morphogenetic proteins in tissue engineering: the road from laboratory to clinic, part II (BMP delivery). J Tissue Eng Regen Med 2[2;3], 81-96. 2008.

41. Schmoekel H, Schense JC, Weber FE, Gratz KW, Gnagi D, Muller R, Hubbell JA. Bone healing in the rat and dog with nonglycosylated BMP-2 demonstrating low solubility in fibrin matrices. Journal of Orthopaedic Research 22[2], 376-381. 2004.

42. Bessho K, Carnes DL, Cavin R, Ong JL. Experimental studies on bone induction using low-molecular-weight poly (DL-lactide-co-glycolide) as a carrier for recombinant human bone morphogenetic protein-2. J Biomed Mat Res 61[1], 61-65. 2002.

43. http://www.medtronic com/your-health/lumbar-degenerative-disc-disease/surgery/benefits-and-risks/index.htm. accessed 7-7-2010.

44. Mussano F, Ciccone G, Ceccarelli M, Baldi I, Bassi F. Bone morphogenetic proteins and bone defects: a systematic review. Spine 32[7], 824-830. 2007.

45. DRG-Entgelttarif für Krankenhäuser im Anwendungsbereich des KHEntgG und Unterrichtung des Patienten gemäß § 8 KHEntgG. St. Joseph Krankenhaus Berlin-Tempelhof, Germany; 2010.

46. DRG-Entgelttarif für Krankenhäuser im Anwendungsbereich des KHEntgG, Unterrichtung des Patienten gem. § 8 KHEntgG. RoMed Klinikum Rosenheim, Germany; 2010.

47. Niu X, Feng Q, Wang M, Guo X, Zheng Q. Porous nano-HA/collagen/PLLA scaffold containing chitosan microspheres for controlled delivery of synthetic peptide derived from BMP-2. J Control Rel 134[2], 111-117. 2009.

48. Patel ZS, Yamamoto M, Ueda H, Tabata Y, Mikos AG. Biodegradable gelatin microparticles as delivery systems for the controlled release of bone morphogenetic protein-2. Acta Biomat 4[5], 1126-1138. 2008.

49. Wang CK, Ho ML, Wang GJ, Chang JK, Chen CH, Fu YC, Fu HH. Controlled-release of rhBMP-2 carriers in the regeneration of osteonecrotic bone. Biomaterials 30[25], 4178-4186. 2009.

50. Lee M, Li W, Siu RK, Whang J, Zhang X, Soo C, Ting K, Wu BM. Biomimetic apatite-coated alginate/chitosan microparticles as osteogenic protein carriers. Biomaterials 30[30], 6094-6101. 2009.

51. Jha AK, Yang W, Kirn-Safran CB, Farach-Carson MC, Jia X. Perlecan domain I-conjugated, hyaluronic acid-based hydrogel particles for enhanced chondrogenic differentiation via BMP-2 release. Biomaterials 30[36], 6964-6975. 2009.

52. Balmayor ER, Feichtinger GA, Azevedo HS, van Griensven M, Reis RL. Starch-poly-epsilon-caprolactone microparticles reduce the needed amount of BMP-2. Clin Orthop Relat Res 467[12], 3138-3148. 2009.

53. Chen F, Chen R, Wang X, Sun H, Wu Z. In vitro cellular responses to scaffolds containing two microencapulated growth factors. Biomaterials 30[28], 5215-5224. 2009.

54. Luginbuehl V, Meinel L, Merkle HP, Gander B. Localized delivery of growth factors for bone repair. European Journal of Pharmaceutics and Biopharmaceutics 58[2], 197-208. 2004.

55. Seeherman H, Wozney J, Li R. Bone morphogenetic protein delivery systems. Spine 27[16 Suppl 1], S16-S23. 2002.

56. Wozney JM, Li RH. Engineering what comes naturally. Nature Biotechnology 21[5], 506-508. 2003.

57. Uludag H, Gao T, Porter TJ, Friess W, Wozney JM. Delivery systems for BMPs: factors contributing to protein retention at an application site. J Bone Joint Surg Am 83-A Suppl 1[Pt 2], S128-S135. 2001.

58. Woo BH, Fink BF, Page R, Schrier JA, Jo YW, Jiang G, DeLuca M, Vasconez HC, DeLuca PP. Enhancement of bone growth by sustained delivery of recombinant human bone morphogenetic protein-2 in a polymeric matrix. Pharm Res 18[12], 1747-1753. 2001.

59. Li RH, Wozney JM. Delivering on the promise of bone morphogenetic proteins. Trends Biotechnol 19[7], 255-265. 2001.

60. Takahashi Y, Yamamoto M, Yamada K, Kawakami O, Tabata Y. Skull Bone Regeneration in Nonhuman Primates by Controlled Release of Bone Morphogenetic Protein-2 from a Biodegradable Hydrogel. Tissue Eng 13[2], 293-300. 2007.

61. Tabata Y. The importance of drug delivery systems in tissue engineering. Pharm Sci Technol Today 3[3], 80-89. 2000.

62. Brekke J. A rationale for Delivery of Osteoinductive Proteins. Tiss Eng 2[2], 97-114. 1996.

63. De Long WG, Jr., Einhorn TA, Koval K, McKee M, Smith W, Sanders R, Watson T. Bone grafts and bone graft substitutes in orthopaedic trauma surgery. A critical analysis. J Bone Joint Surg Am 89[3], 649-658. 2007.

64. Babensee JE, McIntire LV, Mikos AG. Growth factor delivery for tissue engineering. Pharm Res 17[5], 497-504. 2000.

65. Bergeron E, Marquis ME, Chretien I, Faucheux N. Differentiation of preosteoblasts using a delivery system with BMPs and bioactive glass microspheres. J Mater Sci: Mater Med 18[2], 255-263. 2007.

66. Schrier JA, Fink BF, Rodgers JB, Vasconez HC, DeLuca PP. Effect of a freeze-dried CMC/PLGA microsphere matrix of rhBMP-2 on bone healing. AAPS PharmSciTech 2[3], E18. 2001.

67. Shen H, Hu X, Yang F, Bei J, Wang S. An injectable scaffold: rhBMP-2-loaded poly(lactide-co-glycolide)/hydroxyapatite composite microspheres. Acta Biomater 6[2], 455-465. 2010.

68. Schrier JA, DeLuca PP. Recombinant human bone morphogenetic protein-2 binding and incorporation in PLGA microsphere delivery systems. Pharm Dev Technol 4[4], 611-621. 1999.

69. El-Ghannam A, Ning CQ, Mehta J. Cyclosilicate nanocomposite: A novel resorbable bioactive tissue engineering scaffold for BMP and bone-marrow cell delivery. J Biomed Mat Res A 71A[3], 377-390. 2004.

70. Laschke MW, Witt K, Pohlemann T, Menger MD. Injectable nanocrystalline hydroxyapatite paste for bone substitution: in vivo analysis of biocompatibility and vascularization. J Biomed Mat Res B 82B[2], 494-505. 2007.

71. Nitzsche H, Lochmann A, Metz H, Hauser A, Syrowatka F, Hempel E, Mueller T, Thurn-Albrecht T, Maeder K. Fabrication and characterization of a biomimetic composite scaffold for bone defect repair. J Biomed Mater Res A 94A[1], 298-307. 2010.

72. Whang K, Tsai DC, Nam EK, Aitken M, Sprague SM, Patel PK, Healy KE. Ectopic bone formation via rhBMP-2 delivery from porous bioabsorbable polymer scaffolds. J Biomed Mater Res 42[4], 491-499. 1998.

73. Lutolf MP, Lauer-Fields JL, Schmoekel HG, Metters AT, Weber FE, Fields GB, Hubbell JA. Synthetic matrix metalloproteinase-sensitive hydrogels for the conduction of tissue regeneration: Engineering cell-invasion characteristics. Proc Nat Acad Sci USA 100[9], 5413-5418. 2003.

74. Shi S, Cheng X, Wang J, Zhang W, Peng L, Zhang Y. RhBMP-2 microspheres-loaded chitosan/collagen scaffold enhanced osseointegration: an experimental in dog. J Biomater Appl 23[4], 331-346. 2009.

75. Chen Fm, Zhao YM, Sun HH, Jin T, Wang Qt, Zhou W, Wu Zf, Jin Y. Novel glycidyl methacrylated dextran (Dex-GMA)/gelatin hydrogel scaffolds containing microspheres loaded with bone morphogenetic proteins: Formulation and characteristics. J Control Rel 118[1], 65-77. 2007.

76. Ruhe PQ, Boerman OC, Russel FGM, Spauwen PHM, Mikos AG, Jansen JA. Controlled release of rhBMP-2 loaded poly(dl-lactic-co-glycolic acid)/calcium phosphate cement composites in vivo. J Control Rel 106[1-2], 162-171. 2005.

77. Varde NK, Pack DW. Microspheres for controlled release drug delivery. Expert Opin Biol Therapy 4[1], 35-51. 2004.

78. Benita, S (Ed.). Microencapsulation - Methods and Industrial Applications. 2nd ed. Boca Raton, US: Taylor & Francis; 2006.

79. Mäder K, Weidenauer U (Eds.). Innovative Arzneiformen. 1st ed. Stuttgart, Germany: Wissenschaftliche Verlagsgesellschaft; 2010.

80. Schwartz D. Development of an Aqueous Suspension of Recombinant Human Bone Morphogenetic Protein-2 (rhBMP-2) PhD thesis LMU Munich, Germany, 2005.

81. Chen F, Wu Z, Wang Q, Wu H, Zhang Y, Nie X, Jin Y. Preparation of recombinant human bone morphogenetic protein-2 loaded dextran-based microspheres and their characteristics. Acta Pharmacol Sin 26[9], 1093-1103. 2005.

82. Uchegbu, IF (Ed.). Polymers in Drug Delivery. Boca Raton, US: Taylor and Francis; 2006.

83. Freitas S, Merkle HP, Gander B. Microencapsulation by solvent extraction/evaporation: reviewing the state of the art of microsphere preparation process technology. J Control Rel 102[2],313-332. 2005.

84. Mikos AG, Temenoff JS. Formation of highly porous biodegradable scaffolds for tissues engineering. EJB Electronic Journal of Biotechnology [online computer file] 3[2], 2000.

85. Database of the ABDA - Federal Union of German Associations of Pharmacists. http://www.justscience de/de/drugbase/abda-datenbank/fertigarzneimittel.html. accessed 17-7-2010.

86. Park JH, Ye M, Park K. Biodegradable polymers for microencapsulation of drugs. Molecules 10[1], 146-161. 2005.

87. Wischke C, Schwendeman SP. Principles of encapsulating hydrophobic drugs in PLA/PLGA microparticles. Int J Pharm 364[2], 298-327. 2008.

88. Cohen S, Yoshioka T, Lucarelli M, Hwang LH, Langer R. Controlled delivery systems for proteins based on poly(lactic/glycolic acid) microspheres. Pharm Res 8[6], 713-720. 1991.

89. Crotts G, Park TG. Protein delivery from poly(lactic-co-glycolic acid) biodegradable microspheres: release kinetics and stability issues. J Microencaps 15[6], 699-713. 1998.

90. Ruhe PQ, Hedberg EL, Padron NT, Spauwen Paul HM, Jansen JA, Mikos AG. rhBMP-2 release from injectable poly(DL-lactic-co-glycolic acid)/calcium-phosphate cement composites. J Bone Joint Surg Am 85-A Suppl 3, 75-81. 2003.

91. Kempen DHR, Yaszemski MJ, Heijink A, Hefferan TE, Creemers LB, Britson J, Maran A, Classic KL, Dhert WJA, Lu L. Non-invasive monitoring of BMP-2 retention and bone formation in composites for bone tissue engineering using SPECT/CT and scintillation probes. J Control Rel 134[3], 169-176. 2009.

92. Isobe M, Yamazaki Y, Oida S, Ishihara K, Nakabayashi N, Amagasa T. Bone morphogenetic protein encapsulated with a biodegradable and biocompatible polymer. J Biomed Mat Res 32[3], 433-438. 1996.

93. Oldham JB, Lu L, Zhu X, Porter BD, Hefferan TE, Larson DR, Currier BL, Mikos AG, Yaszemski MJ. Biological activity of rhBMP-2 released from PLGA microspheres. J Biomech Eng 122[3], 289-292. 2000.

94. Vasita R, Katti DS. Growth factor-delivery systems for tissue engineering: a materials perspective. Expert Rev Med Devices 3[1], 29-47. 2006.

95. Valentin-Opran A, Wozney J, Csimma C, Lilly L, Riedel GE. Clinical evaluation of recombinant human bone morphogenetic protein-2. Clin Orthop Relat Res [395], 110-120. 2002.

96. Laub M, Chatzinikolaidou M, Jennissen HP. Aspects of BMP-2 binding to receptors and collagen: influence of cell senescence on receptor binding and absence of high-affinity stoichiometric binding to collagen. Materialwiss Werkstofftech 38[12], 1019-1026. 2007.

97. Gao T, Kousinioris N, Winn SR, Wozney JM, Uludag H. Enhanced retention of rhBMP-2 in vivo by thermoreversible polymers. Materialwiss Werkstofftech 32[12], 953-961. 2001.

98. Shahlaie K, Kim KD. Occipitocervical fusion using recombinant human bone morphogenetic protein-2: adverse effects due to tissue swelling and seroma. Spine 33[21], 2361-2366. 2008.

99. Benglis D, Wang MY, Levi AD. A comprehensive review of the safety profile of bone morphogenetic protein in spine surgery. Neurosurgery 62[5 Suppl 2], ONS423-ONS431. 2008.

100. Boakye M, Mummaneni P, V, Garrett M, Rodts G, Haid R. Anterior cervical discectomy and fusion involving a polyetheretherketone spacer and bone morphogenetic protein. J Neurosurg Spine 2[5], 521-525. 2005.

101. Brower RS, Vickroy NM. A case of psoas ossification from the use of BMP-2 for posterolateral fusion at L4-L5. Spine 33[18], E653-E655. 2008.

102. Tumialan LM, Pan J, Rodts GE, Mummaneni P, V. The safety and efficacy of anterior cervical discectomy and fusion with polyetheretherketone spacer and recombinant human bone morphogenetic protein-2: a review of 200 patients. J Neurosurg Spine 8[6], 529-535. 2008.

103. Axelrad TW, Einhorn TA. Bone morphogenetic proteins in orthopaedic surgery. Cytokine Growth Factor Rev 20[5;6], 481-488. 2009.

104. Talwar R, Di Silvio L, Hughes FJ, King GN. Effects of carrier release kinetics on bone morphogenetic protein-2-induced periodontal regeneration in vivo. J Clin Periodontol 28[4], 340-347. 2001.

105. Bae HW, Zhao L, Kanim Linda EA, Wong P, Delamarter RB, Dawson EG. Intervariability and intravariability of bone morphogenetic proteins in commercially available demineralized bone matrix products. Spine 31[12], 1299-1306. 2006.

106. Pietrzak WS, Woodell-May J, McDonald N. Assay of bone morphogenetic protein-2, -4, and -7 in human demineralized bone matrix. J Craniofac Surg 17[1], 84-90. 2006.

107. Mäder K, Bittner B, Li Y, Wohlauf W, Kissel T. Monitoring microviscosity and microacidity of the albumin microenvironment inside degrading microparticles from poly(lactide-co-glycolide) (PLG) or ABA-triblock polymers containing hydrophobic poly(lactide-co-glycolide) A blocks and hydrophilic poly(ethylene oxide) B blocks. Pharm Res 15[5], 787-793. 1998.

108. Pean JM, Boury F, Venier-Julienne MC, Menei P, Proust JE, Benoit JP. Why does PEG 400 co-encapsulation improve NGF stability and release from PLGA biodegradable microspheres? Pharm Res 16[8], 1294-1299. 1999.

109. Al-Azzam W, Pastrana EA, King B, Mendez J, Griebenow K. Effect of the covalent modification of horseradish peroxidase with poly(ethylene glycol) on the activity and stability upon encapsulation in polyester microspheres. J Pharm Sci 94[8], 1808-1819. 2005.

110. Hillger F. Recombinant production and biophysical characterization of proBMP-2, BMP-2 and the BMP 2-propeptide. PhD thesis, MLU Halle-Wittenberg, Germany, 2006.

111. Hillger F, Herr G, Rudolph R, Schwarz E. Biophysical Comparison of BMP-2, ProBMP-2, and the Free Pro-peptide Reveals Stabilization of the Pro-peptide by the Mature Growth Factor. J Biol Chem 280[15], 14974-14980. 2005.

112. Rudolph R, Böhm G, Lilie H, Jaenicke R. Folding Proteins. In: Creighton, TE. Protein Function: A Practical Approach. 2nd Edition. Oxford: Oxford University Press. 1997.

113. Vallejo LF, Rinas U. Optimized procedure for renaturation of recombinant human bone morphogenetic protein-2 at high protein concentration. Biotechnol Bioeng 85[6], 601-609. 2004.

114. Ruppert R, Hoffmann E, Sebald W. Human bone morphogenetic protein 2 contains a heparin-binding site which modifies its biological activity. Eur J Biochem 237[1], 295-302. 1996.

115. Schwartz D, Sofia S, Friess W. Integrity and stability studies of precipitated rhBMP-2 microparticles with a focus on ATR-FTIR measurements. Eur J Pharm Biopharm 63[3], 241-248. 2006.

116. Scheufler C, Sebald W, Hülsmeyer M. Crystal structure of human bone morphogenetic protein-2 at 2.7 Å resolution. J Mol Biol 287[1], 103-115. 1999.

117. Augsten C, Mäder K. Characterizing molar mass distributions and molecule structures of different chitosans using asymmetrical flow field-flow fractionation combined with multi-angle light scattering. Int J Pharm 351[1-2], 23-30. 2008.

118. Vakurov A, Pchelintsev NA, Forde J, O'Fagain C, Gibson T, Millner P. The preparation of size-controlled functionalized polymeric nanoparticles in micelles. Nanotechnology 20[29], 295605. 2009.

119. Technical Note: Direct Visualisation, Sizing and Counting of Aggregation in Proteins. Nanosight Ltd. http://www.nanosight.com/appnotes/M115E%20Application%20Note%20Direct%20Visualisation%20Sizing%20and%20Counting%20of%20Aggregation%20in%20Proteins.pdf. 2009.

120. Domingos RF, Baalousha MA, Ju-Nam Y, Reid MM, Tufenkji N, Lead JR, Leppard GG, Wilkinson KJ. Characterizing Manufactured

Nanoparticles in the Environment: Multimethod Determination of Particle Sizes. Environ Sci Technol 43[19], 7277-7284. 2009.

121. Directorate for the Quality of Medicines & HealthCare of the Council of Europe (EDQM): European Pharmacopeia 6.08. 2009.

122. Quantikine BMP-2 Immunoassay Package Insert. RnD Systems. Last update 15-1-2007.

123. Augsten C, Kiselev MA, Gehrke R, Hause G, Mäder K. A detailed analysis of biodegradable nanospheres by different techniques-A combined approach to detect particle sizes and size distributions. J Pharm Biomed Anal 47[1], 95-102. 2008.

124. Cuifang C, Shirui M, Germershaus O, Schaper A, Rytting E, Chen D, Kissel T. Influence of morphology and drug distribution on the release process of FITC-dextran-loaded microspheres prepared with different types of PLGA. J Microencapsul 26[4], 334-45. 2009.

125. Witschi C, Doelker E. Influence of the microencapsulation method and peptide loading on poly(lactic acid) and poly(lactic-co-glycolic acid) degradation during in vitro testing. J Control Rel 51[2,3], 327-341. 1998.

126. Mao S, Xu J, Cai C, Germershaus O, Schaper A, Kissel T. Effect of WOW process parameters on morphology and burst release of FITC-dextran loaded PLGA microspheres. Int J Pharm 334[1-2] 137-48. 2007.

127. Luca L, Capelle MAH, Machaidze G, Arvinte T, Jordan O, Gurny R. Physical instability, aggregation and conformational changes of recombinant human bone morphogenetic protein-2 (rhBMP-2). Int J Pharm 391[1-2], 48-54. 2010.

128. Schliecker G, Schmidt C, Fuchs S, Kissel T. Characterization of a homologous series of D,L-lactic acid oligomers; a mechanistic study on the degradation kinetics in vitro. Biomaterials 24[21] 3835-44. 2003.

129. Katou H, Wandrey AJ, Gander B. Kinetics of solvent extraction/ evaporation process for PLGA microparticle fabrication. Int J Pharm 364[1], 45-53. 2008.

130. Wischke C. Protein loaded microparticles with modified surfaces for the targeting of dendritic cells. PhD thesis, FU Berlin, Germany 2006.

131. Patterson J, Stayton PS, Li X. In situ characterization of the degradation of PLGA microspheres in hyaluronic acid hydrogels by optical coherence tomography. IEEE Trans Med Imaging 28[1], 74-81. 2009.

132. Musumeci T, Ventura CA, Giannone I, Ruozi B, Montenegro L, Pignatello R, Puglisi G. PLA/PLGA nanoparticles for sustained release of docetaxel. Int J Pharm 325[1-2], 172-179. 2006.

133. Mie G. Contributions to the Optics of Turbid Media, Especially Colloidal Metal Solutions. Ann Phys 25, 377-445. 1908.

134. Rawle A, Kippax P. Setting New Standards for Laser Diffraction Particle Analysis. Available at www.iscpubs.com, accessed 04-02-2010.

135. ISO 13320:2009 Particle size analysis - Laser diffraction methods. 2009.

136. Rawle A. Basic principles of particle-size analysis. Surf Coat Int A 86[A2], 58-65. 2003.

137. Perez-Rodriguez C, Montano N, Gonzalez K, Griebenow K. Stabilization of alpha -chymotrypsin at the CH2Cl2/water interface and upon water-in-oil-in-water encapsulation in PLGA microspheres. J Control Rel 89[1], 71-85. 2003.

138. Castellanos IJ, Crespo R, Griebenow K. Poly(ethylene glycol) as stabilizer and emulsifying agent: a novel stabilization approach preventing aggregation and inactivation of proteins upon encapsulation in bioerodible polyester microspheres. J Control Rel 88[1], 135-145. 2003.

139. Hauburger A, von Einem S, Schwaerzer GK, Buttstedt A, Zebisch M, Schraml M, Hortschansky P, Knaus P, Schwarz E. The pro-form of BMP-2 interferes with BMP-2 signalling by competing with BMP-2 for IA receptor binding. FEBS J 276[21], 6386-6398. 2009.

140. Nitzsche H. Development and Characterization of Nano-Hydroxyapatite - Collagen - Chitosan Scaffolds for Bone Regeneration. PhD thesis, MLU Halle-Wittenberg, Germany, 2010.

141. Hu Y, Zhang C, Zhang S, Xiong Z, Xu J. Development of a porous poly(L-lactic acid)/hydroxyapatite/collagen scaffold as a BMP delivery system and its use in healing canine segmental bone defect. J Biomed Mat Res A 67A[2], 591-598. 2003.

142. Itoh S, Kikuchi M, Takakuda K, Nagaoka K, Koyama Y, Tanaka J, Shinomiya K. Implantation study of a novel hydroxyapatite/collagen (HAp/Col) composite into weight-bearing sites of dogs. J Biomed Mat Res 63[5], 507-515. 2002.

143. Leach JB, Schmidt CE. Characterization of protein release from photocrosslinkable hyaluronic acid-polyethylene glycol hydrogel tissue engineering scaffolds. Biomaterials 26[2], 125-135. 2005.

144. Finelli I, Chiessi E, Galesso D, Renier D, Paradossi G. Gel-like structure of a hexadecyl derivative of hyaluronic acid for the treatment of osteoarthritis. Macromol Biosci 9[7], 646-653. 2009.

145. Schein CH. Production of soluble recombinant proteins in bacteria. Nature Biotechnology 7[11],1141-1149. 1989.

146. Klages J, Kotzsch A, Coles M, Sebald W, Nickel J, Mueller T, Kessler H. The Solution Structure of BMPR-IA Reveals a Local Disorder-to-Order Transition upon BMP-2 Binding. Biochemistry 47[46], 11930-11939. 2008.

147. Keller S, Nickel J, Zhang JL, Sebald W, Mueller TD. Molecular recognition of BMP-2 and BMP receptor IA. Nat Struct Mol Biol 11[5], 481-488. 2004.

148. von Einem S, Schwarz E, Rudolph R. A novel TWO-STEP renaturation procedure for efficient production of recombinant BMP-2. Protein Expression Purif 73[1] 65-69. 2010.

149. Vallejo LF, Brokelmann M, Marten S, Trappe S, Cabrera-Crespo J, Hoffmann A, Gross G, Weich HA, Rinas U. Renaturation and purification of bone morphogenetic protein-2 produced as inclusion bodies in high-cell-density cultures of recombinant Escherichia coli. J Biotechnol 94[2], 185-194. 2002.

150. Frokjaer S, Hovgaard L, (Eds.). Pharmaceutical Formulation Development of Peptides and Proteins. 1st ed., London: Taylor and Francis; 2000.

151. Wang W. Protein aggregation and its inhibition in biopharmaceutics. Int J Pharm 289[1-2], 1-30. 2005.

152. Wang W. Instability, stabilization, and formulation of liquid protein pharmaceuticals. Int J Pharm 185[2], 129-188. 1999.

153. van der Walle CF, Sharma G, Kumar MNVR. Current approaches to stabilising and analysing proteins during microencapsulation in PLGA. Expert Opin Drug Delivery 6[2], 177-186. 2009.

154. Wang W, Nema S, Teagarden D. Protein aggregation-Pathways and influencing factors. Int J Pharm 390[2], 89-99. 2010.

155. Hermanson GT. Bioconjugate Techniques. Second ed. Oxford: Elsevier; 2008.

156. Rohatgi-Mukherjee KK, Lopez-Arbeloa I. Correlation of liquid structure with the photophysics of Rhodamine B (acidic, basic and ester forms) in water-ethanol mixed solvent. J Photochem Photobiol A 58[3], 277-288. 1991.

157. Karas M, Hillenkamp F. Laser desorption ionization of proteins with molecular masses exceeding 10,000 daltons. Anal Chem 60[20], 2299-2301. 1988.

158. Dreisewerd K. The desorption process in MALDI. Chem Rev 103[2], 395-425. 2003.

159. Kjellstroem S, Jensen ON. Phosphoric Acid as a Matrix Additive for MALDI MS Analysis of Phosphopeptides and Phosphoproteins. Anal Chem 76[17], 5109-5117. 2004.

160. Technical Note: High Mass Linear Analysis of intact Proteins on the 4800 MALDI TOF/TOF Analyzer. Applied Biosystems; 2005. http://docs.appliedbiosystems.com/pebiodocs/00114273.pdf.

161. Laub M, Chatzinikolaidou M, Rumpf H, Jennissen HP. Modelling of protein-protein interactions of bone morphogenetic protein-2 (BMP-2) by 3D-Rapid Prototyping. Materialwiss Werkstofftech 33[12], 729-737. 2002.

162. Matthews BW. Solvent content of protein crystals. J Mol Biol 33[2], 491-497. 1968.

163. Erickson HP. Size and shape of protein molecules at the nanometer level determined by sedimentation, gel filtration, and electron microscopy. Biol Proced Online 11[1], 32-51. 2009.

164. Nguyen TH, Ward C. Stability characterization and formulation development of alteplase, a recombinant tissue plasminogen activator. Pharm Biotechnol 5, 91-134. 1993.

165. Keskin DS, Tezcaner A, Korkusuz P, Korkusuz F, Hasirci V. Collagen-chondroitin sulfate-based PLLA-SAIB-coated rhBMP-2 delivery system for bone repair. Biomaterials 26[18], 4023-4034. 2005.

166. Jeon O, Song SJ, Kang SW, Putnam AJ, Kim BS. Enhancement of ectopic bone formation by bone morphogenetic protein-2 released from a heparin-conjugated poly(-lactic-co-glycolic acid) scaffold. Biomaterials 28[17], 2763-2771. 2007.

167. Maeda H, Sano A, Fujioka K. Controlled release of rhBMP-2 from collagen minipellet and the relationship between release profile and ectopic bone formation. Int J Pharm 275[1-2], 109-122. 2004.

168. Geiger M. Porous Collagen/Ceramic Composite Carriers for Bone Regeneration Using Recombinant Human Bone Morphogenetic Protein-2 (rhBMP-2). PhD thesis, FAU Erlangen-Nürnberg, Germany, 2001.

169. Frokjaer S, Otzen DE. Protein drug stability: a formulation challenge. Nat Rev Drug Discovery 4[4], 298-306. 2005.

170. Yang YY, Chung TS, Bai XL, Chan WK. Effect of preparation conditions on morphology and release profiles of biodegradable polymeric microspheres containing protein fabricated by double-emulsion method. Chem Eng Sci 55[12], 2223-2236. 2000.

171. Wischke C, Lorenzen D, Zimmermann J, Borchert H. Preparation of protein loaded poly(D,L-lactide-co-glycolide) microparticles for the antigen delivery to dendritic cells using a static micromixer. Eur J Pharm Biopharm 62[3], 247-253. 2006.

172. Wischke C, Borchert HH. Influence of the primary emulsification procedure on the characteristics of small protein-loaded PLGA microparticles for antigen delivery. J of Microencapsul 23[4], 435-448. 2006.

173. Kang J, Schwendeman SP. Pore Closing and Opening in Biodegradable Polymers and Their Effect on the Controlled Release of Proteins. Mol Pharmaceutics 4[1], 104-118. 2007.

174. Ho ML, Fu YC, Wang GJ, Chen HT, Chang JK, Tsai TH, Wang CK. Controlled release carrier of BSA made by W/O/W emulsion method containing PLGA and hydroxyapatite. J Control Rel 128[2], 142-148. 2008.

175. Chen JL, Yeh MK, Chiang CH. The mechanism of surface-indented protein-loaded PLGA microparticle formation: The effects of salt (NaCl) on the solidification process. J of Microencapsul 21[8], 877-888. 2004.

176. Carrasquillo KG, Cordero RA, Ho S, Franquiz JM, Griebenow K. Structure-guided encapsulation of bovine serum albumin in poly(DL-lactic-co-glycolic) acid. Pharm Pharmacol Commun 4[12], 563-571. 1998.

177. Boury F, Marchais H, Proust JE, Benoit JP. Bovine serum albumin release from poly(alpha -hydroxy acid) microspheres: effects of polymer molecular weight and surface properties. J Control Rel 45[1], 75-86. 1997.

178. ExPASy Proteomics Server; database and therefrom calculated protein parameters. Swiss Intitute of Bioinformatics http://www.expasy.org/cgi-bin/protparam1?P12643@283-396@; http://www expasy org/cgi-bin/protparam1?P02769@25-607@. Accessed 13-4-2010.

179. Kyte J, Doolittle RF. A simple method for displaying the hydropathic character of a protein. J Mol Biol 157[1], 105-132. 1982.

180. Van de Weert M, Hennink WE, Jiskoot W. Protein instability in poly(lactic-co-glycolic acid) microparticles. Pharm Res 17[10], 1159-1167. 2000.

181. Jeffery H, Davis SS, O'Hagan DT. The preparation and characterization of poly(lactide-co-glycolide) microparticles. II. The entrapment of a model protein using a (water-in-oil)-in-water emulsion solvent evaporation technique. Pharm Res 10[3], 362-368. 1993.

182. Sah H. Microencapsulation techniques using ethyl acetate as a dispersed solvent: effects of its extraction rate on the characteristics of PLGA microspheres. J Control Rel 47[3], 233-245. 1997.

183. Sansdrap P, Moës AJ. Influence of manufacturing parameters on the size characteristics and the release profiles of nifedipine from poly(DL-lactide-co-glycolide) microspheres. Int J Pharm 98[1-3], 157-164. 1993.

184. Gabor F, Ertl B, Wirth M, Mallinger R. Ketoprofen-poly(D,L-lactic-co-glycolic acid) microspheres: influence of manufacturing parameters and type of polymer on the release characteristics. J Microencapsul 16[1], 1-12. 1999.

185. Yang YY, Chung TS, Ping Ng N. Morphology, drug distribution, and in vitro release profiles of biodegradable polymeric microspheres containing protein fabricated by double-emulsion solvent extraction/evaporation method. Biomaterials 22[3], 231-241. 2000.

186. Malzert-Freon A, Benoit JP, Boury F. Interactions between poly(ethylene glycol) and protein in dichloromethane/water emulsions: A study of interfacial properties. Eur J Pharm Biopharm 69[3], 835-843. 2008.

187. Zhu G, Mallery SR, Schwendeman SP. Stabilization of proteins encapsulated in injectable poly(lactide-co-glycolide). Nature Biotechnol 18[1], 52-57. 2000.

188. Dunn KD. Determination of polyvinyl alcohol in a poly(DL-lactide-co-glycolide) matrix by size exclusion chromatography using evaporative light scattering detection. J Pharm Biomed Anal 25[3-4], 539-543. 2001.

189. Yang YY, Chia HH, Chung TS. Effect of preparation temperature on the characteristics and release profiles of PLGA microspheres containing protein fabricated by double-emulsion solvent extraction/evaporation method. J Control Rel 69[1], 81-96. 2000.

190. Sipos P, Csoka I, Srcic S, Pintye-Hodi K, Eroes I. Influence of preparation conditions on the properties of eudragit microspheres produced by a double emulsion method. Drug Dev Res 64[1], 41-54. 2005.

191. Gangrade N, Price JC. Simple gas chromatographic headspace analysis of residual organic solvent in microspheres. J Pharm Sci 81[2], 201-202. 1992.

192. Rouse JJ, Mohamed F, van der Walle CF. Physical ageing and thermal analysis of PLGA microspheres encapsulating protein or DNA. Int J Pharm 339[1-2], 112-120. 2007.

193. Reich G. Use of DSC to study the degradation behavior of PLA and PLGA microparticles. Drug Dev Industr Pharm 23[12], 1177-1189. 1997.

194. Kissel T, Li Y, Unger F. ABA-triblock copolymers from biodegradable polyester A-blocks and hydrophilic poly(ethylene oxide) B-blocks as a candidate for in situ forming hydrogel delivery systems for proteins. Adv Drug Deliv Rev 54[1], 99-134. 2002.

195. Berkland C, King M, Cox A, Kim K, Pack DW. Precise control of PLG microsphere size provides enhanced control of drug release rate. J Control Rel 82[1], 137-147. 2002.

196. Berkland C, Kim K, Pack DW. PLG Microsphere Size Controls Drug Release Rate Through Several Competing Factors. Pharm Res 20[7], 1055-1062. 2003.

197. Ding AG, Schwendeman SP. Acidic Microclimate pH Distribution in PLGA Microspheres Monitored by Confocal Laser Scanning Microscopy. Pharm Res 25[9], 2041-2052. 2008.

198. Kranz H, Yilmaz E, Brazeau GA, Bodmeier R. In Vitro and In Vivo Drug Release from a Novel In Situ Forming Drug Delivery System. Pharm Res 25[6], 1347-1354. 2008.

199. Lam XM, Duenas ET, Cleland JL. Encapsulation and stabilization of nerve growth factor into poly(lactic-co-glycolic) acid microspheres. J Pharm Sci 90[9], 1356-1365. 2001.

200. Faisant N, Akiki J, Siepmann F, Benoit JP, Siepmann J. Effects of the type of release medium on drug release from PLGA-based microparticles: Experiment and theory. Int J Pharm 314[2], 189-197. 2006.

201. Jeong JH, Lim DW, Han DK, Park TG. Synthesis, characterization and protein adsorption behaviors of PLGA/PEG di-block co-polymer blend films. Colloids Surf B 18[3,4], 371-379. 2000.

202. van de Weert M, van 't Hof R, van der Weerd J, Heeren RMA, Posthuma G, Hennink WE, Crommelin DJA. Lysozyme distribution and conformation in a biodegradable polymer matrix as determined by FTIR techniques. J Control Rel 68[1], 31-40. 2000.

203. Kang F, Singh J. Effect of additives on the release of a model protein from PLGA microspheres. AAPS PharmSciTech 2[4], 30. 2001.

204. Kempe S, Metz H, Pereira PGC, Mäder K. Non-invasive in vivo evaluation of in situ forming PLGA implants by benchtop magnetic resonance imaging (BT-MRI) and EPR spectroscopy. Eur J Pharm Biopharm 74[1], 102-108. 2010.

205. Malzert-Freon A, Schoenhammer K, Benoit JP, Boury F. Interactions between poly(ethylene glycol) and protein in dichloromethane/water emulsions. 2. Conditions required to obtain spontaneous emulsification allowing the formation of bioresorbable poly(D,L lactic acid) microparticles. Eur J Pharm Biopharm 73[1], 66-73. 2009.

206. Choi SH, Park TG. G-CSF loaded biodegradable PLGA nanoparticles prepared by a single oil-in-water emulsion method. Int J Pharm 311[1-2], 223-228. 2006.

207. Sharif S, O'Hagan DT. A comparison of alternative methods for the determination of the levels of proteins entrapped in poly(lactide-co-glycolide) microparticles. Int J Pharm 115[2], 259-263. 1995.

208. Sah H. A New Strategy To Determine the Actual Protein Content of Poly(lactide-co-glycolide) Microspheres. J Pharm Sci 86[11], 1315-1318. 1997.

209. Makino K, Arakawa M, Kondo T. Preparation and in vitro degradation properties of polylactide microcapsules. Chem Pharm Bull 33[3], 1195-1201. 1985.

210. Makino K, Ohshima H, Kondo T. Mechanism of hydrolytic degradation of poly(L-lactide) microcapsules: effects of pH, ionic strength and buffer concentration. J Microencapsul 3[3], 203-212. 1986.

211. Reeve MS, McCarthy SP, Downey MJ, Gross RA. Polylactide stereochemistry: effect on enzymic degradability. Macromolecules 27[3], 825-831. 1994.

212. Cai Q, Shi G, Bei J, Wang S. Enzymatic degradation behavior and mechanism of poly(lactide-co-glycolide) foams by trypsin. Biomaterials 24[4], 629-638. 2003.

213. D'Souza SS, DeLuca PP. Methods to Assess in Vitro Drug Release from Injectable Polymeric Particulate Systems. Pharm Res 23[3], 460-474. 2006.

214. Sah H. Stabilization of proteins against methylene chloride/water interface-induced denaturation and aggregation. J Control Rel 58[2], 143-151. 1999.

215. Fu K, Pack DW, Klibanov AM, Langer R. Visual evidence of acidic environment within degrading poly(lactic-co-glycolic acid) (PLGA) microspheres. Pharm Res 17[1], 100-106. 2000.

216. Brunner A, Mäder K, Göpferich A. pH and osmotic pressure inside biodegradable microspheres during erosion. Pharm Res 16[6], 847-853. 1999.

217. Shao PG, Bailey LC. Porcine insulin biodegradable polyester microspheres: stability and in vitro release characteristics. Pharm Dev Technol 5[1], 1-9. 2000.

218. Witt C, Mäder K, Kissel T. The degradation, swelling and erosion properties of biodegradable implants prepared by extrusion or compression moulding of poly(lactide-co-glycolide) and ABA triblock copolymers. Biomaterials 21[9], 931-938. 2000.

219. Sansdrap P, Moees AJ. In vitro evaluation of the hydrolytic degradation of dispersed and aggregated poly(DL-lactide-co-glycolide) microspheres. J Control Rel 43[1], 47-58. 1997.

220. Anderson JM, Shive MS. Biodegradation and biocompatibility of PLA and PLGA microspheres. Adv Drug Delivery Rev 28[1], 5-24. 1997.

221. Yoo HS, Lee EA, Park TG. Doxorubicin-conjugated biodegradable polymeric micelles having acid-cleavable linkages. J Control Rel 82[1], 17-27. 2002.

222. Kim S, Healy KE. Synthesis and Characterization of Injectable Poly(N-isopropylacrylamide-co-acrylic acid) Hydrogels with Proteolytically Degradable Cross-Links. Biomacromolecules 4[5], 1214-1223. 2003.

223. Riley T, Stolnik S, Heald CR, Xiong CD, Garnett MC, Illum L, Davis SS, Purkiss SC, Barlow RJ, Gellert PR. Physicochemical Evaluation of Nanoparticles Assembled from Poly(lactic acid)-Poly(ethylene glycol) (PLA-PEG) Block Copolymers as Drug Delivery Vehicles. Langmuir 17[9], 3168-3174. 2001.

224. Heald CR, Stolnik S, Kujawinski KS, De Matteis C, Garnett MC, Illum L, Davis SS, Purkiss SC, Barlow RJ, Gellert PR. Poly(lactic acid)-Poly(ethylene oxide) (PLA-PEG) Nanoparticles: NMR Studies of the Central Solidlike PLA Core and the Liquid PEG Corona. Langmuir 18[9], 3669-3675. 2002.

225. Hrkach JS, Peracchia MT, Domb A, Lotan N, Langer R. Nanotechnology for biomaterials engineering: structural characterization of amphiphilic polymeric nanoparticles by 1H NMR spectroscopy. Biomaterials 18[1], 27-30. 1997.

226. Klose D, Azaroual N, Siepmann F, Vermeersch G, Siepmann J. Towards More Realistic In Vitro Release Measurement Techniques for Biodegradable Microparticles. Pharm Res 26[3], 691-699. 2009.

227. Lagarce F, Faisant N, Desfontis J, Marescaux L, Gautier F, Richard J, Menei P, Benoit J. Baclofen-loaded microspheres in gel suspensions for intrathecal drug delivery: in vitro and in vivo evaluation. Eur J Pharm Biopharm 61[3], 171-180. 2005.

228. Seeherman HJ, Li XJ, Bouxsein ML, Wozney JM. rhBMP-2 induces transient bone resorption followed by bone formation in a nonhuman primate core-defect model. J Bone Joint Surg Am 92[2], 411-426. 2010.

229. Ruhe PQ, Boerman OC, Russel FGM, Mikos AG, Spauwen PHM, Jansen JA. In vivo release of rhBMP-2 loaded porous calcium phosphate cement pretreated with albumin. Journal of Materials Science: Materials in Medicine 17[10], 919-927. 2006.

230. Kempen DHR, Lu L, Classic KL, Hefferan TE, Creemers LB, Maran A, Dhert WJA, Yaszemski MJ. Non-invasive screening method for simultaneous evaluation of in vivo growth factor release profiles from multiple ectopic bone tissue engineering implants. J Control Rel 130[1], 15-21. 2008.

231. Kempen DHR, Lu L, Hefferan TE, Creemers LB, Maran A, Classic KL, Dhert WJA, Yaszemski MJ. Retention of in vitro and in vivo BMP-2 bioactivities in sustained delivery vehicles for bone tissue engineering. Biomaterials 29[22], 3245-3252. 2008.

232. Takahashi Y, Yamamoto M, Tabata Y. Enhanced osteoinduction by controlled release of bone morphogenetic protein-2 from biodegradable sponge composed of gelatin and b-tricalcium phosphate. Biomaterials 26[23], 4856-4865. 2005.

233. Yamamoto M, Takahashi Y, Tabata Y. Controlled release by biodegradable hydrogels enhances the ectopic bone formation of bone morphogenetic protein. Biomaterials 24[24], 4375-4383. 2003.

234. Hosseinkhani H, Hosseinkhani M, Khademhosseini A, Kobayashi H. Bone regeneration through controlled release of bone morphogenetic protein-2 from 3-D tissue engineered nano-scaffold. J Control Rel 117[3], 380-386. 2007.

235. Yokota S, Sonohara S, Yoshida M, Murai M, Shimokawa S, Fujimoto R, Fukushima S, Kokubo S, Nozaki K, Takahashi K, Uchida T, Yokohama S, Sonobe T. A new recombinant human bone morphogenetic protein-2 carrier for bone regeneration. Int J Pharm 223[1-2], 69-79. 2001.

236. Siepmann J, Siepmann F. Mathematical modeling of drug delivery. Int J Pharm 364[2], 328-343. 2008.

237. Siepmann J, Elkharraz K, Siepmann F, Klose D. How autocatalysis accelerates drug release from PLGA-based microparticles: a quantitative treatment. Biomacromolecules 6[4], 2312-2319. 2005.

238. Siepmann J, Faisant N, Benoit JP. A new mathematical model quantifying drug release from bioerodible microparticles using monte carlo simulations. Pharm Res 19[12], 1885-1893. 2002.

239. Hofmann M. ELISA und Wiederfindung biol. aktiver Proteine. RnD Systems, eMail communication. 28-5-2010.

240. Puleo DA, Huh WW, Duggirala SS, DeLuca PP. In vitro cellular responses to bioerodible particles loaded with recombinant human bone morphogenetic protein-2. J Biomed Mater Res 41[1], 104-110. 1998.

241. Lin ZY, Duan ZX, Guo XD, Li JF, Lu HW, Zheng QX, Quan DP, Yang Sh. Bone induction by biomimetic PLGA-(PEG-ASP)n copolymer loaded with a novel synthetic BMP-2-related peptide in vitro and in vivo. J Control Rel 144[2], 190-195. 2010.

242. Hora MS, Rana RK, Nunberg JH, Tice TR, Gilley RM, Hudson ME. Release of human serum albumin from poly(lactide-co-glycolide) microspheres. Pharm Res 7[11], 1190-1194. 1990.

243. Dorati R, Genta I, Montanari L, Cilurzo F, Buttafava A, Faucitano A, Conti B. The effect of gamma -irradiation on PLGA/PEG microspheres containing ovalbumin. J Control Rel 107[1], 78-90. 2005.

244. Kwon YM, Kim SW. Biodegradable triblock copolymer microspheres based on thermosensitive Sol-gel transition. Pharm Res 21[2], 339-343. 2004.

245. Aubert-Pouessel A, Bibby DC, Vernier-Julienne MC, Hindré F, Benoit JP. A Novel in Vitro Delivery System for Assessing the Biological Integrity of Protein upon Release from PLGA Microspheres. Pharm Res 19[7], 1046-1051. 2002.

246. Jiang W, Schwendeman SP. Stabilization and controlled release of bovine serum albumin encapsulated in poly(D, L-lactide) and poly(ethylene glycol) microsphere blends. Pharm Res 18[6], 878-885. 2001.

247. Duggirala SS, Mehta RC, DeLuca PP. Interaction of recombinant human bone morphogenetic protein-2 with poly(DL-lactide-co-glycolide) microspheres. Pharm Dev Technol 1[1], 11-19. 1996.

248. Hoemann CD, El-Gabalawy H, McKee MD. In vitro osteogenesis assays: Influence of the primary cell source on alkaline phosphatase activity and mineralization. Pathol Biol 57[4], 318-323. 2009.

249. Kean T, Thanou M. Biodegradation, biodistribution and toxicity of chitosan. Adv Drug Delivery Rev 62[1], 3-11. 2010.

250. Kumar MN, V, Muzzarelli RAA, Muzzarelli C, Sashiwa H, Domb AJ. Chitosan chemistry and pharmaceutical perspectives. Chem Rev 104[12], 6017-6084. 2004.

251. Synowiecki J, Al-Khateeb NA. Production, properties, and some new applications of chitin and its derivatives. Critical Reviews in Food Science and Nutrition 43[2], 145-171. 2003.

252. Cho MH, Kim KS, Ahn HH, Kim MS, Kim SH, Khang G, Lee B, Lee HB. Chitosan Gel as an In Situ-Forming Scaffold for Rat Bone Marrow Mesenchymal Stem Cells In Vivo. Tissue Eng A 14[6], 1099-1108. 2008.

253. Engstrand T, Veltheim R, Arnander C, Docherty-Skogh AC, Westermark A, Ohlsson C, Adolfsson L, Larm O. A novel biodegradable delivery system for bone morphogenetic protein-2. Plastic and Reconstructive Surgery 121[6], 1920-1928. 2008.

254. Nitzsche H, Metz H, Lochmann A, Bernstein A, Hause G, Groth T, Mäder K. Characterization of Scaffolds for Tissue Engineering by Benchtop-Magnetic Resonance Imaging. Tissue Eng C 15[3], 513-521. 2009.

255. Marchand C, Rivard G-E, Sun J, Hoemann CD. Solidification mechanisms of chitosan-glycerol phosphate/blood implant for articular cartilage repair. Osteoarthritis Cartilage 17[7], 950-957. 2009.

256. Chen F, Wu Z, Wang Q, Wu H, Zhang Y, Nie X, Jin Y. Preparation and Biological Characteristics of Recombinant Human Bone Morphogenetic Protein-2-Loaded Dextran-co-Gelatin Hydrogel Microspheres, in vitro and in vivo Studies. Pharmacology 75[3], 133-144. 2005.

257. Park YJ, Kim KH, Lee JY, Ku Y, Lee SJ, Min BM, Chung CP. Immobilization of bone morphogenetic protein-2 on a nanofibrous chitosan membrane for enhanced guided bone regeneration. Biotechnol Appl Biochem 43[1], 17-24. 2006.

258. Abarrategi A, Moreno-Vicente C, Ramos V, Aranaz I, Sanz Casado JV, Lopez-Lacomba JL. Improvement of Porous beta -TCP Scaffolds with rhBMP-2 Chitosan Carrier Film for Bone Tissue Application. Tissue Eng A 14[8], 1305-1319. 2008.

259. Oliveira SM, Mijares DQ, Turner G, Amaral IF, Barbosa MA, Teixeira CC. Engineering Endochondral Bone: In Vivo Studies. Tissue Eng A 15[3], 635-643. 2009.

260. Blanquaert F, Barritault D, Caruelle JP. Effects of heparan-like polymers associated with growth factors on osteoblast proliferation and phenotype expression. J Biomed Mat Res 44[1], 63-72. 1999.

261. Hurley MM, Gronowicz G, Kream BE, Raisz LG. Effect of heparin on bone formation in cultured fetal rat calvaria. Calc Tiss Int 46[3], 183-188. 1990.

262. Goldhaber P. Heparin enhancement of factors stimulating bone resorption in tissue culture. Science 147[3656], 407-408. 1965.

263. Ruel-Gariepy E, Chenite A, Chaput C, Guirguis S, Leroux JC. Characterization of thermosensitive chitosan gels for the sustained delivery of drugs. Int J Pharm 203[1-2], 89-98. 2000.

264. Kempe S, Metz H, Bastrop M, Hvilsom A, Contri R, V, Mäder K. Characterization of thermosensitive chitosan-based hydrogels by rheology and electron paramagnetic resonance spectroscopy. Eur J Pharm Biopharm 68[1], 26-33. 2008.

265. Ganji F, Abdekhodaie MJ, Ramazani SA. Gelation time and degradation rate of chitosan-based injectable hydrogel. J Sol-Gel Sci Technol 42[1], 47-53. 2007.

266. King GN. The importance of drug delivery to optimize the effects of bone morphogenetic proteins during periodontal regeneration. Curr Pharm Biotechnol 2[2], 131-142. 2001.

267. Maus U, Andereya S, Gravius S, Siebert CH, Ohnsorge Jorg AK, Niedhart C. Lack of effect on bone healing of injectable BMP-2 augmented hyaluronic acid. Arch Orthop Trauma Surg 128[12], 1461-1466. 2008.

268. Aebli N, Stich H, Schawalder P, Theis JC, Krebs J. Effects of bone morphogenetic protein-2 and hyaluronic acid on the osseointegration of hydroxyapatite-coated implants: An experimental study in sheep. J Biomed Mater Res A 73A[3], 295-302. 2005.

269. Kim HD, Valentini RF. Retention and activity of BMP-2 in hyaluronic acid-based scaffolds in vitro. J Biomed Mater Res 59[3], 573-584. 2002.

270. Itoh S, Matubara M, Kawauchi T, Nakamura H, Yukitake S, Ichinose S, Shinomiya K. Enhancement of bone ingrowth in a titanium fiber mesh implant by rhBMP-2 and hyaluronic acid. J Mat Sci: Materials in Medicine 12[7], 575-581. 2001.

271. Luca L, Rougemont A-L, Walpoth BH, Gurny R, Jordan O. The effects of carrier nature and pH on rhBMP-2-induced ectopic bone formation. J Control Rel 147 [1] 38-44. 2010.

272. Lee YM, Nam SH, Seol YJ, Kim TI, Lee SJ, Ku Y, Rhyu IC, Chung CP, Han SB, Choi SM. Enhanced bone augmentation by controlled release of recombinant human bone morphogenetic protein-2 from bioabsorbable membranes. J Periodontol 74[6], 865-872. 2003.

273. Mori M, Isobe M, Yamazaki Y, Ishihara K, Nakabayashi N. Restoration of segmental bone defects in rabbit radius by biodegradable capsules containing recombinant human bone morphogenetic protein-2. J Biomed Mater Res 50[2], 191-198. 2000.

274. Kato M, Toyoda H, Namikawa T, Hoshino M, Terai H, Miyamoto S, Takaoka K. Optimized use of a biodegradable polymer as a carrier material for the local delivery of recombinant human bone morphogenetic protein-2 (rhBMP-2). Biomaterials 27[9], 2035-2041. 2006.

275. Dickerman RD, Reynolds AS, Bennett M. Brower RS, Vickrov NM. A case of psoas ossification from the use of BMP-2 for posterolateral fusion at L4-L5. Spine 2008;33:E653-55. Spine 34[7], 749. 2009.

276. Einhorn TA. Clinical applications of recombinant human BMPs: early experience and future development. J Bone Joint Surg Am 85-A Suppl 3, 82-88. 2003.

277. Eyres KS, Bell MJ, Kanis JA. Methods of assessing new bone formation during limb lengthening. Ultrasonography, dual energy X-ray absorptiometry and radiography compared. J Bone Joint Surg Br 75[3], 358-364. 1993.

278. IRDye 800CW BoneTag Optical Probe Product Information. Li-Cor Biosciences. 2008.

279. Saito N, Okada T, Horiuchi H, Ota H, Takahashi J, Murakami N, Nawata M, Kojima S, Nozaki K, Takaoka K. Local bone formation by injection of recombinant human bone morphogenetic protein-2 contained in polymer carriers. Bone 32[4], 381-386. 2003.

280. Kaito T, Myoui A, Takaoka K, Saito N, Nishikawa M, Tamai N, Ohgushi H, Yoshikawa H. Potentiation of the activity of bone morphogenetic protein-2 in bone regeneration by a PLA-PEG/hydroxyapatite composite. Biomaterials 26[1], 73-79. 2005.

281. Visscher GE, Robison RL, Maulding HV, Fong JW, Pearson JE, Argentieri GJ. Biodegradation of and tissue reaction to 50:50 poly(DL-lactide-co-glycolide) microcapsules. J Biomed Mater Res 19[3], 349-365. 1985.

282. Seeherman H, Wozney J, Li R. Bone morphogenetic protein delivery systems. Spine 27[16 Suppl 1], S16-S23. 2002.

Acknowledgements

First of all, I would like to express my gratitude to my mentor Karsten Mäder for the opportunity to join his working group, the suggestion of the research subject, his enduring interest and support of the work, his challenging ideas and the constantly open door. I want to thank Elisabeth Schwarz, who invited me to her lab, introduced me to the secrets of BMPs and provided the raw material and facilities for the extraction and purification of rhBMP-2. From her group, I would like to set apart Sabrina von Einem for her introduction to the lab protocols as well as to cell culture testing.

First ideas on rhBMP-2 aggregation were gathered with the help of Judith Kuntsche (AF4), Christian Schmelzer and Michael Jung (MALDI-TOF). The labelling procedure of insuline of Ahmed Besheer was used as starting point to perform the labelling of rhBMP-2.

The microsphere characterization based on a variety of sophisticated methods. Sylke Meyer, with her assistance with the confocal laser scanning microscope, and Frank Syrowatka, acquiring the ESEM pictures, helped to visualize the small but important details in microsphere morphology. Thermal analyses were performed by Kerstin Schwarz. Mandy Koch conducted the GC measurements on residual organic solvents within the microspheres. The successful combination of microspheres with a scaffold matrix was enabled by Hagen Nitzsche, who provided scaffolds in their nascent state for these studies. Ute Mentzel assisted in some LD measurements. Katja Meersteiner, Martin Windorf and Matthias Hecker helped as students in the optimization of production and administration of microspheres.

Implants and bone formation were monitored for extended periods of time in vivo. I am very grateful to Hendrik Metz for MRI measurements and fruitful discussions on result evaluation modalities and to Manfred Knörgen for CT measurements. The calcification measurements would have been much more time- and nerve-consuming without the save and sound analyte administration to the mice by Thomas Müller. Johannes Kutza provided the HHA gels in the dispersant comparison study.

I am indebted to Ilona Schön due to her great support during the histological evaluation. Furthermore, I would like to acknowledge Sabine Koitzsch and Gerd Hause for the conduction of histological stainings. Friederike Eisenächer and Verena Gläßer lent their eyes more than once to score the bone formation of *ex vivo* samples.

Last, but not least, I would like to thank my colleagues for giving me such a great time in the group. I am very grateful for the fruitful discussions and lots of fun we had during the last 3½ years. Here, I would like to acknowledge in particular my room- and labmates Hagen Nitzsche and Andreas Noack as well as Johannes Kutza and Andreas Schädlich.

This work was made possible in part by funding from the German Federal Ministry of Education and Research (BMBF, PtJ-Bio, 0313909) and by constant support of the Translational Centre for Regenerative Medicine, Leipzig (TRM Leipzig).

Publikationen

Peer reviewed manuscripts

A. Lochmann, H. Nitzsche, S. von Einem, E. Schwarz, K. Mäder:

The influence of covalently linked and free polyethylene glycol on the structural and release properties of rhBMP-2 loaded microspheres

J Control Rel 147[1] 92-100. 2010

H. Nitzsche, A. Lochmann, H. Metz, A. Hauser, F. Syrowatka, E. Hempel, T. Müller, T. Thurn-Albrecht, K. Mäder: Fabrication and Characterization of a Biomimetic Composite Scaffold for Bone Defect Repair

J Biomed Mat Res A 94A[1], 298-307. 2010

H. Nitzsche, H. Metz, A. Lochmann, A. Bernstein, G. Hause, T. Groth, K. Mäder: Characterization of Scaffolds for Tissue Engineering by Benchtop-MRI

Tissue Eng. C 15[3], 513-521. 2009

Oral Presentations

A. Lochmann, K. Mäder: Controlled drug delivery systems for rhBMP-2 in osseous defect reconstruction.

MDT Leipzig, Leipzig, Nov 25, 2009

Abstract and Poster Presentations

A. Lochmann, H. Nitzsche, A. Schädlich, S. von Einem, E. Schwarz, K. Mäder: Applicability testing of in situ forming implants with incorporated microspheres: In vivo monitoring of Calcification.
Regen. Med. 4[6] S218-S219. 2009 (Abstract)

A. Lochmann, H. Nitzsche, A. Schädlich, S. von Einem, E. Schwarz, K. Mäder: Controlled Delivery of rhBMP-2 from Injectable Delivery systems
Tiss Eng Regen Med 6[12] S184. 2009 (Abstract)
TERMIS World Congress, Aug 31 – Sept 3, 2009, Seoul, Korea

A. Lochmann, H. Nitzsche, S. von Einem, E. Schwarz, K. Mäder: Microspherical delivery of a growth factor.
Saxon Biotechnology Symposium, May 26, 2009, Leipzig, Germany; Abstract book ISBN: 978-3-00-027884-6

A. Lochmann, H. Nitzsche, S. von Einem, E. Schwarz, K. Mäder: Controlled Delivery of rhBMP-2 from Biodegradable Delivery Systems.
CRS German Chapter Annual Meeting, March 19 - 20, 2009, Halle, Germany (Poster)

A. Lochmann, H. Nitzsche, S. von Einem, E. Schwarz, K. Mäder: Microparticles with rhBMP-2 for Incorporation in in situ-forming Implants.
7th International Conference on Bone Morphogenetic Proteins July 9 - 13, 2008, Lake Tahoe, United States (Poster)

H. Nitzsche, A. Noack, A. Lochmann, C. Oliveira, A. Besheer, H. Metz, A. Bernstein, G. Hause, T. Groth, K. Mäder: Scaffold Properties and Interaction with Cells Investigated By Magnetic Resonance Methods.
Tissue Eng. A 14[5], 907. 2008 (Abstract),
TERMIS-EU Meeting, June 22 – 26, 2008, Porto, Portugal (Poster)

A. Lochmann, H. Nitzsche, S. von Einem, E. Schwarz, K. Mäder: Microparticles for Incorporation in In Situ-Forming Implants in Osseous Defect Reconstruction

Tissue Eng. A 14[5], 879-880. 2008 (Abstract),

TERMIS-EU Meeting, June 22 – 26, 2008, Porto, Portugal (Poster)

A. Lochmann, H. Nitzsche, S. von Einem, E. Schwarz, K. Mäder: Biodegradable Delivery Systems for the Controlled Release of Recombinant Human Bone Morphogenetic Protein 2

9th Advanced Summer Course in Cell-Materials Interactions, June 16 – 20, 2008, Porto, Portugal (Poster)

A. Lochmann, S. von Einem, E. Schwarz, K. Mäder: rhBMP-2 Loaded Microparticles for Osseous Defect Reconstruction

CRS German Chapter Annual Meeting, March 4 - 5, 2008, Braunschweig, Germany (Poster)

A. Lochmann, H. Nitzsche, S. Kempe, S. von Einem, E. Schwarz, K. Mäder: rhBMP-2 Delivery From Scaffolds, Microparticles And In Situ-forming Gels

6th research festival for life sciences 2007, Dec 14, 2007, Leipzig, Germany, (Poster), Abstract book ISBN 3-9810760-2-8

A. Lochmann, H. Nitzsche, S. Kempe, S. von Einem, E. Schwarz, K. Mäder: rhBMP-2 Delivery From Scaffolds And In Situ-forming Gels

Regen. Med. 2[5] 649-650. 2007 (Abstract),

3rd World Congress on Regenerative Medicine, Oct 18 – 20, 2007, Leipzig, Germany (Poster)

Curriculum Vitae

Alexander Lochmann

Geburtsdatum: 22.06.1981

Geburtsort: Karl-Marx-Stadt, jetzt Chemnitz

Familienstand: verheiratet

Theorie

01/2007 – 09/2010	Promotionsstudium in Pharmazeutischer Technologie an der Martin-Luther-Universität Halle-Wittenberg, Stipendiat des Translations-zentrums für Regenerative Medizin in Leipzig; Thema der Arbeit: „Development of controlled drug delivery systems for rhBMP-2 in osseous defect reconstruction"
12/2006	Approbation zum Apotheker
12/2006	Drittes Staatsexamen
09/2005	Zweites Staatsexamen
09/2003	Erstes Staatsexamen
09/2001	Beginn des Pharmaziestudiums an der Universität Leipzig
07/2000 – 04/2001	Sanitätsdienst bei der Bundeswehr
09/1988 – 07/2000	Schulausbildung und Abitur in Chemnitz

Praxis

05/2008 – 06/2010	Teilzeittätigkeit als Apotheker, Burg-Apotheke, Halle
01/2007 – 05/2010	Lehrtätigkeit an der MLU Halle-Wittenberg Seminare und Praktika „Arzneiformenlehre I", „Arzneiformenlehre II" Seminare „Statistik für Pharmazeuten"

05/2006 – 10/2006	Pharmazeut im Praktikum, Grassi-Apotheke, Leipzig
11/2005 – 04/2006	Pharmazeut im Praktikum, Hexal Pharmaforschung, Holzkirchen
10/2003 – 03/2005	Studentische Hilfskraft am Institut für Pharmazie, Universität Leipzig, AK Prof. Kurt Eger
09/2002 – 08/2003	Studentische Hilfskraft am Institut für Biochemie, Universität Leipzig, AK Prof. Annette Beck-Sickinger

Famulaturen und Firmenpraktikum

02/2004 – 03/2004	Aeropharm GmbH/Hexal AG, Rudolstadt Abteilung F&E Ophthalmika
07/2002 – 08/2002	Klinikum Chemnitz, Zentralapotheke
03/2002	Bären-Apotheke, Chemnitz

Sonstiges

07/2004 – 12/2006	Freie Mitarbeit bei der Deutschen Apotheker Zeitung, Stuttgart; Übersetzen und Verfassen von Artikeln für die Fachpresse

Erklärung

Hiermit erkläre ich, dass ich mich mit der vorliegenden Arbeit erstmals um die Erlangung eines Doktorgrades bewerbe.

Ferner erkläre ich, dass ich die Ergebnisse der vorliegenden Dissertationsarbeit an der Martin-Luther-Universität Halle-Wittenberg unter Anleitung von Herrn Professor Dr. rer. nat. habil. Karsten Mäder selbständig erarbeitet bzw. im Rahmen der angegebenen Kooperationen erhalten und die Dissertation ohne fremde Hilfe angefertigt habe. Dazu habe ich keine anderen als die angegebenen Quellen und Hilfsmittel benutzt und die den verwendeten Werken wörtlich oder inhaltlich entnommenen Stellen als solche kenntlich gemacht.

Halle, den 13.09.2010

Alexander Lochmann

Nothing in the universe can travel at the speed of light, they say, forgetful of the shadow's speed.

Howard Nemerov